Challenge Journal of
CONCRETE RESEARCH LETTERS

Vol.13 No.1 (2022)

acoustic emission aerated concrete compressive strength concrete corrosion cracking curing ductility durability energy absorption ferrocement fly ash fracture mechanical properties mortar nanoparticle palm oil fuel ash reinforced concrete self-compacting concrete silica fume strengthening superplasticizer tensile strength workability waste disposal water absorption

ISSN 2548-0928

TULPAR ACADEMIC PUBLISHING

Challenge Journal of Concrete Research Letters

E-mail: *cjcrl@challengejournal.com*

Web page: *cjcrl.challengejournal.com*

TULPAR Academic Publishing
www.tulparpublishing.com

Challenge Journal of Concrete Research Letters

CONTENTS

TULPAR ACADEMIC PUBLISHING

Challenge Journal of Concrete Research Letters

Research Article

Optimization of axial load carrying capacity of CFST stub columns

Celal Cakiroglu [a,*], Gebrail Bekdaş [b]

[a] *Department of Civil Engineering, Turkish-German University, 34820 İstanbul, Turkey*
[b] *Department of Civil Engineering, İstanbul University-Cerrahpaşa, 34320 İstanbul, Turkey*

ABSTRACT

Concrete filled steel tubular (CFST) columns are widely used due to their enhanced mechanical properties. The interaction between the concrete core and the steel casing increases structural stability and magnifies the compressive strength of concrete. Besides the structural performance, in alignment with the commitment of the concrete industry to reduce its environmental impact, lowering the carbon emissions caused by the production of concrete structures is gaining importance in recent years. The current paper gives an overview of the equations available in the literature that predict the axial load carrying capacity of rectangular CFST columns. A modified version of the Jaya metaheuristic algorithm is being proposed and the outcome of this algorithm is being presented. The algorithm is used in order to maximize the axial load-carrying capacity of a stub column. As an optimization constraint the CO_2 emission associated with the production of the CFST column is being kept below a predefined level throughout the optimization process. The optimization process as well as the cross-sectional dimensions associated with the optimum solution are presented.

ARTICLE INFO

Article history:
Received 3 September 2021
Revised 7 October 2021
Accepted 1 November 2021

Keywords:
Metaheuristic
Optimization
CFST
Columns
Axial load carrying capacity

1. Introduction

Concrete-filled steel tubular (CFST) columns are an extensively investigated field of structural engineering. A major reason for this is the ease of construction, high ductility, and strength of these composite members. Some of the application areas of these structures are piles, columns and bridge piers (Wang et al. 2017). Although a large number of experimental studies have been conducted in this field, these studies are mostly related to the displacement and compressive strength properties of CFST columns. Some of the notable works done in this field include the experimental studies of Lai and Varma (2015), Johansson and Gylltoft (2002), Wei et al. (2020) about circular CFST columns. In the area of CFST columns with rectangular cross-sections the works of Xiong et al. (2017), Zhu et al. (2017) and Chen et al. (2018) can be mentioned.

While the experimental and numerical study of CFST columns is an extensively investigated area, the research in the field of optimization of CFST columns is relatively neglected. In recent years particularly metaheuristic optimization algorithms found application in a broad range of engineering problems. Cakiroglu et al. (2021) used metaheuristic methods to minimize the CO_2 emission associated with the production of CFST columns with circular cross-section. Besides CFST columns, laminated composite plates (Cakiroglu et al. 2020), cylindrical walls (Kayabekir 2021), water networks (Geem 2009), reinforced concrete cantilever soldier piles (Arama et al. 2020), active tuned mass dampers (Kayabekir et al. 2020a) and plane stress systems (Kayabekir et al. 2020b) are some of the engineering systems to which metaheuristic methods were applied. In the current study a modified Jaya optimization is applied to the problem of axial load-carrying capacity maximization. The variables of this optimization problem are the cross-sectional dimensions shown in Figure 1. The constraints of optimization are the upper and lower bounds of the design variables for which Eqs. (1-5) are applicable and the amount of CO_2 emission related to the production process of concrete. These ranges are given in Table 1. During the production of 1 kg of concrete approximately 0.12 kg of CO_2 is emitted into the atmosphere, and during

* *Corresponding author*. E-mail address: cakiroglu@tau.edu.tr (C. Cakiroglu)
ISSN: 2548-0928 / DOI: https://doi.org/10.20528/cjcrl.2022.01.001

the production of 1 kg of steel approximately 1.38 kg of CO_2 is being emitted (Fantilli et al. 2019). Besides the ranges of applicability also, the amount of CO_2 associated with the production of a stub column is introduced as an additional optimization constraint.

Nomenclature

N_u	Ultimate axial load-carrying capacity
N_s	Contribution of the steel casing to N_u
N_c	Contribution of the concrete core to N_u
A_s	Cross-sectional area of the steel casing
A_c	Cross-sectional area of the concrete core
η_s	Reduction factor that introduces the effect of confinement on the steel casing
η_c	Amplification factor that introduces the effect of confinement on the concrete core
k_s	Equivalent confining coefficient incorporating the lack of concrete confinement
H	Longer side length of a rectangular cross-section
B	Shorter side length of a rectangular cross-section
t	Wall thickness of the steel casing
D'	Equivalent diameter of the rectangular cross-section
f_c'	Compressive strength of concrete
f_y	Yield strength of the steel casing

1.1. Equations for the prediction of N_u

The literature about CFST columns includes various equations for the prediction of N_u of stub columns. Furthermore, there are separate equations for CFST columns with circular and rectangular cross-sections. The current study focuses on rectangular cross-sections. The equations developed by Wang et al. (2017) are used since these equations are shown to deliver the most satisfactory results in terms of the prediction of N_u (Vu et al. 2021).

$$N_u = N_s + N_c \tag{1}$$

$$N_s = \eta_s f_y A_s \ , \ N_c = \eta_c f_c' A_c \tag{2}$$

$$\eta_s = 0.91 + 7.31 \cdot 10^{-5} f_y - (1.28 \cdot 10^{-6} + 2.26 \cdot 10^{-8} f_y)\left(\frac{D'}{t}\right)^2 \tag{3}$$

$$\eta_c = 0.98 + 29.5(f_y)^{-0.48} k_s^{0.2} \left(\frac{t f_y}{D' f_c'}\right)^{1.3} \tag{4}$$

$$k_s = \frac{1}{3}\left(\frac{B-2t}{H-2t}\right)^2 \tag{5}$$

The equivalent diameter in Eq. (3) is calculated as $D' = \sqrt{(B^2 + H^2)}$. The equivalent confining coefficient k_s is needed due to lack of concrete confinement caused by the rectangular shape of the cross-section. Eqs. (1) to (5) are applicable only for certain ranges of the design variables B, H and t shown in Fig. 1. These ranges are listed in Table 1.

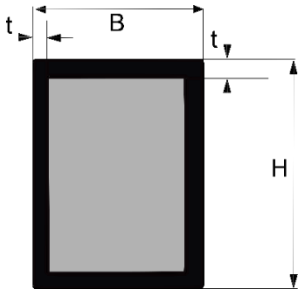

Fig. 1. Dimensions of a rectangular CFST column.

Table 1. Ranges of design variables.

Width to thickness ratio	$12 \leqslant B/t \leqslant 100$
Height to width ratio	$1 \leqslant H/B \leqslant 2$
Yield strength of the steel tube	175 MPa $\leqslant f_y \leqslant$ 960 MPa
Compressive strength of the concrete	20 MPa $\leqslant f_c' \leqslant$ 120 MPa
Steel wall thickness [mm]	$3 \leqslant t \leqslant 30$

2. Methods

The goal of the optimization is to maximize N_u while keeping the CO_2 emission associated with the production of the stub column below a certain threshold level at all times. Furthermore, throughout the iterations the design variables are kept within their corresponding upper and lower bounds of applicability as given in Table 1. The class of concrete has been varied between C25, C40, C60 and the yield stress of steel is fixed at 500 MPa.

2.1. Optimization process

A modified version of a metaheuristic optimization algorithm called Jaya optimization has been utilized in this study. The algorithm starts with the random generation of a population of solution candidates. Each solution candidate consists of a list of design variable values. In the current study these lists contain the cross-section side lengths, steel casing wall thickness and the corresponding axial load-carrying capacity and CO_2 emission. Once the initial population has been created all vectors in the population go through a Jaya iteration given in Eq. (6) (Venkata Rao 2016).

$$x_i^{k+1} = x_i^k + r1 \cdot \left(x_b^k - \left|x_i^k\right|\right) - r1 \cdot \left(x_w^k - \left|x_i^k\right|\right) \tag{6}$$

In Eq. (6) x_i^k is the $i-th$ vector in the population after k Jaya iterations and x_i^{k+1} is the updated version of this vector. x_b^k and x_w^k are the best- and worst-performing members of the population respectively in the $k-th$ Jaya iteration step. r_1 and r_2 are three dimensional vectors of random numbers between zero and one. In the proposed modified Jaya algorithm r_1 and r_2 are assigned according to the Lévy distribution given in Eq. (7) (Nolan 2020). The Lévy distributions for different values of γ and $\delta = 0$ are shown in Fig. 2. For each design variable the parameters of the Lévy distribution are tuned separately. A flowchart of the modified Jaya algorithm can be seen in Fig. 3.

$$f(x) = \sqrt{\frac{\gamma}{2\pi}} \frac{1}{(x-\delta)^{1.5}} e^{\frac{-\gamma}{2(x-\delta)}}, \quad \delta < x < \infty \tag{7}$$

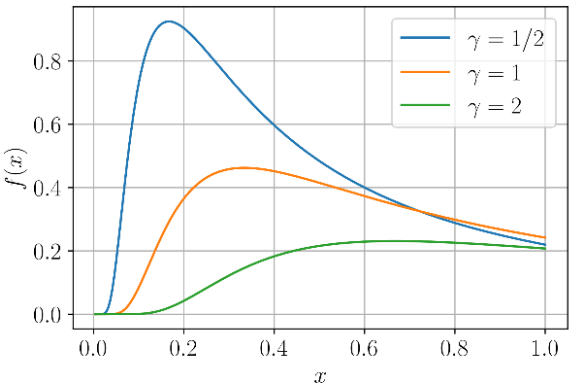

Fig. 2. Lévy distributions.

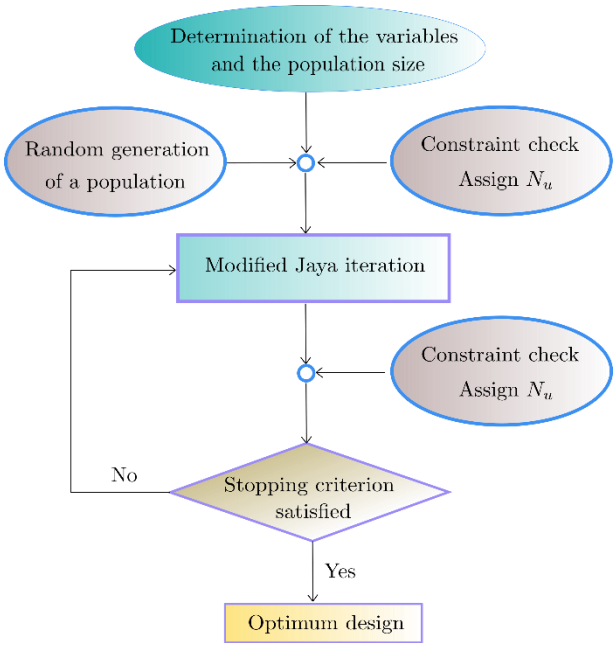

Fig. 3. Flow chart of the modified Jaya algorithm.

3. Results

Fig. 4 shows the optimization process where the best- and worst-performing solution vectors and the average value of the entire population are shown in different colors. It is observed that after the first ten iterations no more major update happened in the best solution vector. On the other hand, the convergence of the worst and average solution vectors to the optimum solution is observed after twenty-five iterations. The maximum axial load that could be achieved through the optimization was around 10759 kN in case of C25 concrete class. Similarly, Figs. 5 and 6 show the development of the best, worst and average solutions throughout the Jaya iteration steps for C40 and C60 concrete classes respectively. For all three concrete classes the corresponding cross-sectional dimensions and the maximum axial load-carrying capacities are listed in Table 2.

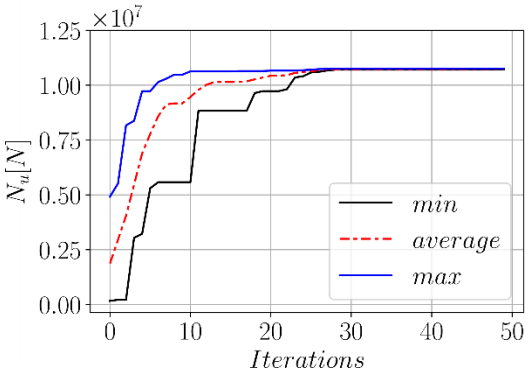

Fig. 4. Modified Jaya optimization for C25 concrete.

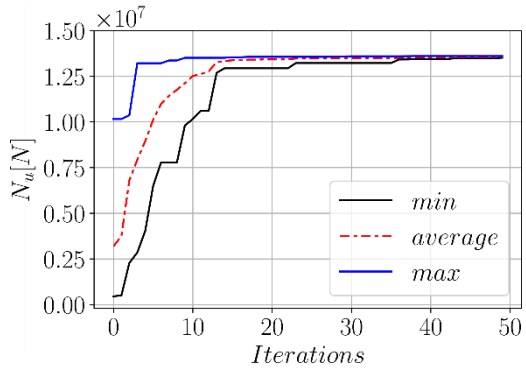

Fig. 5. Modified Jaya optimization for C40 concrete.

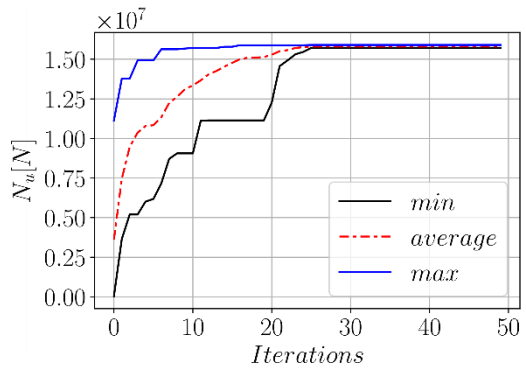

Fig. 6. Modified Jaya optimization for C60 concrete.

Table 2. Optimized cross-sections.

	B	H	t	$N_{u,\max}$ (kN)
C25	300	537	3	10759
C40	300	433	3	13618
C60	230	443	3	15905

4. Conclusions

Concrete-filled steel tubular (CFST) columns are widely used due to their favorable properties such as increased ductility and stability. Although structural performance is the primary concern of design engineers, the construction industry in general is aiming to reduce its

carbon footprint in the recent years. The current study is considering both of these aspects of structural design. The cross-sectional dimensions of a stub column are optimized to increase the ultimate load-carrying capacity of the CFST structure while keeping the carbon emission below a predetermined level. To this end the modified version of a metaheuristic technique called Jaya algorithm has been used. The optimization process has been done for C25, C40 and C60 concrete classes. The results showed that through optimization the performance of a CFST column can be significantly increased without causing excessive carbon emissions.

Acknowledgements

None declared.

Funding

The authors received no financial support for the research, authorship, and/or publication of this manuscript.

Conflict of Interest

The authors declared no potential conflicts of interest with respect to the research, authorship, and/or publication of this manuscript.

References

Arama ZA, Kayabekir AE, Bekdaş G, Geem ZW (2020). CO_2 and cost optimization of reinforced concrete cantilever soldier piles: A parametric study with harmony search algorithm. *Sustainability*, 12, 5906.

Cakiroglu C, Bekdaş G, Geem ZW (2020). Harmony search optimisation of dispersed laminated composite plates. *Materials*, 13(12), 2862.

Cakiroglu C, Islam K, Bekdaş G, Billah M (2021). CO_2 emission and cost optimization of concrete-filled steel tubular (CFST) columns using metaheuristic algorithms. *Sustainability*, 13(14), 8092.

Chen S, Zhang R, Jia LJ, Wang JY, Gu P (2018). Structural behavior of UHPC filled steel tube columns under axial loading. *Thin-Walled Structures*, 130, 550-563.

Fantilli AP, Mancinelli O, Chiaia B (2019). The carbon footprint of normal and high-strength concrete used in low-rise and high-rise buildings. *Case Studies in Construction Materials*, 11, e00296.

Geem ZW (2009). Harmony search optimization to the pump-included water distribution network design. *Civil Engineering and Environmental Systems*, 26(3), 211-221.

Johansson M, Gylltoft K (2002). Mechanical behavior of circular steel-concrete composite stub columns. *Journal of Structural Engineering*, 128(8), 1073-1081.

Kayabekir AE (2021). Effects of constant parameters on optimum design of axially symmetric cylindrical reinforced concrete walls. *The Structural Design of Tall and Special Buildings*, 30(6), e1838.

Kayabekir AE, Bekdaş G, Nigdeli SM, Geem ZW (2020a). Optimum design of PID controlled active tuned mass damper via modified harmony search. *Applied Sciences*, 10, 2976.

Kayabekir AE, Toklu YC, Bekdaş G, Nigdeli SM, Yücel M, Geem ZW (2020b). A novel hybrid harmony search approach for the analysis of plane stress systems via total potential optimization. *Applied Sciences*, 10, 2301.

Lai Z, Varma AH (2015). Noncompact and slender circular CFT members: Experimental database, analysis, and design. *Journal of Constructional Steel Research*, 106, 220–233.

Nolan JP (2020). Univariate Stable Distributions, Models for Heavy Tailed Data. Springer International Publishing, Switzerland.

Venkata Rao R (2016). Jaya: A simple and new optimization algorithm for solving constrained and unconstrained optimization problems. *International Journal of Industrial Engineering Computations*, 7(2016), 19–34.

Vu QV, Truong VH, Thai HT (2021). Machine learning-based prediction of CFST columns using gradient tree boosting algorithm. *Composite Structures*, 259, 113505.

Wang ZB, Tao Z, Han LH, Uy B, Lam D, Kang WH (2017). Strength, stiffness and ductility of concrete-filled steel columns under axial compression. *Engineering Structures*, 135, 209-221.

Wei J, Luo X, Lai Z, Varma AH (2020). Experimental behavior and design of high-strength circular concrete-filled steel tube short columns. *Journal of Structural Engineering*, 146(1), 04019184.

Xiong MX, Xiong DX, Liew JYR (2017). Axial performance of short concrete filled steel tubes with high- and ultra-high- strength materials. *Engineering Structures*, 136, 494-510.

Zhu A, Zhang X, Zhu H, Zhu J, Lu Y (2017). Experimental study of concrete filled cold-formed steel tubular stub columns. *Journal of Constructional Steel Research*, 134, 17-27.

Challenge Journal of Concrete Research Letters

Research Article

Structural behavior of ferrocement composite hollow-cored panels for roof construction

Yousry B. I. Shaheen [a], Zeinab A. Etman [a,b,*], Aya M. Elrefy [b]

[a] *Department of Civil Engineering, Menoufia University, Shebin ElKoum, Menofia, Egypt*
[b] *Department of Civil Engineering, Higher Institute of Engineering and Technology, Menofia, Egypt*

ABSTRACT

The main objective of the following work is to study the effect of using different types of metallic and non-metallic mesh reinforcement materials on the flexural behavior of ferrocement hollow-cored panels as a viable alternative for conventional reinforced concrete roofs. The proposed panels are lighter in weight relative to the conventional reinforced concrete panels. Three types of the steel meshes were used to reinforce the ferrocement skin layers. Namely: welded wire mesh, expanded metal mesh, and tenax mesh with various numbers of layers. Experimental investigation was conducted on the proposed panels. A total of ten slabs having the total dimensions of 2000 mm length, 500 mm width and 120 mm thickness were cast and tested under flexural loadings until failure. The deformation characteristics and cracking behavior were recorded and observed for each panel at all stages of loadings. The results showed that high ultimate and serviceability loads, crack resistance control, high ductility, and good energy absorption properties could be achieved by using the proposed panels. This could be of true construction merits for both developed and developing countries alike. The experimental results were then compared to analytical models using (ABAQUS/Explicit) programs. The finite element (FE) simulations achieved better results in comparison with the experimental results.

ARTICLE INFO

Article history:
Received 13 July 2021
Revised 28 September 2021
Accepted 28 December 2021

Keywords:
Hollow core slab
Ferrocement
Composite materials
Tenax mesh
Experimental program

1. Introduction

A hollow core slab, known as a void slab, hollow core plank or simply a concrete plank is a precast concrete slab typically used in the construction of roofs in multi-story apartment buildings. Precast concrete popularity is linked with low-seismic zones and more economical constructions because of fast building assembly, lower self-weight (less material), etc. The precast hollow core concrete slab has voids extending the full length of the slab which makes the slab much lighter than a massive solid concrete slab of equal thickness or strength. The reduced weight is important because it lowers the costs of transportation as well as material (concrete) costs. Hollow core slabs are most widely known for providing economical, efficient floor and roof systems.

On the other hand, ferrocement is a construction material that proved to yield superior properties in terms of crack control, impact resistance, and toughness, largely due to the close spacing and uniform dispersion of reinforcement within the material. In 1999, the American Concrete Institute ACI committee 549 give the following definition in the state-of-the-art report on ferrocement (ACI 549R) "ferrocement is a type of thin wall reinforced concrete commonly constructed of hydraulic cement mortar reinforced with closely spaced layers of continuous and relatively small size wire mesh. The mesh may be made of metallic or other suitable materials".

A literature review was presented by Koukousel and Mistakid (2014) and Sakthivel and Jagannathan (2005) on ferrocement as a construction material. Ferrocement can be used in different applications due to its properties such as different roofing systems, retaining walls, sculptures, bus shelters, bridge decks, repair works, water structures like tanks, strengthening and precast ferrocement elements (Aboul-Anen et al. 2009; Ali and Abdullah

* *Corresponding author*. Tel.: +2-01-009-727355 ; E-mail address: :zeinab.etman@sh-eng.menofia.edu.eg (Z. A. Etman)
ISSN: 2548-0928 / DOI: https://doi.org/10.20528/cjcrl.2022.01.002

1995; Al-Kubaisy and Jumaat 2000; Elavenil and Chandrasekar 2007; Fahmy et al. 1997). Additionally, ferrocement is lighter than traditional concrete up to 70% elements, which can be suitable for low-cost housing (Leeanansaksiri et al. 2018; Naaman 2015; Shaheen and Eltahawy 2017). The effect of the strength of ferrocement jackets for initially damaged exterior RC beam-column joints is presented by Singh et al. (2015). In this study, the experimental observation noticed an improvement in the ultimate load, yield load carrying capacity with increase in stiffness of the ferrocement-jacketed joints in comparison with the control joint.

Many investigators have reported the advantages of ferrocement in comparing with the conventional reinforced concrete. In addition, numerous test data are available to define its performance criteria for construction and repair of structural elements (Shaheen et al. 2018; Fahmy et al. 2004, 2005). From these investigations, it can be concluded that ferrocement has features included ease of prefabrication and low cost in maintenance and repair. Swamy and Shaheen (1990) investigated the comprehensive test data on the tensile behavior of ferrocement plates, 12.5mm thick. The results showed that the composite properties of elastic modulus and ultimate tensile strength could be very satisfactorily predicted. However, the cracking behavior for a wide range of mesh geometry could not be satisfactorily predicted by a single unique relationship. There was, however, a good correlation between the composite properties of ultimate tensile strength and ultimate flexural strength. The results show that by suitable design of the matrix and the reinforcement, high strength ferrocement sheets with high crack resistance can be developed for a variety of structural applications.

Furthermore, many attempts have been made to improve the practical use of the ferrocement I-beams by developing its ductile behavior. For example, the evaluation of the actual flexural capacity of the ferrocement I-beam with additional layers of wire mesh in the flange section as compared to the theoretical analysis computation is illustrated by Acma et al. (2015). The design and construction of the ferrocement channels were presented with various materials (e.g., meshes and mortar). In addition, an optimal combination of meshes was obtained and finite element FE models of the channels were implemented using ABAQUS Unified FEA (Eskandari and Madadi, 2015). Ferrocement developed sandwich panels for use as wall bearing units, also studied the structural behavior of light weight ferrocement walls. The proposed panels are lighter in weight relative to the conventional reinforced concrete panels (Shaheen et al. 2020; Shaaban et al. 2018).

Bhalsing et al. (2014) studied the tensile strength behavior of ferrocement due to the specific surface area. A relation between the tensile strength of ferrocement and its mechanical properties were determined. Therefore, utilizing ferrocement in hollow core elements can reduce the self-weight of the elements considerably. Furthermore, the hollow core ferrocement elements are generally more ductile when compared with the hollow conventional reinforced concrete units, because of the fact that the reinforcement in ferrocement is uniformly distributed over the entire section of the hollow elements.

Abbas et al. (2020) studied the flexural response of hollow high strength concrete beams considering different size reductions. The test results showed that ductility of hollow beams with size reductions of 16% and 28.4% was higher than that of the reference solid beam, while the ductility of the hollow beam with 44.4% size reduction was quite comparable to that of the solid beam. Naser et al. (2021) applied an experimental investigation to study the effect of using different types of reinforcement on the flexural behavior of ferrocement thin hollow core slabs with embedded PVC pipes. The results showed that the slab reinforced with only macro steel fibers provided the highest flexural strength, while that reinforced with steel bars showed the highest stiffness and lowest deflection among all tested slabs. Prakashan et al. (2016) applied an experimental study on the flexural behavior of hollow core concrete slabs. The results showed that the conventional flexural capacity equation for solid concrete slabs can predict the flexural capacity of hollow core concrete slabs with an accuracy of ± 19%. And the load - deflection behavior and the serviceability performance of hollow core concrete slabs are significantly better than conventional solid concrete slabs.

Shaheen et al. (2016) investigated the behaviour of ferrocement sandwich panels slabs under shear. Their results concluded further that the developed composite ferrocement slabs emphasized better deformation characteristics and higher cracking and ultimate loads. Du et al. (2021) investigated a new mechanical model of polyvinyl alcohol fiber–reinforced ferrocement cementatious composite (PVA-RFCC), which was reinforced with both PVA fiber and steel wire mesh (SWM). A series of experiments were conducted to study their mechanical properties, and a comparative analysis was also performed to evaluate their flexural toughness. In the same vein, Abdul-Fataha (2014) and Shaheen et al. (2014a) employed numerical models and designed an experimental program to investigate the structural behavior ferrocement beams under three point loadings up to failure. The results of the numerical models and experimental tests indicated that the beam with fiberglass meshes gives the lowest first crack load and the maximum load. Shaheen et al. (2014b) estimated the structure performance of ferrocement domes reinforced with composite material. The results of the experimental program indicated that the dome reinforced with fiberglass mesh has the highest service load and ultimate load and the dome reinforced with welded wire meshes achieved highest ductility ratio and energy absorption. Additionally comparing the results of FE simulations with the experimental results showed that the results of FE simulation is closed the experimental results.

Advantages of ferrocement are;

- It can be fabricated into any shape required.
- The material is very dense, but structures made from it are light in weight.
- It is more durable than most woods and more economical than imported steel.
- The basic raw materials for the construction of ferrocement sand, cement, and reinforcing mesh are readily available in most countries.

- Except for highly stressed or critical structures such as deep-water vessels, adequate ferrocement construction does not demand stringent specifications.
- Little new training is required for the laborers, providing a skilled supervisor is on hand.
- Reduction in time and cost.
- Easily repaired.

Disadvantages of ferrocement are;

- Fastening with bolts, screws, nails, and such like, can be difficult on ferrocement.
- The labor-intensive nature of it, which makes it expensive for industrial application in the western world.
- In addition, threats to degradation (rust) of the steel components
- These air voids can turn to pools of water as the cured material absorbs moisture. If the voids occur where there is untreated steel, the steel will rust and expand, causing the system to fail.
- Tying rods and mesh together is time-consuming.

2. Research Signification

The objective of the work presented in this research was to study the influence of several types of metal and non-metal mesh reinforcement materials on the flexural behavior of ferrocement hollow-cored panels as a viable alternative to traditional reinforced concrete panels. Compared with the traditional reinforced concrete part, the weight of the test part is lighter. In order to strengthen these hollow-cored panels, three types of steel mesh, Welded wire mesh, expanded steel wire mesh and tenax mesh with various layers are used. The parameters investigated in this study are:

- Effect of the number of layers of steel reinforcement provided.
- Effect of the type of steel reinforcement used.

An experimental plan was carried out on the test samples. Ten hollow-cored panels with dimensions of 500mm*2000mm*120mm were casted and tested until they failed under flexural load. Record and observe the deformation characteristics and cracking behavior of each sample during the loading process. Experimental results are then compared to analytical models using (ABAQUS/Explicit) programs. According to the results, high ultimate load and serviceability load, crack resistance control, high ductility and strong energy absorption characteristics have been obtained.

This has the chance to be a true construction benefit to developed and poor countries. The test results of the ferrocement hollow-cored panels revealed that using double-layer of expanded steel mesh as the additional reinforcement of the main steel can achieve the best performance of the reinforced concrete hollow-cored panels. The Finite Element (FE) simulations have achieved better results in comparison with the experimental results. Hollow Core Slabs have many applications in residential, social, industrial, commercial and infrastructure construction such as industrial and large commercial roof covering, floors for multistory buildings, used with steel structures and underground car parking.

3. Experimental Program

The experimental program includes the construction and testing of ten hollow-cored panels 2000 mm long 500 mm wide and 120 mm total thickness. The main goal is to investigate the ultimate load, flexural behavior, ductility ratio, energy absorption and mode of failure at collapse of the control panels, which are reinforced with steel bars and, then, to compare their behavior with those ferrocement panels reinforced with welded galvanized steel mesh and expanded metal mesh and tenax mesh. Skeletal steel bars are used with steel and tenax meshes. Five designations series are then developed as shown in Table 1, along with the details of the experimental program of all the test specimens. Fig. 1 also reveals all the details of reinforcement for all specimens.

Table 1. Details of test specimens.

Specimens designation	Code of panels	Reinforcement wire mesh	Reinforcement details		
			Tension steel bars, Ø6 mm	Compression steel bars, Ø6 mm	No. of stirrups, Ø6 mm/m'
A	O1	With fiber	6	6	6
	O2	Without fiber	6	6	6
B	E1	One layer of expanded steel mesh	6	6	------
	E2	Two layers of expanded steel mesh	6	6	------
C	W2	Two layers of welded steel mesh	6	6	------
	W3	Three layers of welded steel mesh	6	6	------
	W4	Four layers of welded steel mesh	4	4	------
D	M1	One layer of expanded steel mesh +one layer of welded steel mesh	6	6	------
E	T1	One layer of tenax LBO SAMP	6	6	------
	T2	Two layers of tenax LBO SAMP	6	6	------

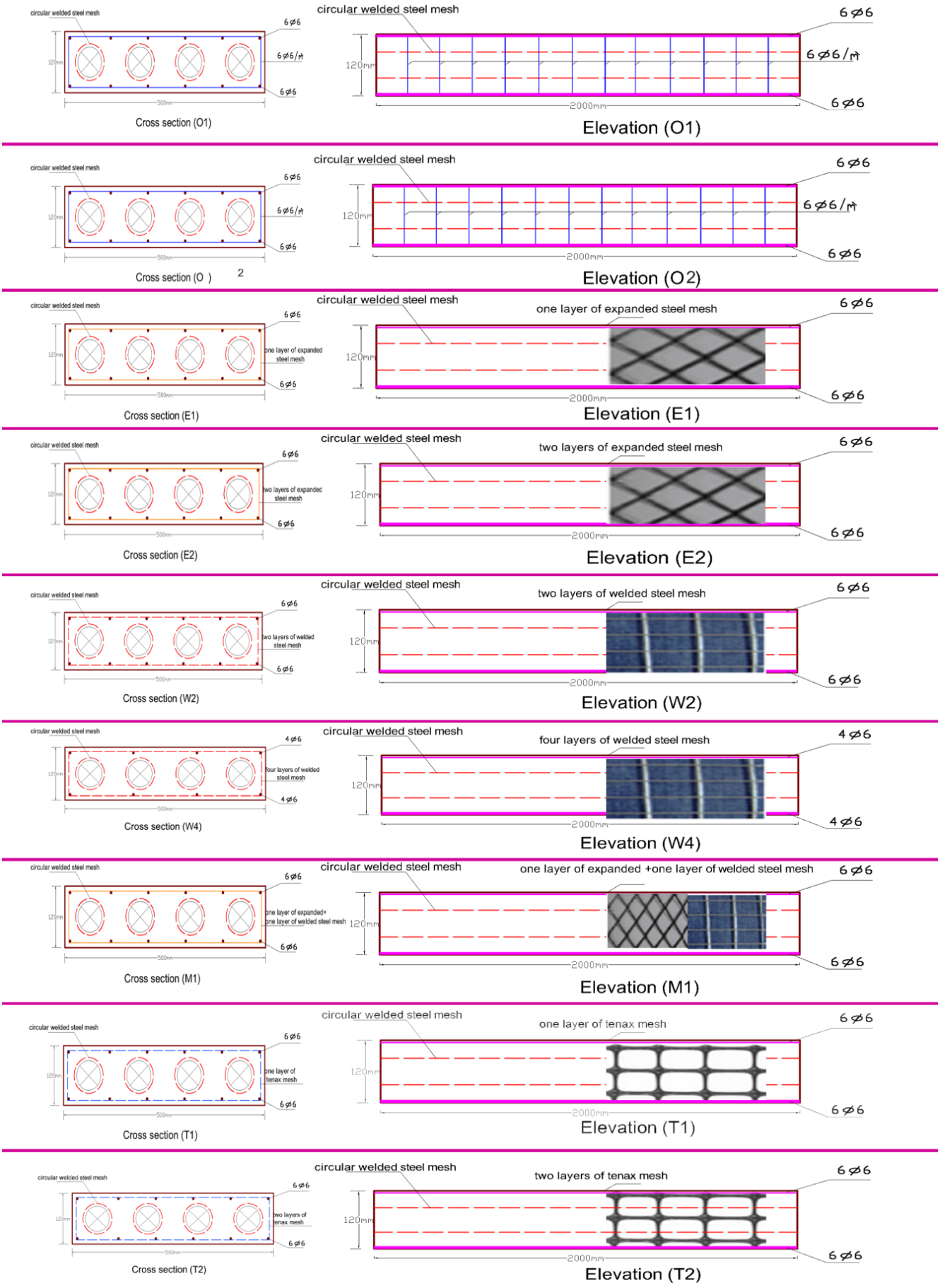

Fig. 1. Reinforcement details of the tested specimens.

3.1. Material properties

• The fine aggregate used in the study is natural siliceous sand. It is clean and nearly free from impurities with a specific gravity of 2.66 and a volume weight of 1.588 t/m^3. Its characteristics satisfy the requirements of the Egyptian Code of Practice (E.C.P. 203/2018) and Egyptian Standard Specifications (E.S.S. 1109/2008).
• The cement used is ordinary Portland cement (CEM I, 42.5 N) (LAFARGE cement). It is physical and chemical properties meeting the requirements of the Egyptian Standard Specifications (E.S.S. 4756-1/2013) as shown.
• Silica fume (S.F) was employed in the present work to increase the strength and permeability of the mortar matrix. It was used as partial replacement by weight of cement in the mortar mixtures. The S.F. had an average particle size of 0.1 micrometer and a silicon dioxide content of 93%.
• Fly ash is a concrete additive of a new generation in fine powder form and spherical particles which reduces the water requirements and creates a lubricating effect that causes concrete to flow and pump better. In addition the concrete is more cohesive and is less prone to segregation. Fly ash had a relatively low specific gravity of 2.20.
• Polypropylene fibres mesh e-300: Using only 100% virgin homopolymer polypropylene graded fibrillated fibers containing no reprocessed olefin components that meets ASTM C-1116, A minimum of 900 grammes (0.9kg/m^3) of application per cubic metre is required. Fibers are commonly utilised to prevent cracking caused by drying shrinkage and thermal expansion/contraction. It was also utilised to reduce permeability in concrete, improve impact capacity, shatter resistance, and abrasion resistance, as well as add fibrillated toughness and residual strength. The technical specifications and mechanical properties of Polypropylene fibres e-300 as provided by producing company are given in Table 2, shown in Fig. 2.
• The water used was clean drinkable water, free from impurities was used for mixing and curing processes. The properties of the used water achieve the Egyptian Code of Practice (E.C.P. 203/2018) requirements.
• Super plasticizer used was a high rang water reducer HRWR. It was used to improve the workability of the mix. The admixture used was produced by CMB GROUP under the commercial name of Addicrete BVF. It meets the requirements of ASTM C494 (type A and F) (Singh et al., 1986). The admixture is a brown liquid having a density of 1.18 kg/liter at room temperature. The amount of HRWR was 1.0% of the cement weight.
• Reinforcing steel: Normal mild steel bars were used, produced from the Ezz Al Dekhila Steel - Alexandria Its chemical and physical characteristics satisfy the Egyptian Standard Specification E.S.S. 262/2011. Mild steel bars of 6 mm diameter were used with yield strength of 240 MPa.
• Reinforcing meshes
- Expanded steel mesh is used as reinforcement for ferrocement girders. The technical specifications and mechanical properties of expanded metal mesh as provided by producing company are given in Table 3 and shown in Fig. 2.
-Welded metal mesh used was obtained from China, and it was used as reinforcement for ferrocement panels. The technical specifications and mechanical properties of welded steel mesh as provided by producing company are given in Table 3. It is complying with of ACI 549.1R-97 (2009) shown in Fig. 2.
-Tenax LBO SAMP (330) is polypropylene Geogrid especially for reinforcement applications. The geogrid is manufactured from a unique process of extrusion and biaxial orientation to enhance their tensile properties. It features consistently high tensile strength and modulus, excellent resistance to construction damages and environmental exposure. Properties of this mesh can be shown in Table 3 and Fig. 2.

Table 2. Chemical and physical properties of fiber mesh e-300.

Fiber Length	Type / Shape	Absorption	Specific Gravity	Electrical Conductivity	Acid & Salt Resistance	Melt Point	Ignition Point	Thermal Conductivity	Alkali Resistance
Various	Graded / Fibrillated	Nil	0.91	Low	High	162°C (324°F)	593°C (1100°F)	Low	Alkali Proof

Table 3. Technical specifications and mechanical properties of expanded metal, welded metal and tenax meshes.

Expanded Metal Mesh		Welded Metal Mesh		Tenax LBO 330	
Style	1532	Dimensions	12.5mm × 12.5mm	Structure	Biaxial geogrid
Sheet Size	1m × 10m	Weight	430 g/m^2	Mesh type	Rectangular apertures
Weight	1.3 kg/m^2	Proof Stress	400 N/mm^2	Standard colour	Black
Diamond size	16mm × 31mm	Ultimate Strain	$58.8 \cdot 10^{-3}$	Polymer type	Polypropylene
Dimensions of strand	1.25 × 1.5mm	Proof Strain	$1.17 \cdot 10^{-3}$	Carbon black content	2%
Proof Stress	199 N/mm^2	Ultimate Strength	600 N/mm^2	Dimensional characteristics	(LBO 330) Samp
Proof Strain	$9.7 \cdot 10^{-3}$			Aperture size MD	40 mm
Ultimate Strength	320 N/mm^2			Aperture size TD	27 mm
Ultimate Strain	$59.2 \cdot 10^{-3}$			Mass per unit area	420 g/m^2

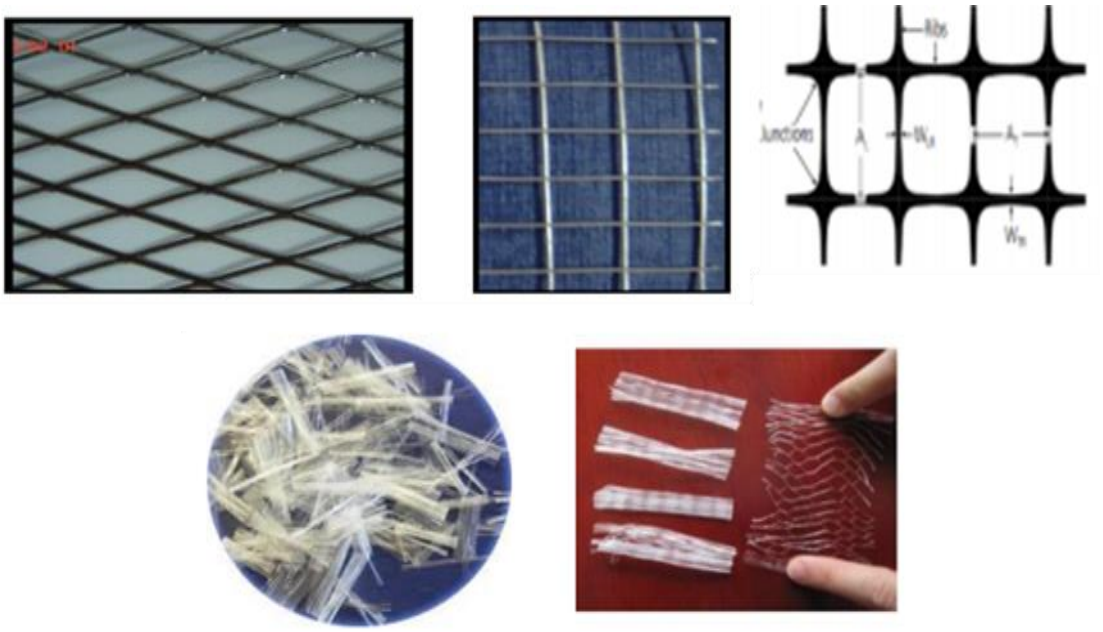

Fig. 2. Types of meshes and fiber e-300.

3.2. Mortar matrix

The sand-cement mortar of ferrocement consisted of sand, ordinary Portland cement, silica fume and fly ash. The main purpose of mix design was to determine how the high amount of cement could be partially replaced by silica fume and fly ash to increase strength of mortar matrix with no detrimental effects on the quality and properties of the mix in both the fresh and hardened states. The requirement of good workability was essential, to allow the mortar matrix to penetrate through the layers of steel mesh reinforcement. A super plasticizing agent was used to increase flow characteristics and accelerate the early strength development. Mortar mixtures for the ferrocement were made using a water / cement ratio of 0.35, super-plasticizer of 2% by weight of cement, while sand/cement ratio of 2.0, 10% by weight of cement was replaced by S.F and 20% by weight of cement was replaced by fly ash and the percentage of addition of fiber e-300 was chosen as 0.9 kg/m^3. The average compressive strength of the ferrocement mortar after 28 days, (fcu), was found to be 35 MPa. For all mixes, mechanical mixer in the laboratory used mechanical mixing with capacity of 0.05 m^3, where the volume of the mixed materials was found to be within this range. The constituent materials were first dry mixed; the mix water was added and the whole patch was re-mixed again in the mixer. The mechanical compaction was applied for all specimens.

3.3. Preparation of test specimens

The mold from rectangular forms from contras wood with entire size of 500x120x2000 mm was prepared and used for casting panels. The pipes from plastic with diameter 50 mm and 2200 mm length were prepared and used to keep the required voids. The ferrocement forms were left for 24 hours in the mold before disassembling the mold. Lastly, the forms were covered with wet burlap for 28 days. All of previous steps are shown in Fig. 3.

3.4. Test setup

At the time of testing, the specimen was painted with white paint to facilitate the visual crack detection during testing process. A set of four "demec" points was placed on one side of the specimen to allow measuring the strain versus load during the test. Demec points were placed as shown in Fig. 4. The specimens were tested on a testing loading frame with a four loading points. The span length was 1800 mm while the distance between the two loading points was 600 mm. dial gauges were used to measure deflection at mid span and under points of loading while strain gauges attached to the top and bottom of the surface of concrete at the critical sections to evaluate its behavior. All the values of deflection at the variable positions and top and bottom strain values were recorded. Cracks were traced throughout bottom of the specimen and then marked with black markers. The first crack-load of each specimen was recorded. The load was increased until complete failure of the specimen was reached. Test setup of specimen can be shown in Fig. 5.

4. Experimental Results and Discussions

The obtained results for the first cracking load, ultimate load, Serviceability Load, ductility ratio and energy absorption as shown in Table 4, Ultimate load and deflection at ultimate load were measured and obtained during the test, while ductility ratio, serviceability load and energy absorption were determined from the load–deflection diagram for each tested panel. Fig. 6 represents the values for the first cracking load and ultimate load for all the tested panels. Maximum ultimate load reached 50 kN for E2 and minimum ultimate load achieved 32 kN.

Fig. 3. Steps of specimen preparation.

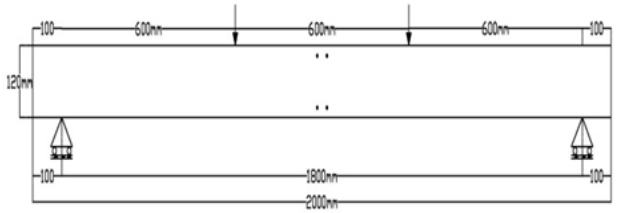

Fig. 4. Locations of demec points.

Fig. 5. Test setup.

4.1. Flexural serviceability load

The flexural serviceability load was calculated from the load-deflection curves. It is defined as the load corresponding to deflection equal to the span of the panel divided by (constant=250) according to The Egyptian Code. Fig. 6 represents the values for the serviceability load for all the tested panels. The main aim of calculating serviceability load is to evaluate the effect of using different meshes.

4.2. Ductility ratio

Ductility ratio is defined here as the ratio between the mid span deflection at ultimate load to that at the first crack load ($\Delta u/\Delta y$), panels reinforced with expanded metal mesh and welded steel meshes were given higher ductility ratio than control beam. Fig. 7 shows ductility ratios for all tested panels.

4.3. Energy absorption

Energy absorption is defined as the area under the load–deflection curve. Microsoft Office (excel sheet) was used to calculate the area under curve by integrated the equation of the load–deflection curve for each beam specimens as follow: ultimate load Energy absorbed = $\int_0^{\Delta u} f(\Delta)d\Delta$; where $f(\Delta)$ is the equation of load–deflection curve, and Δu is the mid-span deflection at failure load. Panels reinforced with expanded steel mesh were achieved higher energy absorption than control panels. Fig. 8 emphasizes energy absorption for all tested panels.

Table 4. Test results for all experimental test specimens.

Specimens designation	Code of panels	First crack load (kN)	Serviceability load (kN)	Ultimate load (kN)	First crack deflection (mm)	Maximum deflection (mm)	Ductility ratio	Energy absorption (kN.mm)
A	O1	12	29.00	36	2.55	16.08	6.30	433.70
	O2	12	28.10	34	2.11	14.71	6.97	375.79
B	E1	8	20.00	38	1.56	21.10	13.52	507.46
	E2	16	29.80	50	2.79	35.27	12.64	1317.19
C	W2	8	32.12	38	1.22	16.50	13.52	454.08
	W3	10	30.69	42	1.42	19.64	13.83	599.20
	W4	12	30.90	44	1	18.97	18.97	602.10
D	M1	8	24.30	40	1.28	23.64	18.46	667.88
E	T1	8	22.50	32	1	18.20	18.20	408.02
	T2	10	22.20	34	2.42	35.60	14.71	937.20

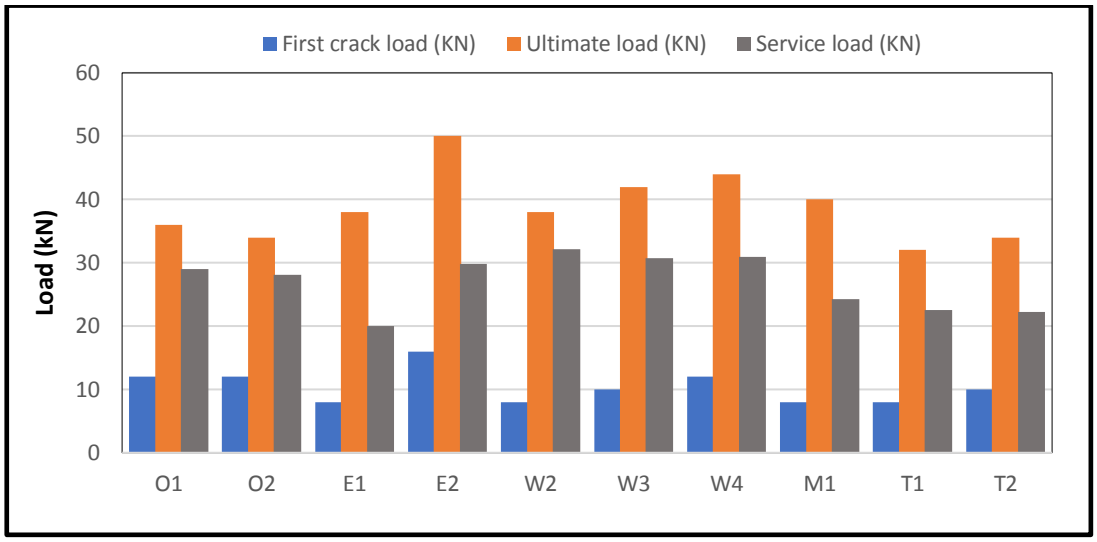

Fig. 6. First crack load, ultimate load and service load of all tested slabs.

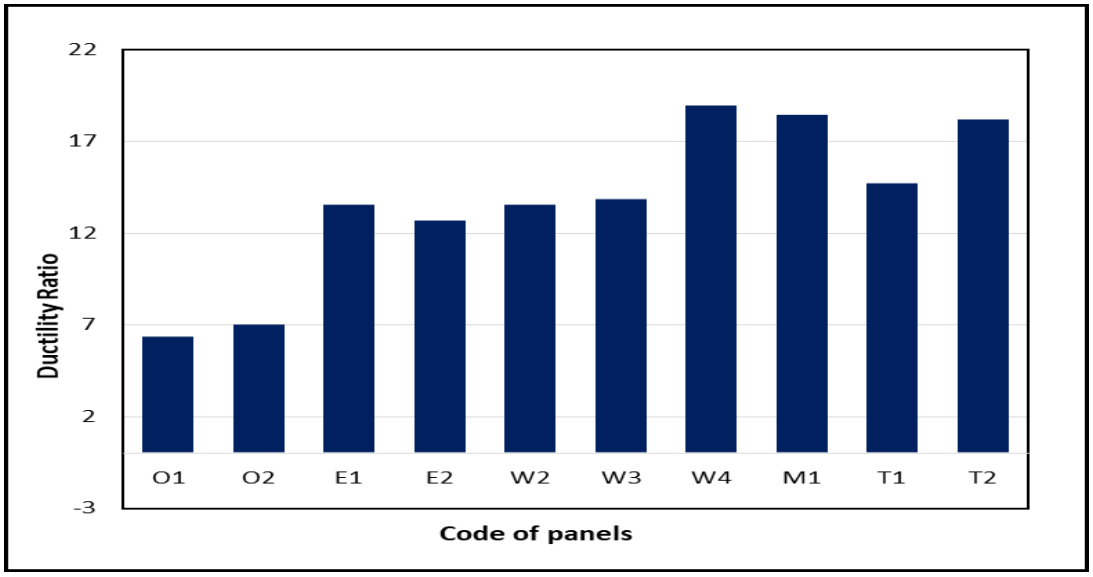

Fig. 7. Ductility ratio of all tested panels.

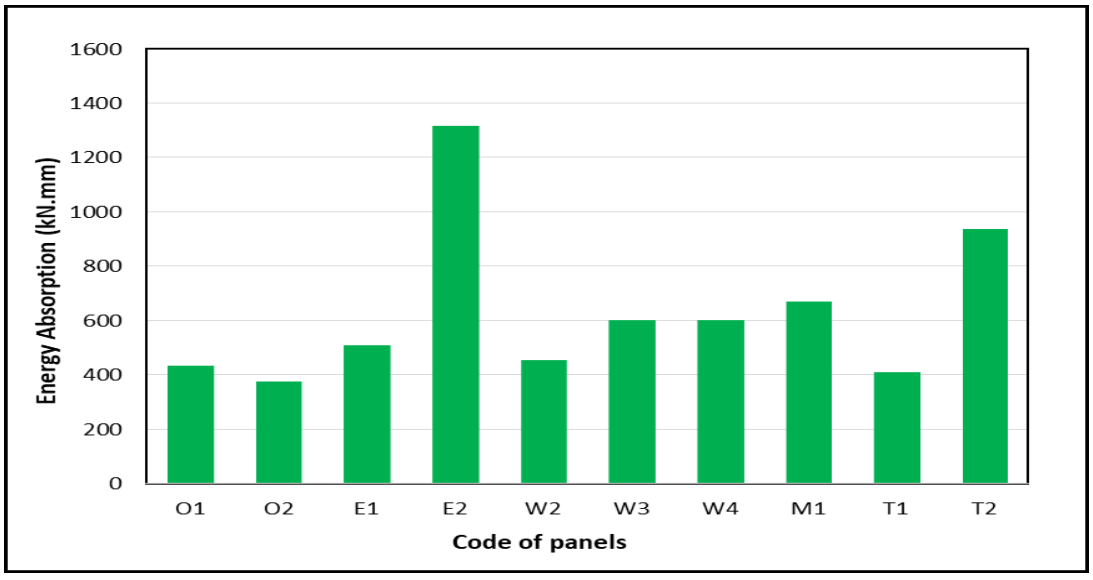

Fig. 8. Energy absorption for all tested panels.

4.4. Load-deflection relationship

Fig. 9 shows the load-deflection curves of the control specimen with fiber (O1) and control specimen without fiber (O2). From figure, group A, the ultimate load for specimen (O1) is more than that of the specimen (O2). This is due to the fiber used in the mix. The percentage of increasing in the ultimate load is 5.5%. Also the deflection of specimen (O2) is decrease by 8.51% compared to specimen (O1). From Fig. 10, group B, the specimens reinforced with expanded steel mesh in addition to steel bars (E1) and (E2). The ultimate load for specimen (E2) is more than that of specimen (E1). This is due to increasing the number of layers. The percentage of increasing in the ultimate load is 31.5%. Also the deflection of specimen (E1) is decrease by 40.1% compared to specimen (E2). Fig. 11 illustrates that, group C, the specimens reinforced with welded wire mesh in addition to steel bars (W2), (W3) and (W4). The ultimate load for specimen (W4, W3) is more than that of specimen (W2). This is due to increasing the number of layers. The percentage of increasing in the ultimate load is 15.7%, 10.5% respectively. Also the deflection of specimen (W4, W3) is increase by 14.9%, 19.09% respectively compared to specimen (W2). Fig. 12 illustrates that, group E, the specimens reinforced with Tenax mesh in addition to steel bars (T1) and (T2). The ultimate load for specimen (T2) is more than that of specimen (T1). This is due to increasing the number of layers. The percentage of increasing in the ultimate load is 6.25 %. Also the deflection of specimen (T2) is increase by 95.6% compared to specimen (T1). Fig. 13 emphasizes comparison of load deflection curves for all the tested panels.

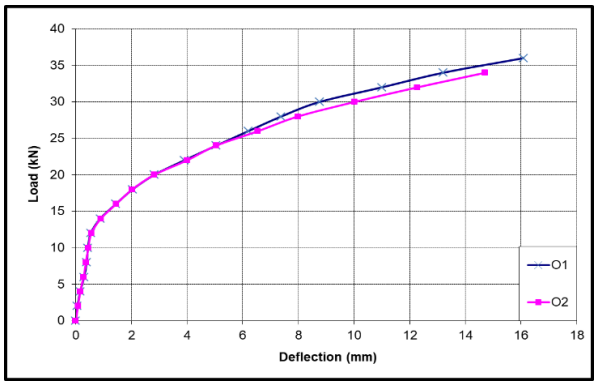

Fig. 9. Load-deflection curves for group (A).

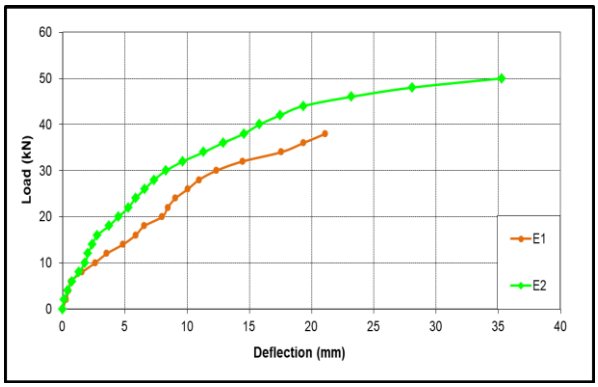

Fig. 10. Load-deflection curves for group (B).

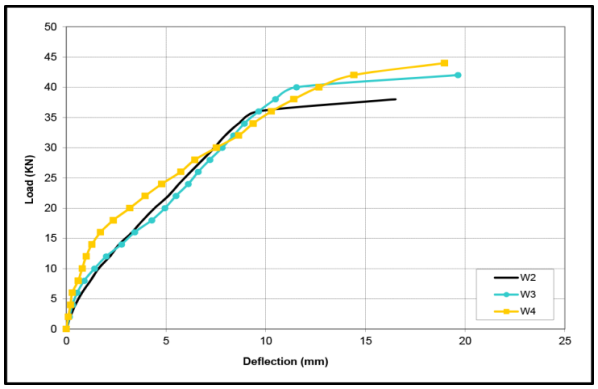

Fig. 11. Load-deflection curves for group (C).

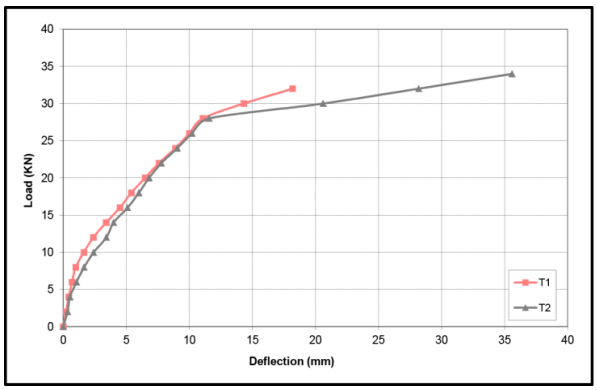

Fig. 12. Load-deflection curves for group (E).

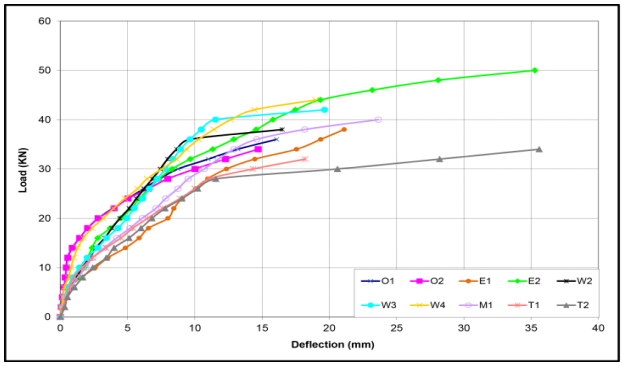

Fig. 13. Load-deflection curves for all tested panels.

4.5. Effect of using various types of meshes

In order to evaluate the effect of the reinforcing steel mesh type, specimens reinforced with expanded steel mesh, welded wire mesh and tenax mesh were compared to control specimen at the same number of layers. Fig. 14 illustrates the load-deflection curves of the control specimen with fiber (O1) is compared to the specimen reinforced with one layer of expanded steel mesh (E1) and the specimen reinforced with one layer of tenax mesh (T1). From figure, the ultimate load for specimen (E1) is more than that of (O1 and T1). This is due to the strength of expanded steel mesh. The percentage of increasing in the ultimate load is 5.5% and 18.7% respectively. Fig. 15 illustrates the load-deflection curves of the control specimen with fiber (O1) is compared to the specimen reinforced with two layers of expanded steel mesh (E2), two layers of welded wire mesh (W2), one layer of welded wire mesh plus one layer of expanded steel mesh (M1) and the specimen reinforced with two layers of tenax mesh (T2). From figure, the ultimate load for specimen (E2) is more than that of (O1, W2, M1 and T2). This is due to the strength of expanded steel mesh. The percentage of increasing in the ultimate load is 38.8%, 31.5% 25% and 47.05%, respectively.

In order to evaluate the effect numbers of steel wire mesh layers, specimens reinforced with expanded steel mesh, welded wire mesh and tenax mesh were compared to control specimen. Fig. 16 illustrates the load-deflection curves of the control specimen with fiber (O1) is compared to the specimen reinforced with one layer of expanded steel mesh (E1) and the specimen reinforced with two layers of expanded steel mesh (E2). From figure, the ultimate load for specimen (E2) is more than that of (O1 and E1). This is due to the number of layers. The percentage of increasing in the ultimate load is 38.8% and 31.5% respectively. Fig. 17 illustrates the load-deflection curves of the control specimen with fiber (O1) is compared to the specimen reinforced with two layers of welded wire mesh (W2), the specimen reinforced with three layers of welded wire mesh (W3) and the specimen reinforced with four layers of welded wire mesh (W4). From figure, the ultimate load for specimen (W4) is more than that of (O1, W2 and W3). This is due to the number of layers. The percentage of increasing in the ultimate load is 22.2%, 15.78% and 4.76%, respectively.

Fig. 18 illustrates the load-deflection curves of the control specimen with fiber (O1) is compared to the specimen reinforced with two layers of tenax mesh (T2), the specimen reinforced with one layer of tenax mesh (T1). From figure, the ultimate load for specimen (O1) is more than that of (T1, T2). The percentage of increasing in the ultimate load is 12.5% and 5.8% respectively.

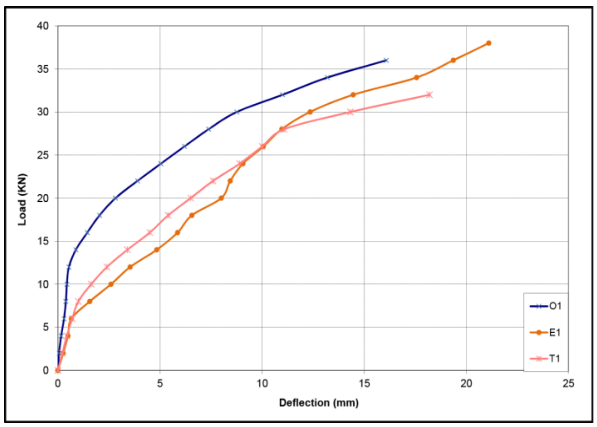

Fig. 14. Effect of type of reinforcement on the load–deflection for the panels.

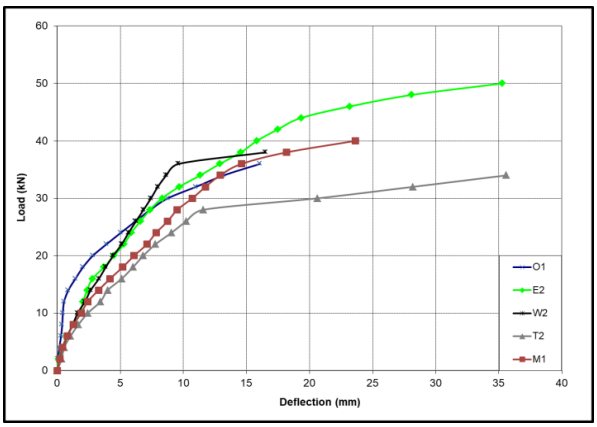

Fig. 15. Effect of type of reinforcement on the load-deflection for the panels.

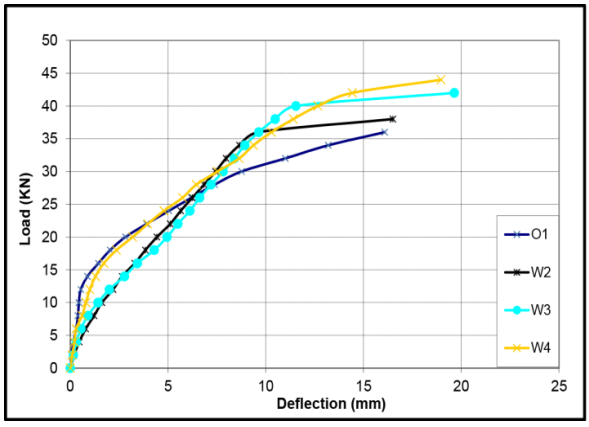

Fig. 16. Effect of number of layers of welded mesh for the panels.

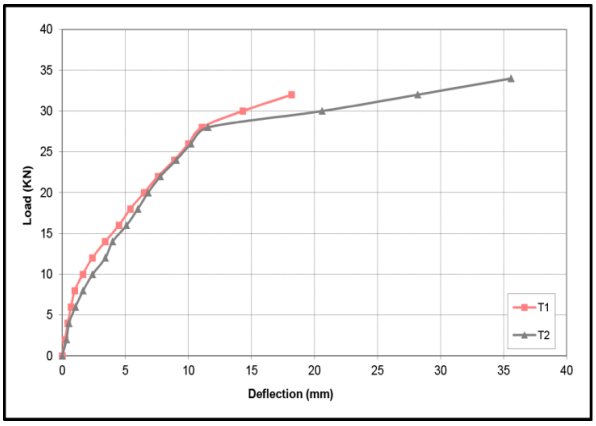

Fig. 17. Effect of number of layers of welded mesh for the panels.

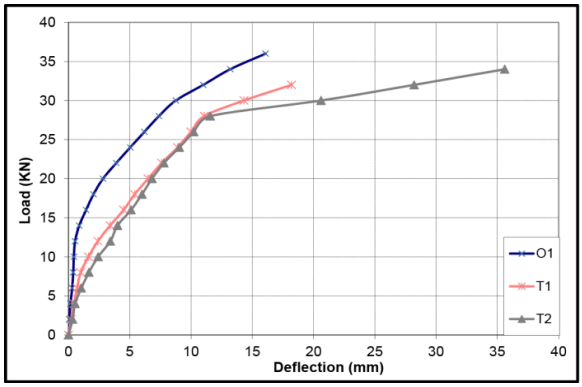

Fig. 18. Effect of number of layers of welded wire mesh for the panels.

4.6. Compressive and tensile strain

Fig. 19 shows load-strain curves for control group (A) specimens (O1 and O2). For panel O1, the compressive strain increased with the increase of the applied load. The maximum compressive strain reached about -0.00142 at maximum load 36 kN. However, the max tensile strain was 0.0015 at the same load. The maximum compressive strain at panel O2 reached about -0.0014at maximum load 34 kN. However, the max tensile strain was 0.00136 at the same load.

The load-compressive and tensile strain curves for group B (panels E1, E2) are plotted in Fig. 20. The curves show that the compressive strain increased with the increase of the applied load. At panel E1 the maximum compressive strain reached about -0.0025 at maximum load 38 kN. However, the max tensile strain was 0.0023 at the same load. For panel (E2), the maximum compressive strain reached about -0.0031 at maximum load 50 kN. However, the max tensile strain was 0.003 at the same load.

For group C (panels W2, W3 and W4), the compressive strain increased with the increase of the applied load. For panel (W2), the maximum compressive strain reached about -0.0015 at maximum load 38 kN. However, the max tensile strain was 0.002 at the same load. The maximum compressive strain at panel W3 reached about -0.00142 at maximum load 42 kN. However, the max tensile strain was 0.00135 at the same load. The maximum compressive strain at panel W4 reached about -0.00255 at maximum load 44 kN. However, the max tensile strain was 0.0025 at the same load as shown in Fig. 21.

For the last group specimens E (specimens T1 and T2), Fig. 22 shows that the compressive strain increased with the increase of the applied load. For panel (T1) the maximum compressive strain reached about -0.0017 at maximum load 32 kN. However, the max tensile strain was 0.00168 at the same load. The maximum compressive strain at panel (T2) reached about -0.0022 at maximum load 34 kN. However, the maximum tensile strain was 0.00217 at the same load.

4.7. Cracking patterns and mode of failure

Cracks were traced and marked throughout the side of the specimen. The first crack-load of each specimen, crack propagation, and failure mode were recorded. Flexural cracks developed near the mid-span of the specimen. With the increase of the load, the cracks propagated vertically and new flexural cracks were developed rapidly. The cracks started to propagate wider when the specimens approached their failure load. As the load increased, more cracks started to develop and the crack at midspan started to propagate vertically towards the top surface of the specimen, while most of the developed cracks did not continue propagating. This could be attributed to the effect of steel mesh in controlling the crack width. The cracks for all tested panels can be shown in Fig. 23.

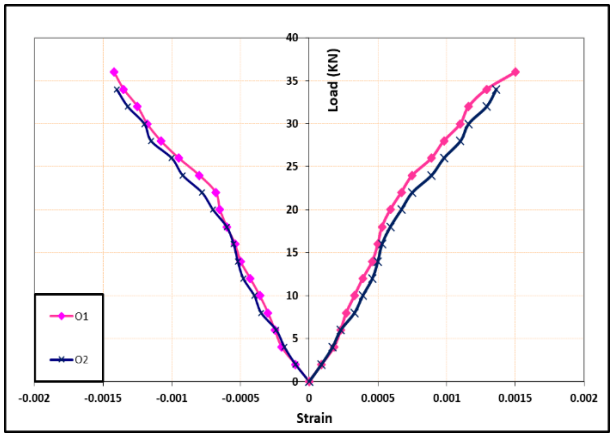

Fig. 19. Load-compressive and tensile strain curves for group (A).

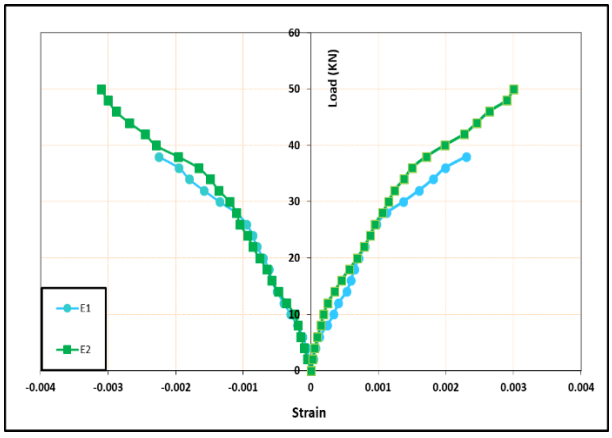

Fig. 20. Load-compressive and tensile strain curves for group (B).

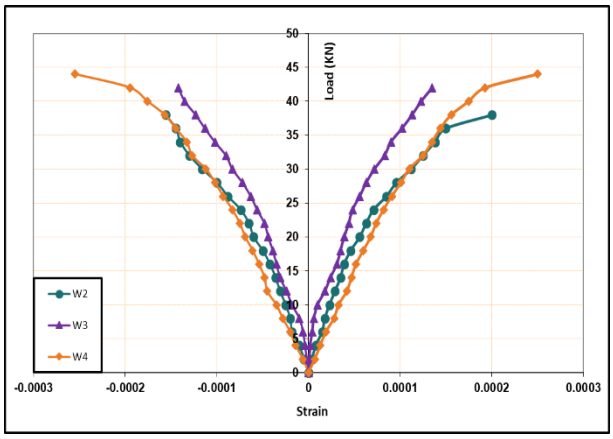

Fig. 21. Load-compressive and tensile strain curves for group (C).

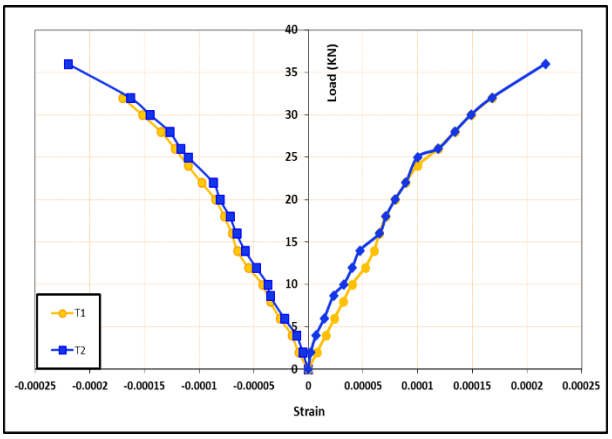

Fig. 22. Load-compressive and tensile strain curves for group (E).

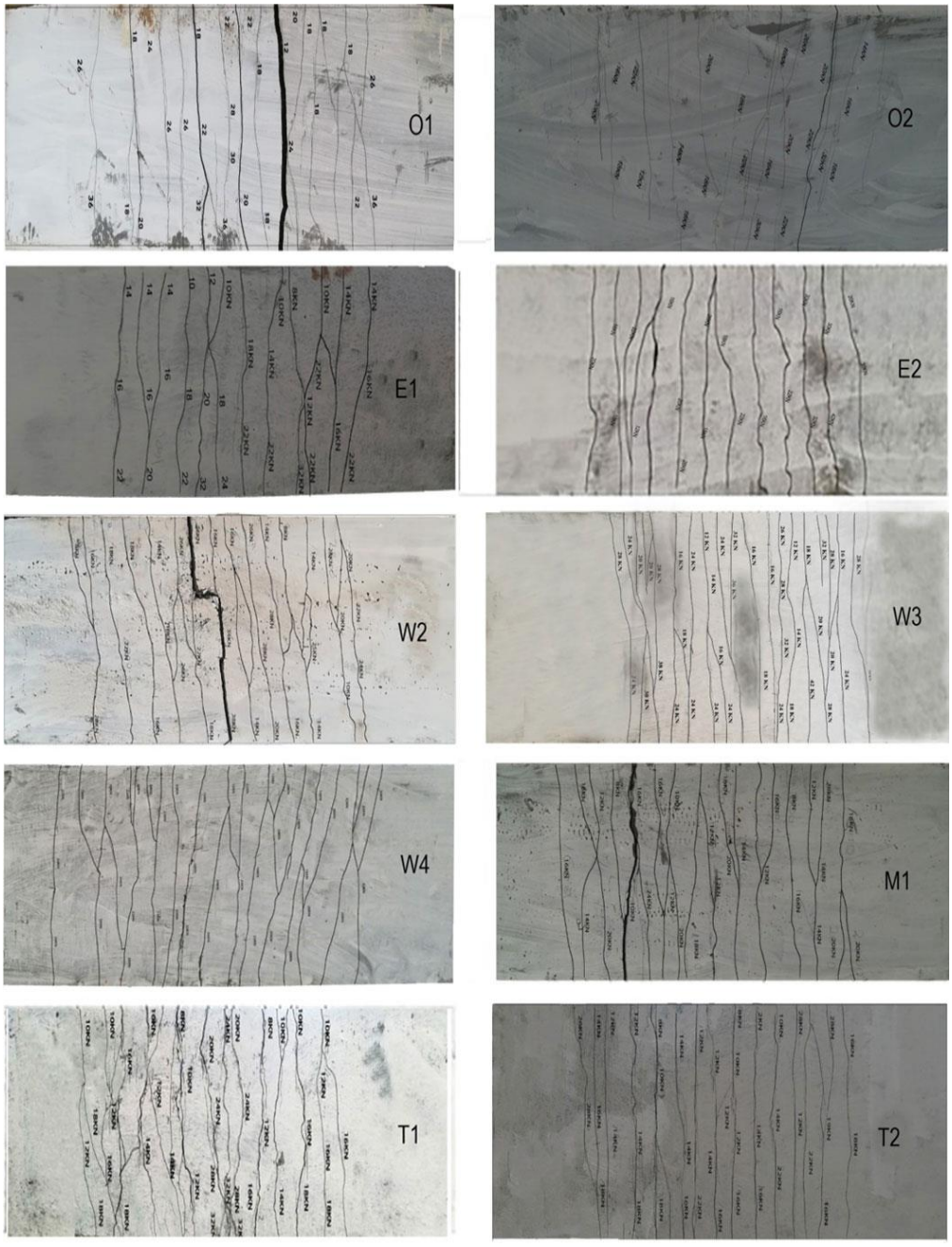

Fig. 23. Cracking patterns for all tested panels.

5. Finite Element Simulation

The specimens of study were modeled as 3D structures in Abaqus. Concrete parts were modeled using C3D8R. Steel bars, welded, expanded steel mesh and tenax mesh were modeled using T3D2 elements. (Fig. 24) shows modeling of all parts (reinforced concrete hollow-core panels, Steel bars, welded, expanded metal mesh, tenax mesh) in Abaqus.

The supports of the concrete panels were prevented from transferring to YZ directions and from rotation about XZ direction at the two lines of contact with underneath roller supports. Concrete panel is exposed to two concentrated loads at equivalent distance from the support line.

Concerning the interaction between the loads, reinforced mesh and concrete target general, contact surfaces of the concrete target can be defined using the Interaction, Create Interaction Property and Create Interaction option. We specify all regions of the model that can potentially come into contact with each other by defining contact surfaces.

6. FE Model Verification

Fig. 25 represents a comparison between failure modes and cracks pattern of the tested beam as published and the corresponding FE models.

The load-deflection curve of experimental work and its associated FE model are shown in Fig. 26.

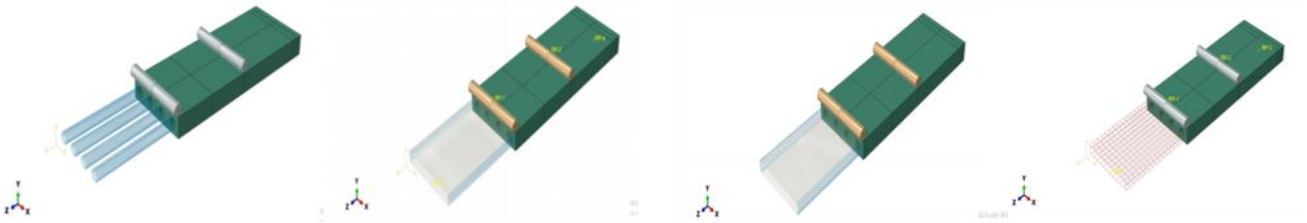

circular mesh welded metal mesh expanded metal mesh tenax mesh

Fig. 24. Modeling of reinforcing metal mesh.

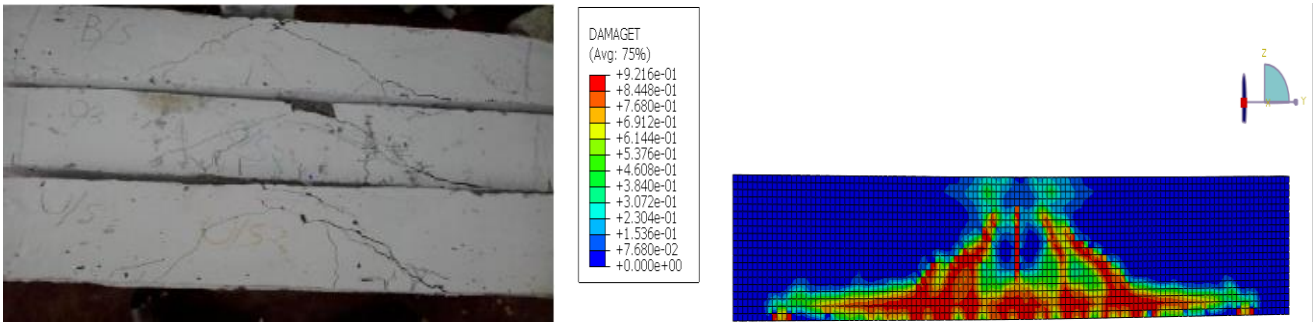

a) Failure shape of experimental model b) Failure shape of FE model

Fig. 25. Failure pattern of model.

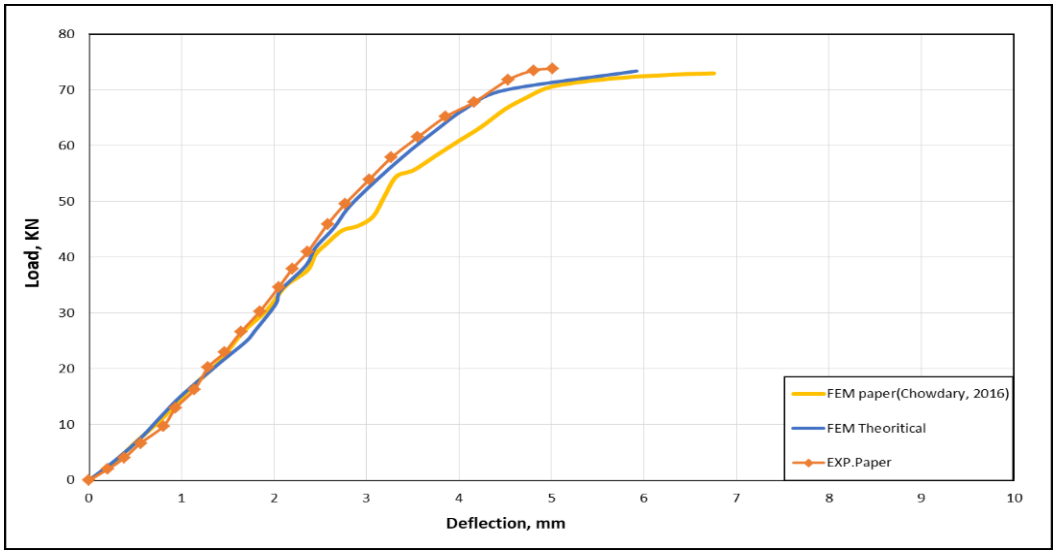

Fig. 26. Load-deflection curve of experimental work and their corresponding FE model.

7. Comparison between Experimental and FE Simulation Results

The comparison between experimental and FE simulation results, ultimate load, 1st crack load, mid span deflection at the ultimate load are illustrated in Table 5. Fig. 27 and Fig. 28 presents the applied load-mid span deflection, and the applied load-strain curves; respectively as obtained from the experimental and theoretical results for the all tested panels. The first crack load was determined as the first deviation from linearity of load deflection curve. The comparison between the experimental and theoretical cracking patterns for all tested specimens are presented in Fig. 29. Stress distribution for all tested panels can be obtained at Fig. 30.

Consequently, it can be concluded that the FE simulations give accurate results in comparing with the experimental results. In addition, these comparisons indicate a good agreement in slope of curves in the linear stage. For nonlinear stage, and due to the possibility of the inaccuracy in modelling the post yield behaviour of steel rebar material, there is somewhat none agreement between the finite element results and those of experimental results.

Table 5. Comparison between experimental and theoretical results.

Specimens designation	Code of panels	First crack load (kN)			Ultimate load (kN)			Maximum deflection (mm)		
		Finite Element Method Results	Experimental Study Results	Percentage of difference	Finite Element Method Results	Experimental Study Results	Percentage of difference	Finite Element Method Results	Experimental Study Results	Percentage of difference
A	O1	12.75	12	1.062	35.85	36	0.995	15.44	16.08	0.960
	O2	12.29	12	1.024	34.85	34	1.025	14.26	14.71	0.969
B	E1	8.78	8	1.097	39.99	38	1.052	23.12	21.10	1.095
	E2	16.68	16	1.042	50.26	50	1.005	33.08	35.27	0.93
C	W2	8.72	8	1.09	39.29	38	1.033	16.52	16.50	1.001
	W3	10.85	10	1.085	43.35	42	1.032	18.76	19.64	0.955
	W4	12.94	12	1.078	44.5	44	1.011	17.91	18.97	0.944
D	M1	8.46	8	1.057	40.98	40	1.024	23.14	23.64	0.978
E	T1	8.83	8	1.103	32.92	32	1.028	17.30	18.20	0.950
	T2	10.8	10	1.080	34.15	34	1.004	34.10	35.60	0.957

8. Conclusions

Based on the results and observations of the theoretical and experimetal study presented in chapter the following conclusions could be drawn as follows:

- The best behavior of ferrocement hollow-cored panels was that of reinforced with two layers of expanded metal mesh in terms of ultimate load and Energy absorption.
- The specimen reinforced with two layers of expanded steel mesh increase the ultimate load by (31.5%) compared to that reinforced with one layer of expanded steel mesh. In addition, the specimen reinforced with four layers of welded wire mesh increase the ultimate load by (15.7% and 4.7%) compared to that reinforced with two layers of welded wire mesh and three layers of welded wire mesh, respectively.
- Using two layers of expanded steel mesh increased the ultimate load by percentage (38.8%) compared to control panel, while using two, three and four layers of welded wire mesh increased the ultimate load by percentage (5.5%, 16.6% and 22.2%) compared to control panel.
- The highest energy absorption property was shared between specimens made of two layers of expanded steel mesh and two layers of tenax mesh by percentage (67.07%, 53.7%) compared to control panel, respectively. and the lowest was found mostly with hollow-cored panels made of one layer of tenax by percentage (6.29%) compared to control panel.
- The highest Ductility ratio was shared between specimens made of four layers of welded wire mesh and specimen reinforced with one layer of expanded steel mesh + one layer of welded wire mesh by percentage (66.7%, 65.8%) compared to control panel, respectively.
- There is a great saving of weight by making voids area in the cross section leading to easy construction especially for weak soil foundations.
- Good agreement was founded between the theoretical and experimental results.
- Out of the point of this research, using ferrocement hollow-cored panels with different types and reinforced with several layers of mesh reinforcement may be have true construction merits for using in a variety of applications.

Further research needs to be conducted to reach sound recommendations for practical use especially for the beams with light polystyrene foam of high densities.

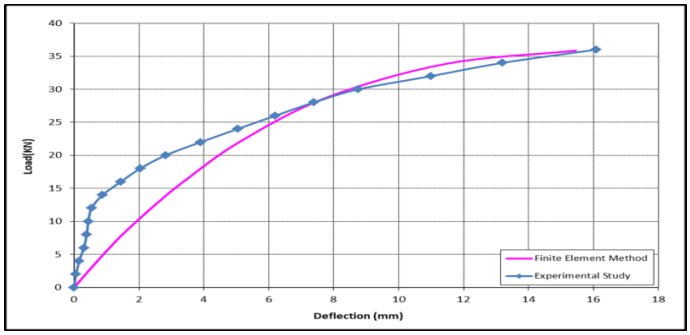

a) Load-deflection curves for panel O1

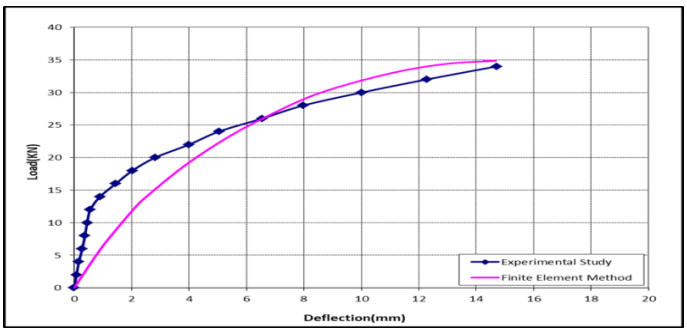

b) Load-deflection curves for panel O2

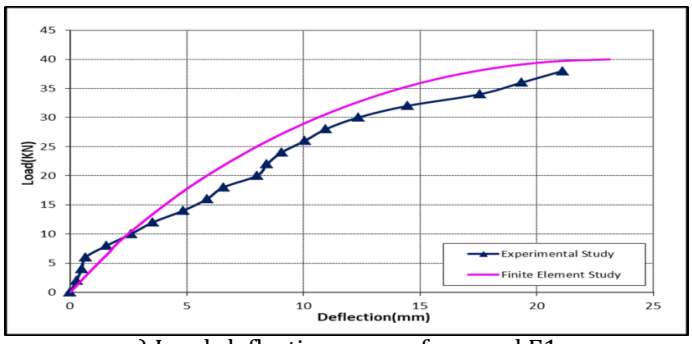

c) Load-deflection curves for panel E1

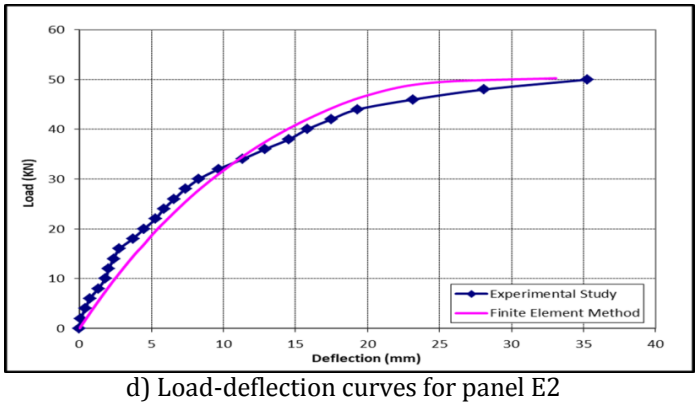

d) Load-deflection curves for panel E2

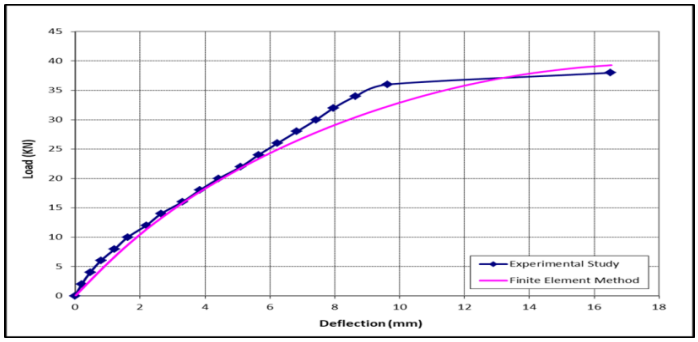

e) Load-deflection curves for panel W2

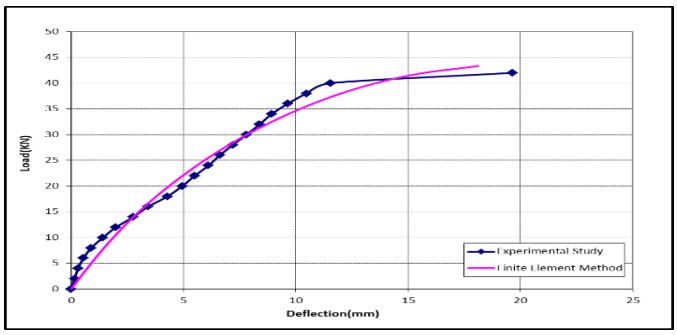

f) Load-deflection curves for panel W3

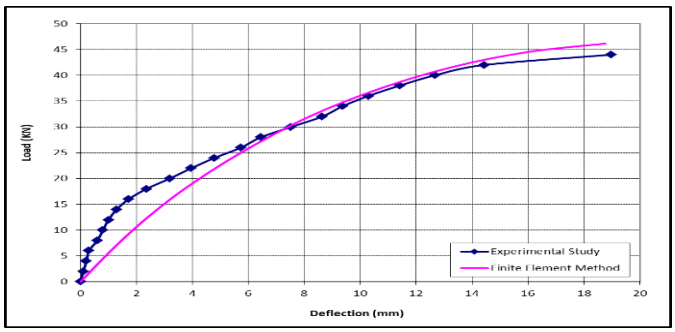

g) Load-deflection curves for panel W4

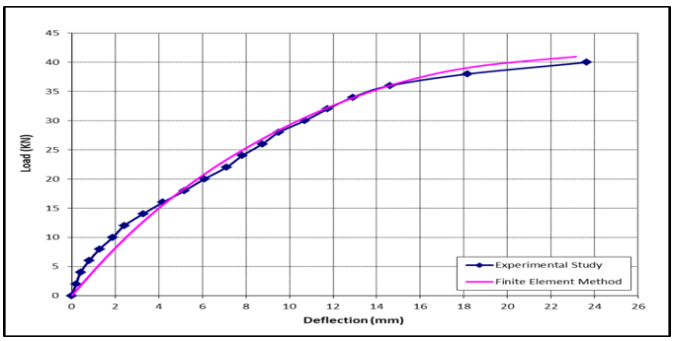

h) Load-deflection curves for panel M1

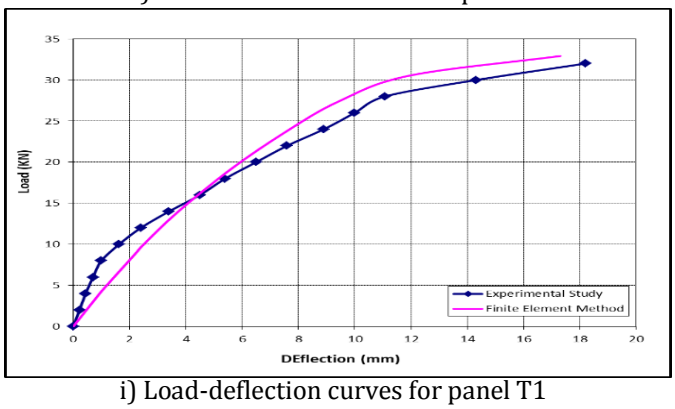

i) Load-deflection curves for panel T1

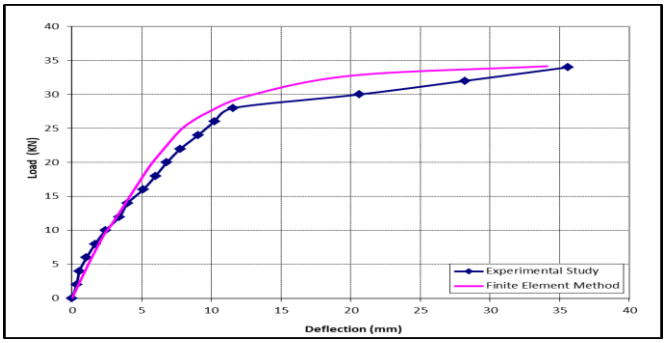

j) Load-deflection curves for panel T2

Fig. 27. Load-deflection curve for test specimens for experimental and theoretical results.

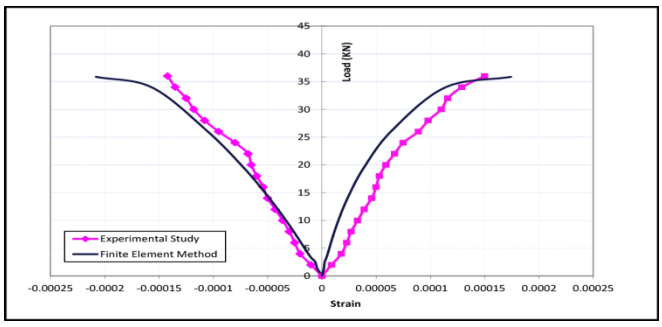

a) Load-strain curves of panel O1

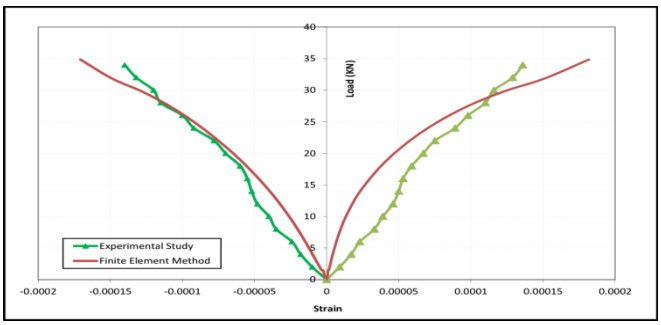

b) Load-strain curves of panel O2

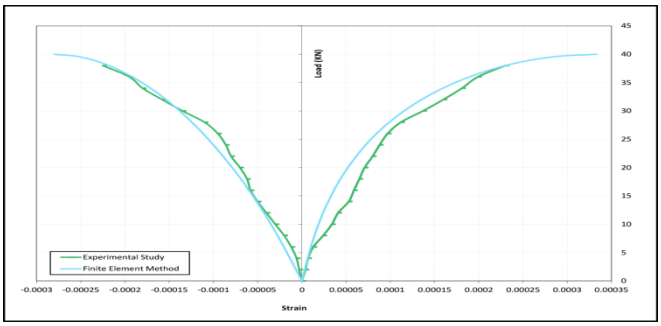

c) Load-strain curves of panel E1

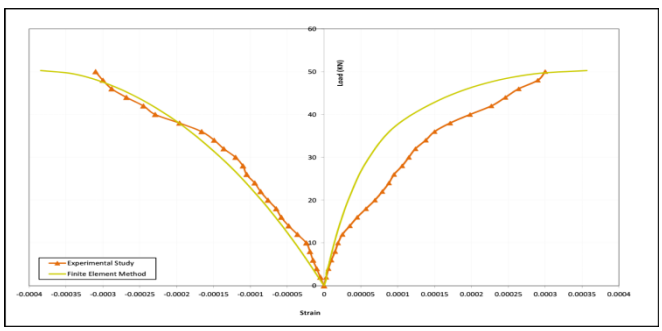

d) Load-strain curves of panel E2

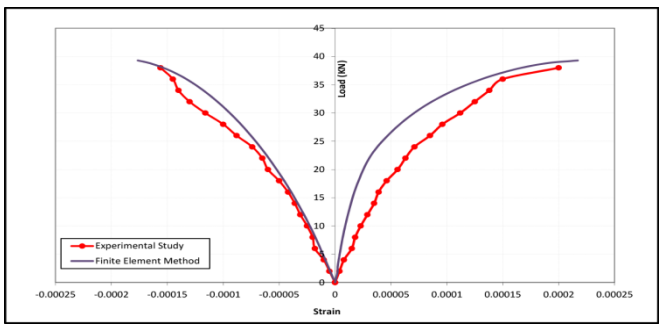

e) Load-strain curves of panel W2

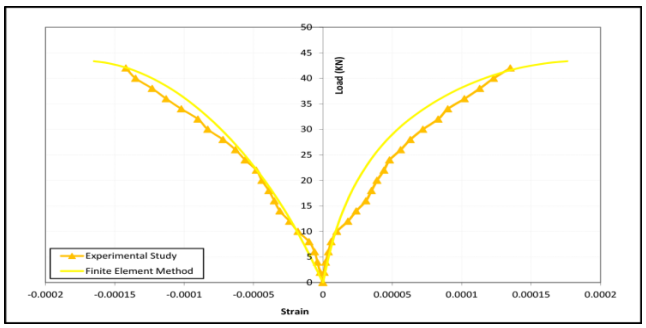

f) Load-strain curves of panel W3

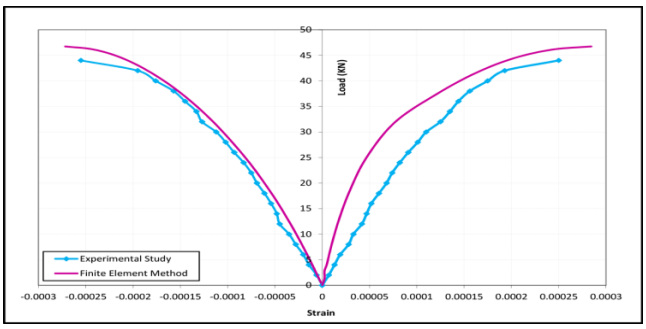

g) Load-strain curves of panel W4

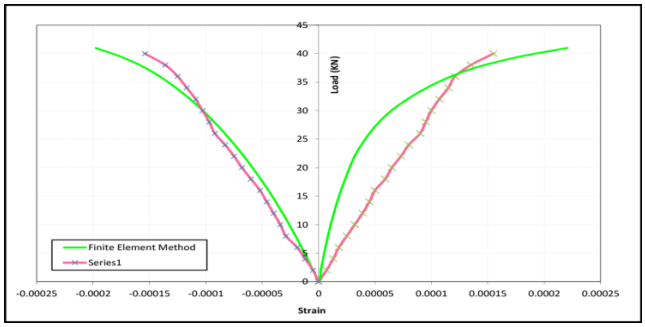

h) Load-strain curves of panel M1

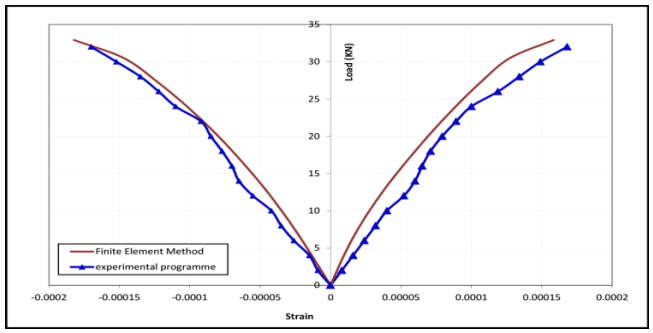

i) Load-strain curves of panel T1

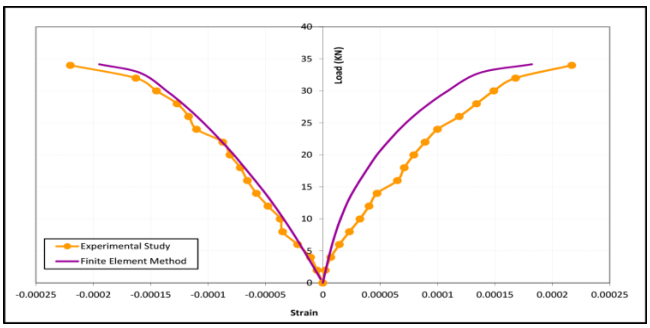

j) Load-strain curves of panel T2

Fig. 28. Load- strain curves for tested specimens and experimental and theoretical results.

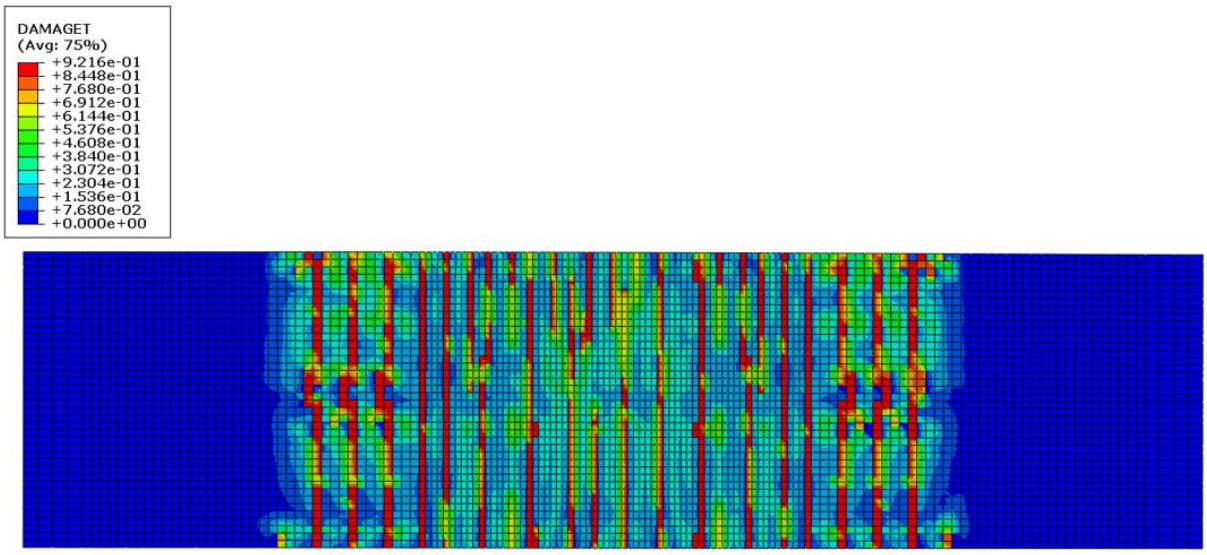

a) Cracking pattern for panel O1 from the theoretical study

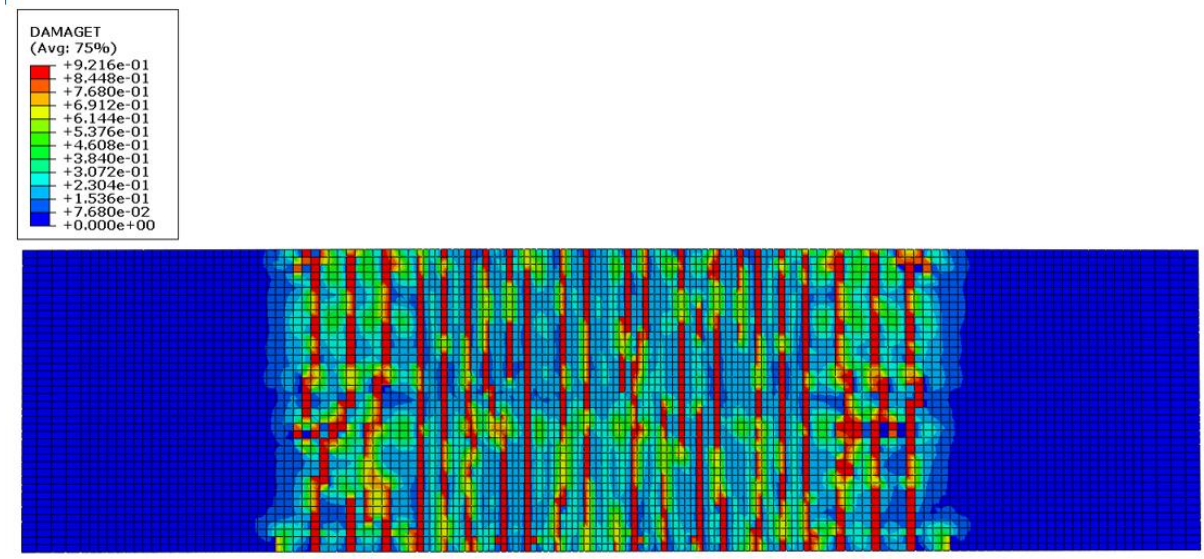

b) Cracking pattern for panel O2 from the theoretical study

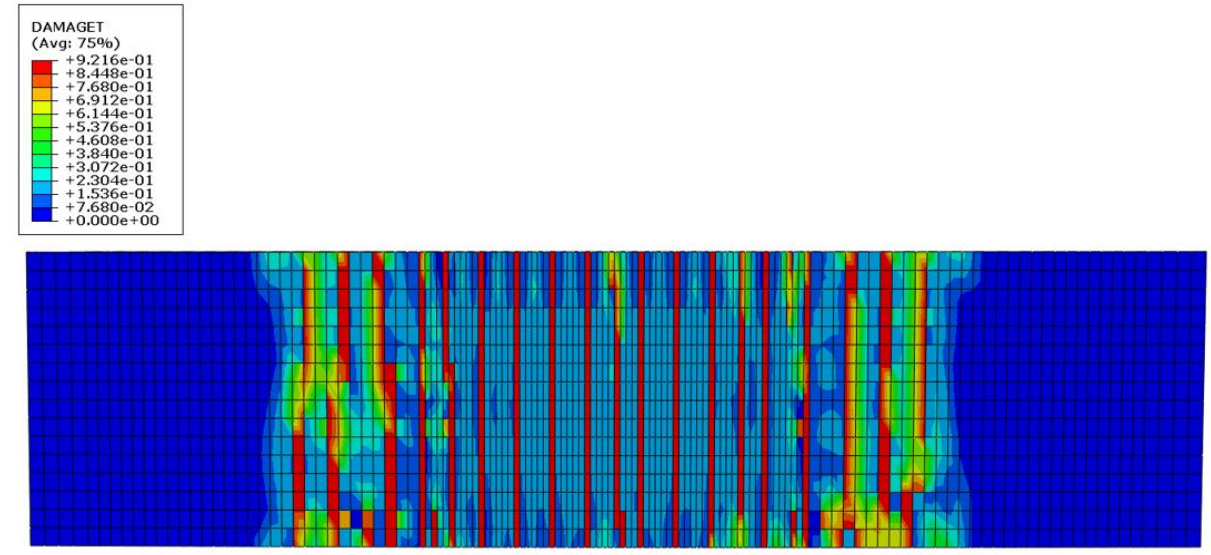

c) Cracking pattern for panel E1 from the theoretical study

Fig. 29. (continued)

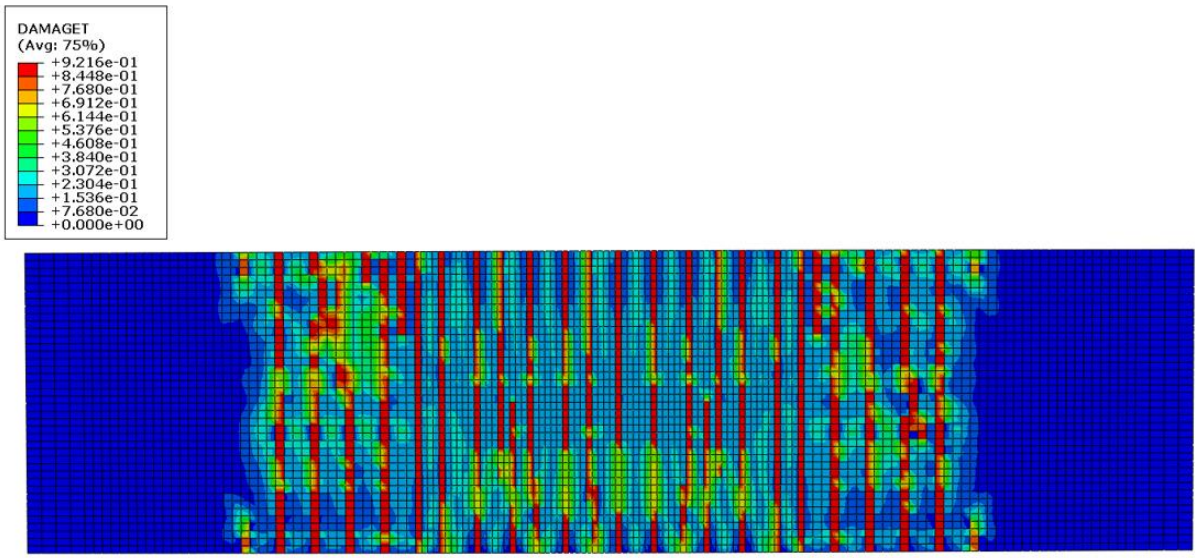

d) Cracking pattern for panel E2 from the theoretical study

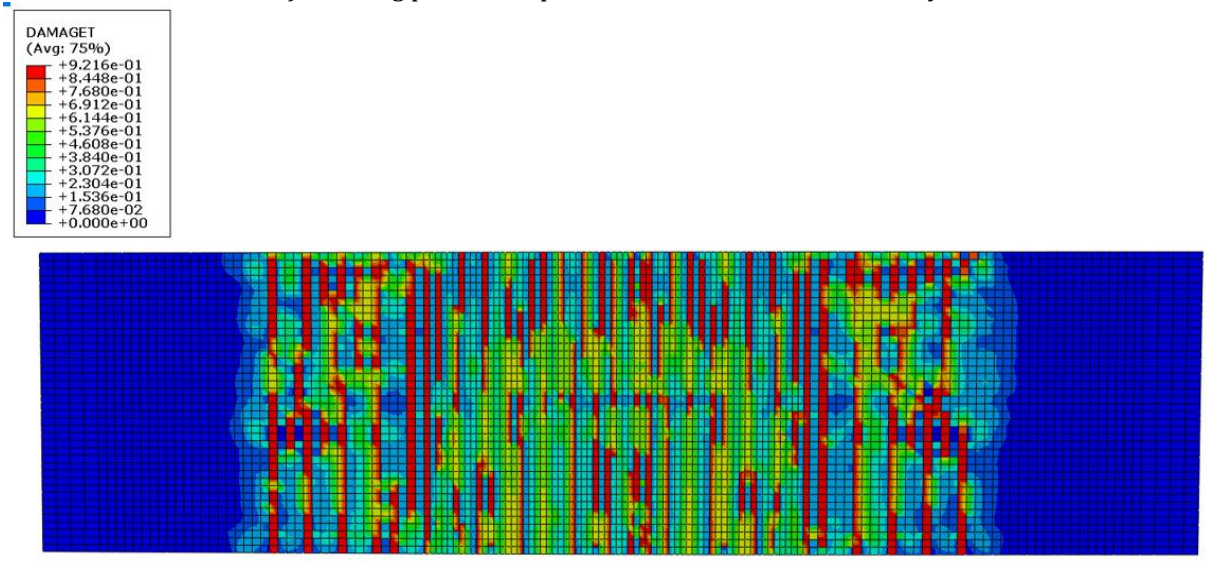

e) Cracking pattern for panel W2 from the theoretical study

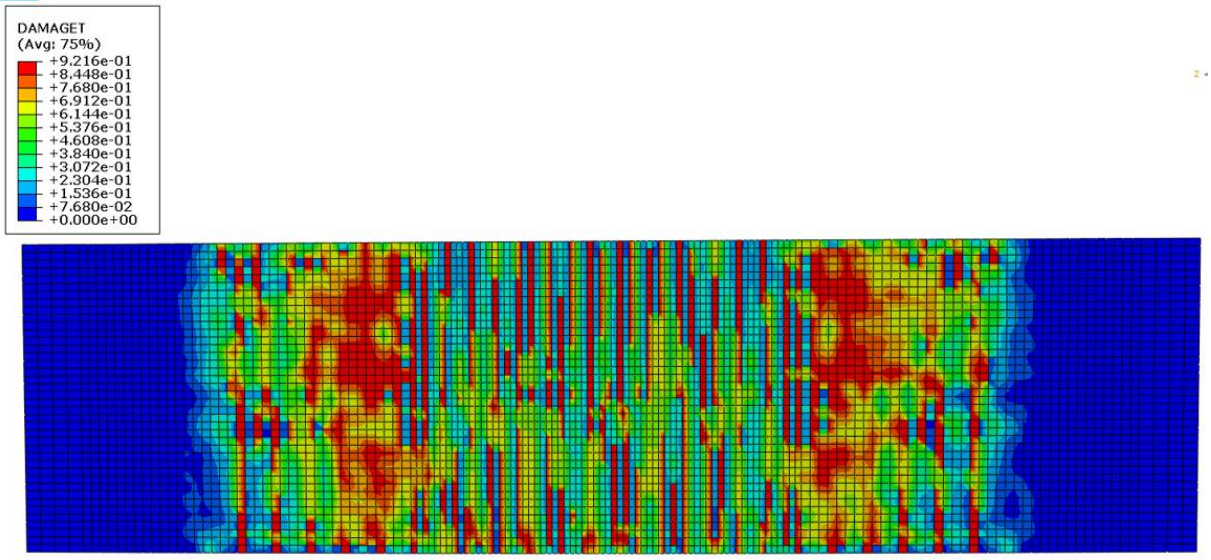

f) Cracking pattern for panel W3 from the theoretical study

Fig. 29. (continued)

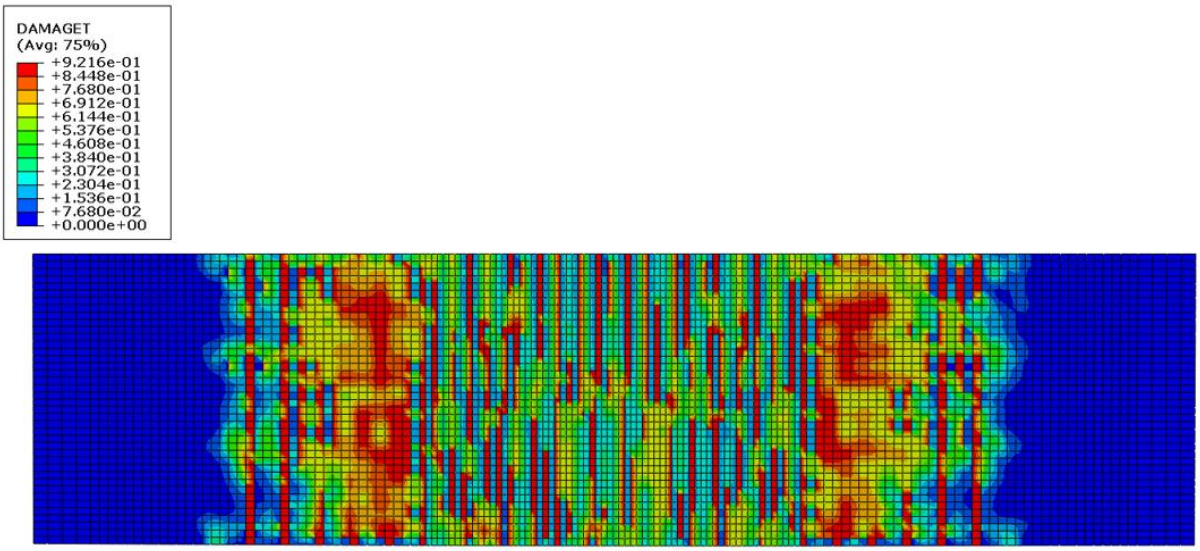

g) Cracking pattern for panel W4 from the theoretical study

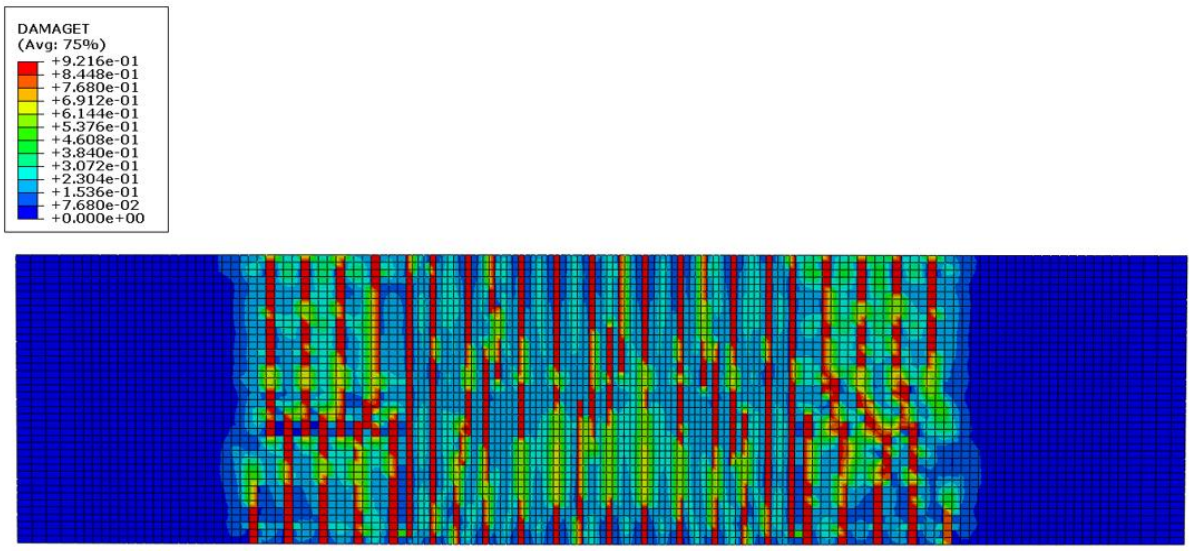

h) Cracking pattern for panel M1 from the theoretical study

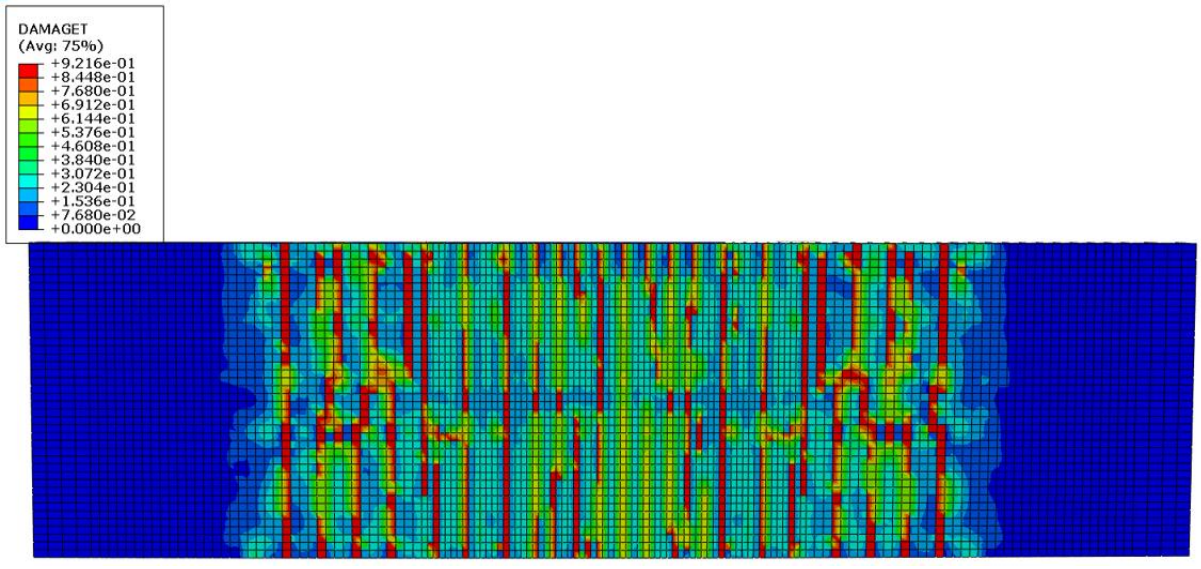

i) Cracking pattern for panel T1 from the theoretical study

Fig. 29. (continued)

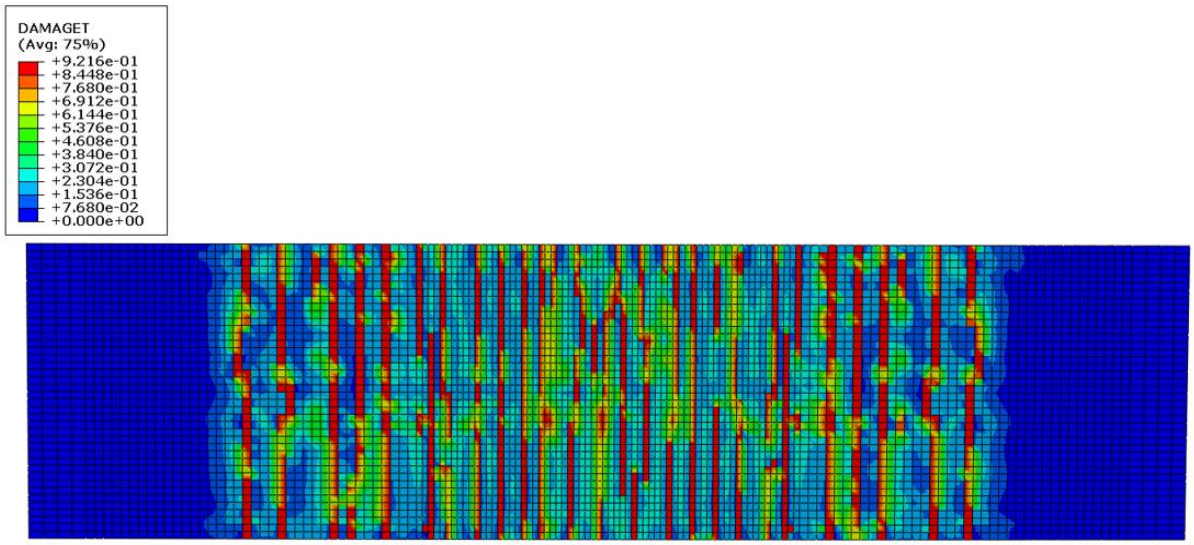

j) Cracking pattern for panel T2 from the theoretical study

Fig. 29. Cracking patterns for all tested specimens from the theoretical study.

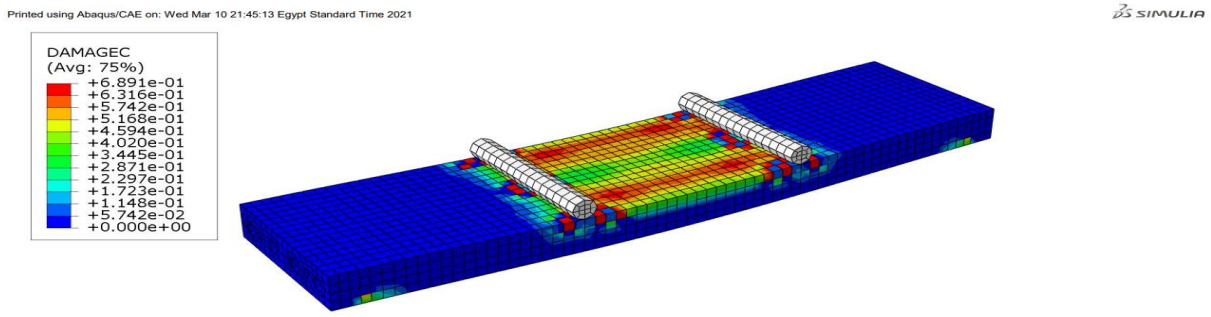

a) Stress distribution for panel O1 from the theoretical study

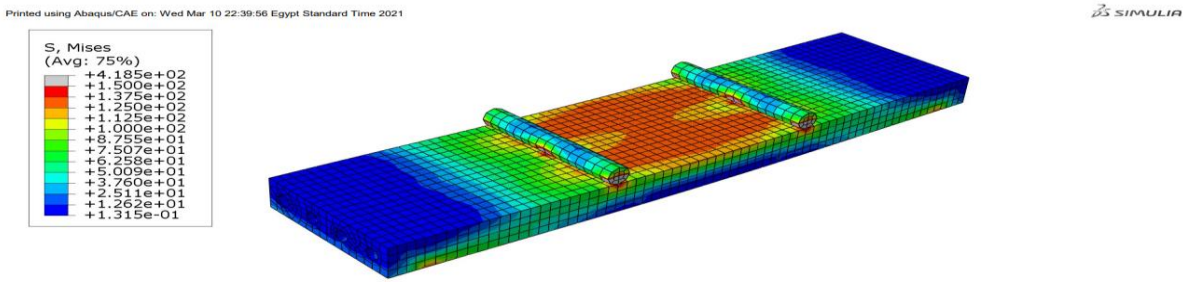

b) Stress distribution for panel O2 from the theoretical study

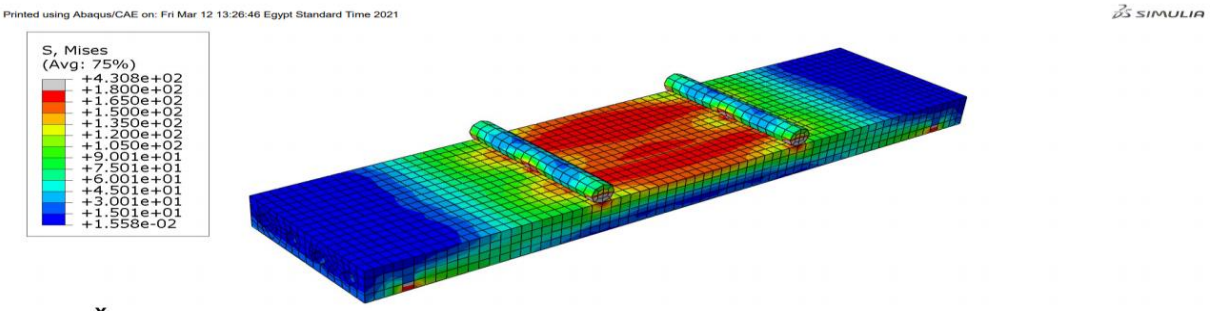

c) Stress distribution for panel E1 from the theoretical study

Fig. 30. (continued)

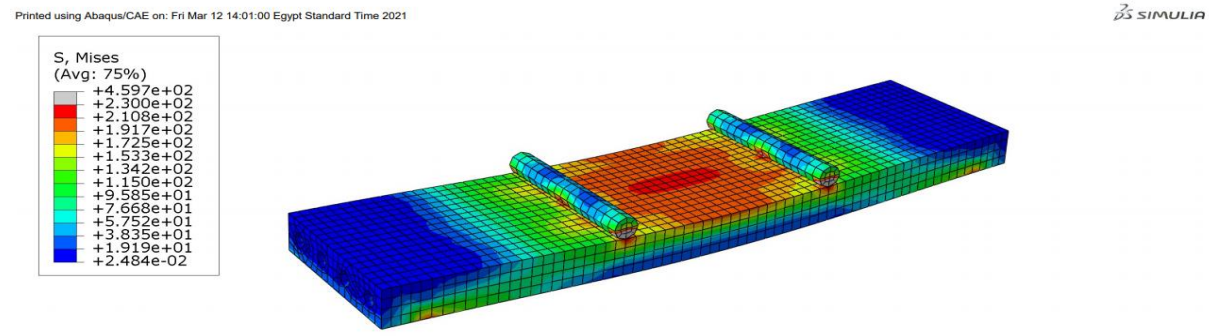

d) Stress distribution for panel E2 from the theoretical study

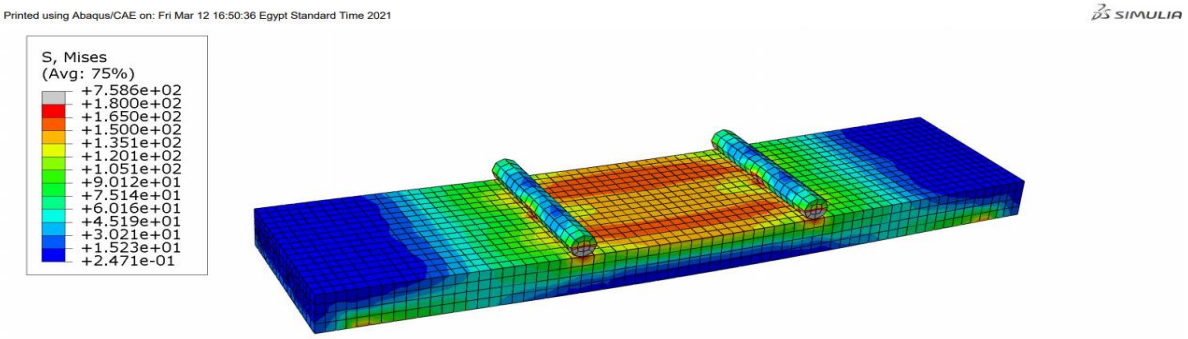

e) Stress distribution for panel W2 from the theoretical study

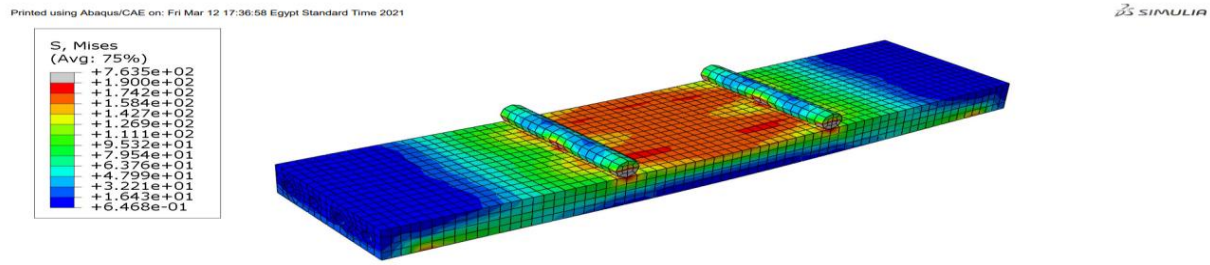

f) Stress distribution for panel W3 from the theoretical study

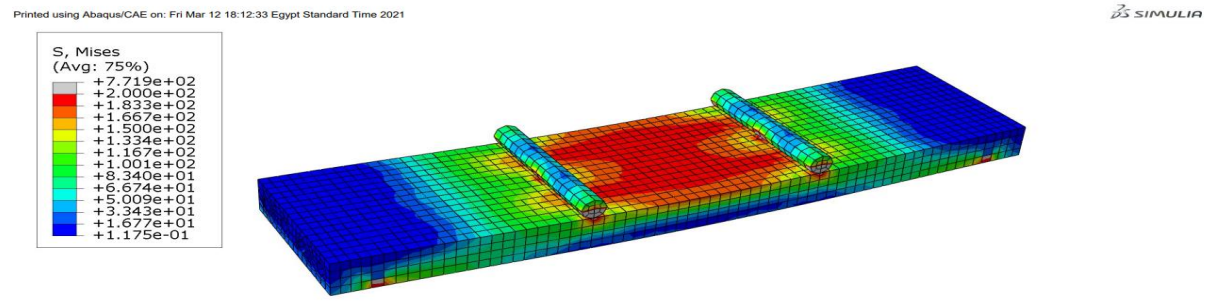

g) Stress distribution for panel W4 from the theoretical study

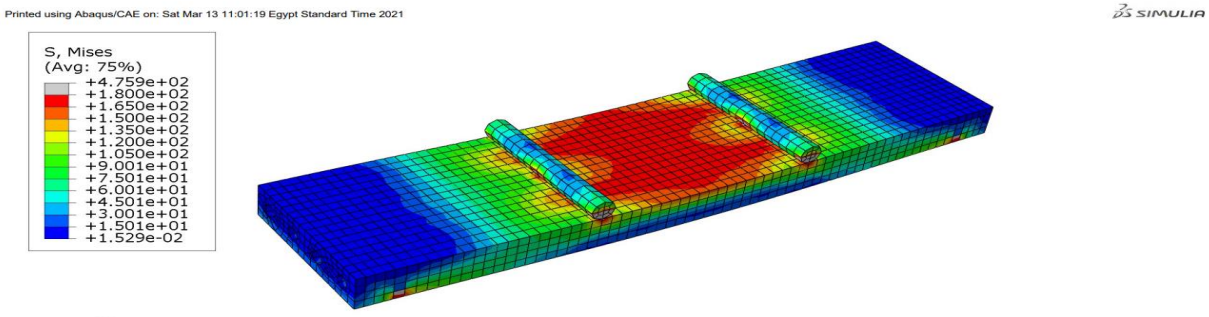

h) Stress distribution for panel M1 from the theoretical study

Fig. 30. (continued)

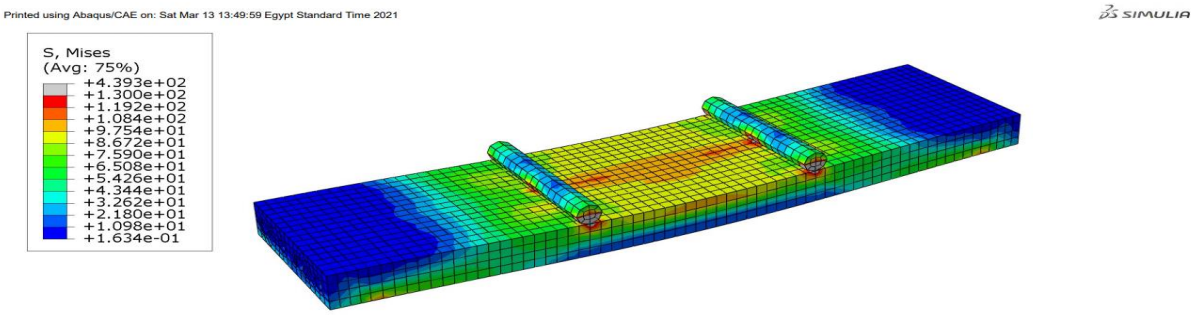

k) Stress distribution for panel T1 from the theoretical study

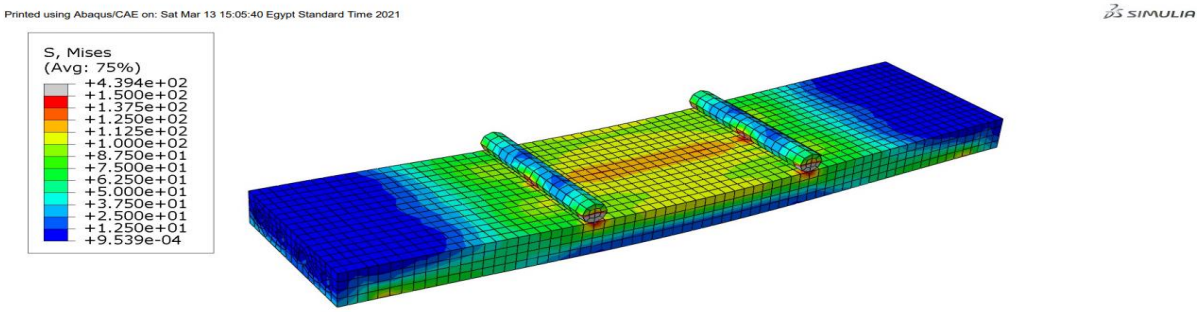

m) Stress distribution for panel T2 from the theoretical study

Fig. 30. Stress distribution for all tested specimens from the theoretical study.

Acknowledgements

None declared.

Funding

The authors received no financial support for the research, authorship, and/or publication of this manuscript.

Conflict of Interest

The authors declared no potential conflicts of interest with respect to the research, authorship, and/or publication of this manuscript.

References

Abbass AA, Abid SR, Arna'ot FH, Al-Ameri R A, Özakça M (2020). Flexural response of hollow high strength concrete beams considering different size reductions. *Journal of Structures*, 23, 69-86.

Abdul-Fataha S (2014). Structural behavior of concrete beams reinforced with innovative materials. *M.Sc. thesis*, Department of Civil Engineering, Menoufia University, Egypt.

Aboul-Anen B, El-Shafey A, El-Shami M (2009). Experimental and analytical model of ferrocement slabs. *International Journal of Recent Trends in Engineering*, 1(6), 25-29.

ACI 549 (1999) .State-of-the-Art Report on Ferrocement. ACI Manual of Concrete Practice, Part 5.

Acma L, Dumpasan G, Salva M, Mansaguiton M, Supremo R, Daquiado N (2015). Flexural strength and ductility behavior of ferrocement I-beam. *Mindanao Journal of Science and Technology*, 13, 99-108.

Al-Kubaisy MA, Jumaat MZ (2000). Flexural behavior of reinforced concrete slabs with ferrocement tension zone cover. *Construction and Building Materials*, 14(5), 245-252.

Ali A, Abdullah A (1995). Applications of ferrocement as a low cost construction material in Malaysia. *Journal of Ferrocement*, 25(2), 123-128.

ASTM C1116/C1116M-10a (2015). Standard specification for fiber reinforced concrete. ASTM international, West Conshohocken, PA.

Bhalsing S, Shoaib S, Autade P (2014). Tensile strength of ferrocement with respect to specifc surface. International *Journal of Innovative Research in Science, Engineering and Technology*, 3(4), 501-507.

Chowdary PA (2016). Experimental analytical and investigation of flexural behavior of reinforced concrete beam. *International Journal of Advanced Scientific Technology in Engineering and Management Sciences*, 2(12).

Du W, Yang C, Wang C, Pan Y, Zhang H, Yuan W (2021). Flexural behavior of polyvinyl alcohol fiber - reinforced ferrocement cementitious composite. *Journal of Materials in Civil Engineering*, 33(4).

E.C.P. 203 (2018). Egyptian Code of Practice: Design and Construction for Reinforced Concrete Structures. Cairo, Egypt.

Elavenil S, Chandrasekar V (2007). Analysis of reinforced concrete beams strengthened with ferrocement. *International Journal of Applied Engineering Research*, 2(3), 431- 440.

Eskandari H, Madadi A (2015). Investigation of ferrocement channels using experimental and finite element analysis. *Engineering Science and Technology, an International Journal*, 18(4), 769-775.

E.S.S. 1109 (2008). Aggregates for Concrete. Egyptian Organization for Standardization & Quality, Cairo, Egypt.

E.S.S. 4756-1 (2013). Portland Cement, Ordinary and Rapid Hardening. Egyptian Organization for Standardization & Quality, Cairo, Egypt.

Fahmy EH, Shaheen YB, Korany YS (1997). Use of ferrocement laminates for repairing reinforced concrete slabs. *Journal of Ferrocement*, 27(3), 219-232.

Fahmy EH, Ezzat H, Shaheen YB, Abou Zeid MN (2004). Development of ferrocement panels for floor and wall construction. *Proceedings of the 5th Structural Specialty Conference of the Canadian Society for Civil Engineering*, Saskatoon, Saskatchewan, Canada.

Fahmy EH, Ezzat H, Shaheen YB, Abou Zeid MN, Abdel Naby AM (2005). Permanent ferrocement forms: a viable alternative for construction

of concrete Beams. Proce*edings of the 30th Conference on Our World in Concrete and Structures*, Singapore, 249-256.

Koukousel A, Mistakid E (2014). Buckling behavior of composite ferrocement plates. *Conference: 8th Hellenic National Conference of Steel Structures*.

Leeanansaksiri A, Payakapo P, Ruangrassamee A (2018). Seismic capacity of masonry infilled RC frame strengthening with expanded metal ferrocement. *Journal of Engineering Structures*, 159, 110-127.

Naaman AE (2015). Ferrocement: Progress review and most critical need for the near future. *11th International Symposium on Ferrocement and Textile Reinforced Concrete 3rd ICTRC*, Germany, 9-14.

Naser FH, Al Mamoori AH, Dhahir MK (2021). Effect of using different types of reinforcement on the flexural behavior of ferrocement hollow core slabs embedding PVC pipes. *Ain Shams Engineering Journal*, 12(1), 303-315.

Prakashan LV, George J, Edayadiyil JB, George JM (2016). Experimental study on the flexural behavior of hollow core concrete slabs. *Journal of Applied Mechanics and Materials*, 857, 107-112.

Sakthivel PB, Jagannathan A (2005). Ferrocement construction technology and its applications – A review. http://dl.lib.mrt.ac.lk/handle/123/9492.

Shaaban IG, Shaheen YB, Elsayed EL, Kamal OA, Adesina PA (2018). Flexural behaviour and theoretical prediction of lightweight ferrocement composite beams. *Case Studies in Construction Materials*, 9.

Shaheen YB, Eltehawy EA (2017). Structural behaviour of ferrocement channels slabs for low cost housing. *Challenge Journal of Concrete Research Letters*, 8(2), 48-64.

Shaheen YB, Eltaly BE, Abdul-Fataha S (2014a). Structural performance of ferrocement beams reinforced with composite materials. *Journal of Structural Engineering & Mechanics*, 50(6), 817-834.

Shaheen YB, Eltaly BE, Hanesh AA (2014b). Experimental and FE simulations of ferrocement domes reinforced with composite materials. *Journal of Concrete Research Letters*, 5(4), 873-887.

Shaheen YB, Nasser AA, El-Habashy WS (2016). Behaviour of ferrocement sandwich panels slabs under shear. *Journal of Concrete Research Letters*, 7(1), 11-23.

Shaheen YB, Soliman NM, El-Araby F (2018). Repairing reinforced concrete beams with openings by ferrocement laminates. *12th International Conference on Civil and Architecture Engineering*, Cairo, Egypt, 1-20.

Shaheen YB, Mousa M, Gamal E (2020). Structural behavior of light weight ferrocement walls. *13th International Conference on Civil and Architecture Engineering*, Cairo, Egypt, 1-21.

Singh V, Bansal PP, Kumar M (2015). Experimental studies on strength and ductility of ferrocement jacketed RC beam-column joints. *International Journal of Civil and Structural Engineering*, 5(3), 199-205.

Swamy RN, Shaheen YB (1990). Tensile behavior of thin ferrocement plates. *ACI Materials Journal*, 357-387.

Challenge Journal of Concrete Research Letters

Research Article

Effect of expanded polystyrene beads on the properties of foam concrete containing polypropylene fiber

Mehmet Canbaz [a,*], Ali Can Türeyen [a]

[a] *Department of Civil Engineering, Eskişehir Osmangazi University, 26480 Eskişehir, Turkey*

ABSTRACT

In this study, foam concrete was produced using 3 different volumes of EPS beads (up to 100%), 3 different volumes of polypropylene(PP) fiber (up to 0.1)%, sand and 40% pre-produced foam which is fixed by volume. The water-cement ratio was 0.4 and the sand-cement ratio was chosen as 1. The foam concrete were cast into molds with a size of 100 x 100 x 500 mm and 150 x 150 x 150 mm prism. Unit weight, ultrasonic pulse, water absorption, splitting tensile strength, bending strength and compressive strength tests were achieved. Foam concrete were kept in laboratory standard conditions. According to the results of study, unit weight and ultrasonic pulse velocity vary between 970-1350 kg/m^3 and 1.6-2.6 km/sec, respectively. The water absorption of the foam concrete decreased up to 65% as the EPS beads ratio increased. Since EPS beads do not contribute to the strength and act like a void, splitting tensile strength in specimens containing EPS beads decreased by up to 70%. The use of fiber contributes to the splitting tensile strength, especially in specimens that do not contain EPS beads, and it increased the strength by 78%. Similarly, the flexural strength of the PP fiber addition increased by up to 70%. As the EPS beads ratio increased, the flexural strengths decreased by 77%. With the addition of PP fiber, the compressive strength increased by 55%. However, since EPS beads' strength is negligible, it caused a 60% decrease in compressive strength.

ARTICLE INFO

Article history:
Received 3 November 2021
Revised 26 January 2022
Accepted 12 February 2022

Keywords:
Foam concrete
EPS beads
Polypropylene fiber
Mechanical properties

1. Introduction

Foam concrete is classified as a type of lightweight concrete in which an air gap is created into cement paste or mortar with the help of foaming agent (Ramamurthy et al. 2009). Foam concrete is a building material designed with a unit weight varying between 400 and 1600 kg/m^3, flowing, self-compacting, and used in non-structural applications with its low compressive strength (Jones and McCarthy 2005; Richard and Ramli 2013; Nambiar and Ramamurthy 2008). The dry unit weight of foam concrete affects many of its physical properties. There are many parameters that affect the dry unit weight, such as the materials used in the mixture, aggregate type, mineral and chemical additives, cement content and type. However, the most important factor affecting all the physical properties of the foam concrete is the foam volume used in the mixture (Bindiganavile and Hoseini 2008). Foam concrete is known as a material with low cement content and lightweight aggregates with high fluidity and excellent thermal insulation (Ramamurthy and Nambiar 2009). Although foam concrete is not a new material and the first patent date goes back to 1920, it could not find a wide usage area because the foam quality was not as stable as desired. However, after the 2000s, the development of foam production machines with technology has led to an increase in foam stability and production volume of foam concrete. Therefore, foam concrete has made it widely used in applications (Brady et al. 2001).

For semi-structural applications, the fresh, mechanical and transport microstructure properties of foam concrete were investigated by adding polycarboxylate superplasticizers at different water/cement ratios of foam

* *Corresponding author*. Tel.: +90-222-239-3750 ; Fax: +90-222-239-3613 ; E-mail address: mcanbaz@ogu.edu.tr (M. Canbaz)
ISSN: 2548-0928 / DOI: https://doi.org/10.20528/cjcrl.2022.01.003

concrete with a unit weight of 1500 kg/m^3. It was concluded that the water/cement ratio and superplasticizer had a significant effect on the properties of foam concrete. With the increase of superplasticizer content, the mechanical and transport properties of foam concrete improved and the optimum results were obtained at a plasticizer content of 1.35. With the use of superplasticizer, it has been observed that a smaller void diameter is formed and better void distribution occurs (Al-Shwaiter et al. 2021). The water absorption, capillarity and compressive strengths of foam concrete produced at different foam volumes and by replacing sand and fly ash with 100% were investigated. The water absorption, capillarity and compressive strength decreased with the increase of the foam volume in the mixture. Fly ash caused an increase in water absorption due to high water-solids requirement (Nambiar and Ramamurthy 2007). In addition, in the other work, it was stated that fly ash plays an important role in the stability and consistency of foam concrete (Nambiar and Ramamurthy 2008). In this study, compressive strengths of foam concretes with unit weights varying between 1000-1500 kg/m^3 with the displacement of cement and fly ash up to 75% were investigated. No strength reduction was observed in the replacement of fly ash with cement up to 67%. According to the article, it was determined that the strength increased over time with the increase in the fly ash content (Kearsley and Wainwright 2000). Foam concrete obtained by replacing fly ash with sand, the structural improvement of foam concrete with the addition of silica fume, fly ash, and PP fiber was investigated. The compressive strength of the foam concrete, which has a density between 1000-1900 kg/m^3, including PP fiber and silica fume, varied between 10-70 MPa. In addition, with the addition of PP fiber, the drying shrinkage, creep resistance and tensile strength of foam concrete were greatly increased. Thus, it was concluded that fibered foam concrete can be used in structural applications (Amran et al. 2020). It is aimed to produce foam concrete with an oven-dry density of 1300 kg/m^3 by replacing up to 30% cement with palm oil fuel ash (POFA). With a 30% POFA displacement, the density was reduced by approximately 43%. This is due to the porous nature of POFA. Displacement of more than 20% POFA caused a decrease in strength (Alnahhal et al. 2021). The fluidity, compressive strength, thermal conductivity and density of foam concretes produced by replacing 75% and 100% of quarry waste with river sand were investigated. The use of quarry sand in high volumes improved the compressive strength, decreased fluidity, and slightly increased thermal conductivity. It has been concluded that foam concrete containing quarry dust will cause less greenhouse gas emissions and less energy consumption (Lim et al. 2017). The hardened properties, void structure and curing method of high porosity foam concrete produced with normal Portland cement were investigated. It was concluded that the porosity, compressive strength and thermal conductivity of the foamed concrete varied between 88.5%-95.4%, 0.12 to 0.75 and 0.036-0.063, respectively (Jiang et al. 2016). The drying shrinkage, compressive strength and splitting tensile strength of foam concrete produced using silica fume, fly ash and PP fiber was focused on. With the addition of silica fume and PP fibers, the dry unit weight and compressive strength of foam concrete vary between 800-1500 kg/m^3 and 10-50 MPa, respectively. Silica fume and polypropylene greatly increase the compressive strength. In addition, PP fiber greatly increases the drying shrinkage and splitting tensile strength of foam concrete (Bing et al. 2012). 3-hour and 28-day compressive strength, thermal conductivity, water resistance and splitting tensile strength of foam concrete produced using magnesium phosphate cement (MPC) were investigated. It has been determined that the 3-hour compressive strength of MPC-based foam concrete is approximately 70% of the 28-day compressive strength. The compressive strength and thermal conductivity of MPC-based foam concrete produced by adding 10% fly ash were found to be 2.4 MPa and 0.072 W/mK (Ma and Chen 2017). Thermal conductivity and compressive strength tests of 6 groups of foam concrete varying between 15%, 17% and 20% air content were examined. It was observed that the dry unit weight, compressive strength and thermal conductivity ranged between 860-1245 kg/m^3, compressive strength 2.5-6.5 MPa and thermal conductivity coefficient between 0.021 and 0.035, respectively (Kumar et al. 2018). Foam concrete was produced with a bentonite slurry of 9.1% of its solid content. The compressive strength decreased with the increase of bentonite slurry. It was concluded that foam concrete with bentonite slurry showed better thermal insulation properties (Xie et al. 2018). Workability and strength properties of foam concrete produced by adding up to 20% of waste tire powder were investigated. It was observed that the workability of foam concrete decreased as the volume of tire waste dust increased. The highest compressive strength was obtained in foam concrete produced with 5% waste rubber powder (Mehrabi et al. 2019). As can be seen in Fig. 1, there are partition wall element applications where EPS beads and foam concrete are used together.

A research was conducted on the thermal insulation and bending strength of wall panels with 3 different percentages of EPS particles on the surface area of foam concrete with a fixed density of 1100 kg/m^3 and a solid/water ratio of 0.25. It has been observed that the flexural strength of the EPS particle decreases at higher volumes and shows lower thermal insulation properties (Priyanka et al. 2021). The compressive strength, fire resistance and thermal conductivity properties of foam concrete containing EPS ranging from 0% to 82.22% by volume were investigated. The density of foam concrete varies between 150 kg/m^3 and 1200 kg/m^3. It was concluded that the fire resistance, thermal conductivity and compressive strength of foam concrete decreased significantly with the increase in EPS volume (Sayadi et al. 2016). It was aimed to investigate a new wall system with foam concrete produced using 50% recycled EPS. It has been concluded that foamed concrete with EPS can compete with precast panel and can be used as the main wall material (Dissanayake et al. 2017).

When the previous studies are examined, there is a lot of research on foam concrete, but there are very few studies evaluating EPS beads in foam concrete. In this

study, apart from using EPS beads in foam concrete, unlike other studies, it was added to PP fiber and its effect on its hardened properties was investigated. High strength is not expected, especially from lightweight concrete. However, these concretes should be made in the form of slabs and should not be shattered while they are attached with dowels. In general, steel fiber is preferred in case of such mechanical need in concrete. However, for lightweight concrete, it was thought that polypropylene fiber would be sufficient to increase adherence and mechanical performance. For this reason, polypropylene fiber was used.

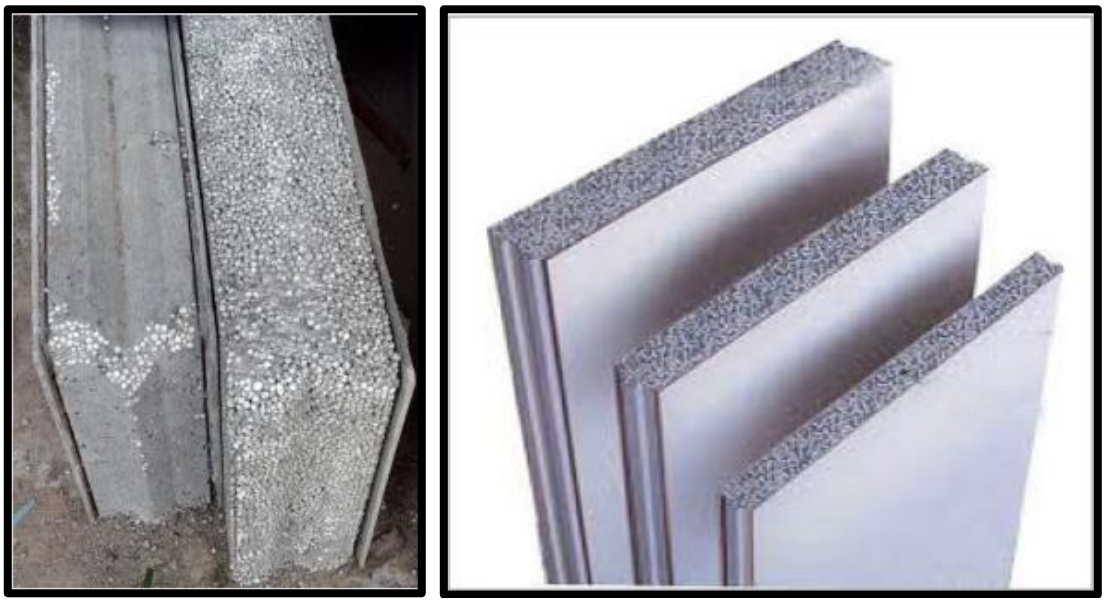

Fig. 1. EPS beads and foam concrete application (Fernando 2015; Dissanayake et al. 2017).

2. Experimental Study

2.1. Materials

Cement: Type R CEM I 42.5 cement was employed in the experiment. The chemical and physical properties of this cement are listed in Table 1.

Aggregate: Fine river sand was used in the foamed concrete mixtures. The sand was taken from Sakarya River in Osmaneli/Bilecik. The granulometry of the sand is provided in Table 2.

Water: Eskişehir tap water was employed. The chemical analysis of the drinkable water is provided in Table 3.

Foam Agent: The foam agent was mixed with the water 2.5 % by mass and foam solution was produced (80 gr/l). The foam agent which is compose of vinyl resin and calcium naphthalene sulfonate is produced by Aydos Chemicals Company. The properties of the foam agent is listed in Table 3.

Fiber: Polypropylene fiber is used as fiber in the production. The properties of this PP fiber is shown in Table 5.

Expanded polystyrene (EPS) beads: The Styrofoam aggregate used is granular and expanded polystyrene based material. Unit volume weight is 0.02 kg/dm^3.

Table 1. Properties of cement.

Chemical properties				Physical properties	
SiO_2	19.19	K_2O	0.63	Density, g/cm^3	3,09
Al_2O_3	4.56	Na_2O	0.31	Specific surface cm^2/g	3590
Fe_2O_3	3.09	SO_3	3.21	Setting Time(initial), min	163
CaO	62.9	CI-	0.013	Setting Time(final), min	227.5
MgO	1.88	LOI	3.8	Expansion, mm	1

Table 2. Granulometry of sand.

Sieve size, mm	2	1	0.5	0.25	0.125
Granulometry, %	100	67.8	47.4	16.6	2

Table 3. Properties of mixing water.

Chemical property, mg/l						Physical property	
Al	0,04	Cu	0.016	Ni	5,07	Conductivity, µS/cm	628
NO_3	11,1	Fe	0.007	K	6,8	Hardness, Fd^0	30.11
NH_4	0,06	Mn	0.015	As	1,19	pH	7.35

Table 4. Properties of foam agent.

pH	Cl^-, %	Freezing point, °C	Color	Density kg/dm³	Alkali, %
5.23	<0.1	-5	Brown	1.041	<0.5

Table 5. Properties of PP fiber.

Type	Length, mm	Diameter, mm	L/d	$\sigma_{tensile}$ MPa	E, GPa	Density, kg/dm³	Melting point, °C
High Grade (fibrofor)	20	0.3	67	400	4.9	0.91	150

2.2. Method and tests

In foam concrete production, the water-cement ratio was chosen as 0.4, and the sand-cement ratio was chosen as 1. PP fiber was added to the prepared cement mortar mixture first, and then EPS beads were added. It was mixed with the previously prepared foam cement mortar. The mixing ratios are given in Table 6. 15 cm cube specimens were taken from the prepared mixture and subjected to standard curing conditions (23±2 ^{0}C, lime-saturated water).

The specimens taken from the mixture prepared with the ingredients shown in Fig. 2 were removed from the cure tank 28 days after production, and unit weight, ultrasonic pulse, water absorption, tensile splitting, compression and bending tests were performed on the specimens. Each experiment was carried on at least three specimens. Considering the results of the experiments, the unit weights, ultrasonic pulse velocities (UPV), water absorption rates, split tensile strength, compressive strength and flexural strength of the specimens were calculated.

Table 6. Mixture ratio.

Water/cement	Sand/cement	EPS beads, %	Fiber, %	Foam, %
0.4	1	0 50 100	0.00 0.05 0.10	40

Fig. 2. Mixture ingredients, specimens and tests on these specimens.

3. Discussion

The change of foam concrete unit weights with EPS Beads and PP fiber are present in Fig. 3. When Fig. 3 was examined, foam concrete unit weights with EPS Beads and PP fiber varies between 970-1350 kg/m^3. It was observed that unit weights decreased by up to 24% by using EPS Beads instead of sand. The low density of EPS beads compared to sand caused a decrease in unit weights. PP fiber addition increased the unit weights below 5% in specimens containing EPS beads, while it increased by 18% in specimens without EPS beads. Since the PP fiber addition negatively affected the foam distribution in foam concrete without EPS beads, it caused an increase in the unit weights.

Fig. 4 shows the effect of EPS beads and PP fiber ratio on UPV of foam concrete specimens. When Fig.4 was examined, foam concrete was seen that the UPV values varied between 1.6-2.6 km/sec. It was observed that the void system and EPS beads contained in foam concrete reduce UPVs. When the rate of EPS beads is 50%, the UPV values decrease by 30%, while the rate of decrease is 8% when the rate of EPS beads is 100%. The effect of the PP fibers on UPV has particularly pronounced in specimens without EPS beads. Increasing the PP fiber ratio in these specimens increased the UPV values by up to 40%. The biggest factor in this increase is that the vibration passes the gaps in a shorter time thanks to the PP fibers.

The water absorption rates by weight found as a result of the water absorption test performed on the foam concrete specimens are given in Fig. 5. When Fig. 5 was examined, as the EPS beads rate increases, the water absorption rate decreased by 65%. The fact that EPS beads do not absorb water has been effective in reducing this rate. In addition, the addition of PP fiber caused a partial closure of the cracks and capillary spaces that caused the water to enter the foam concrete, resulting in a decrease in the water absorption rate up to 69%.

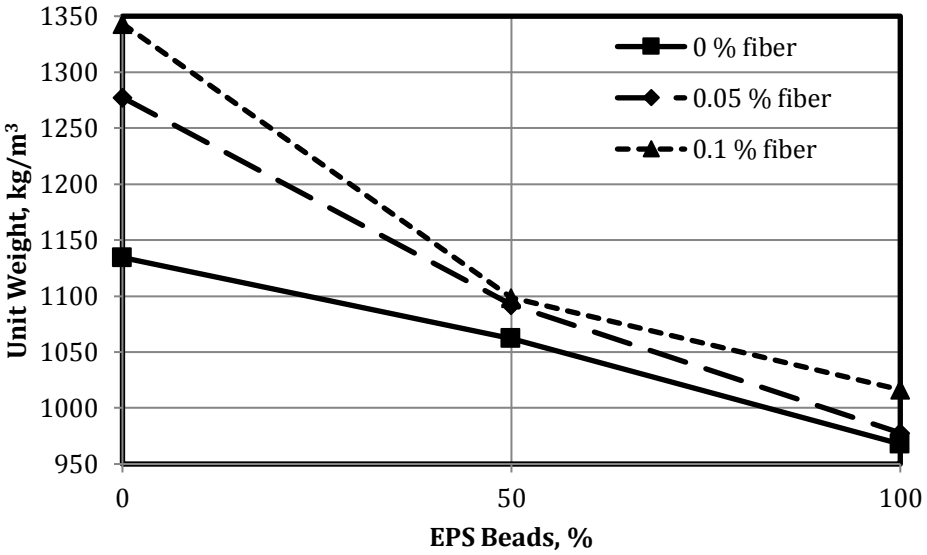

Fig. 3. Unit weight of foam concrete.

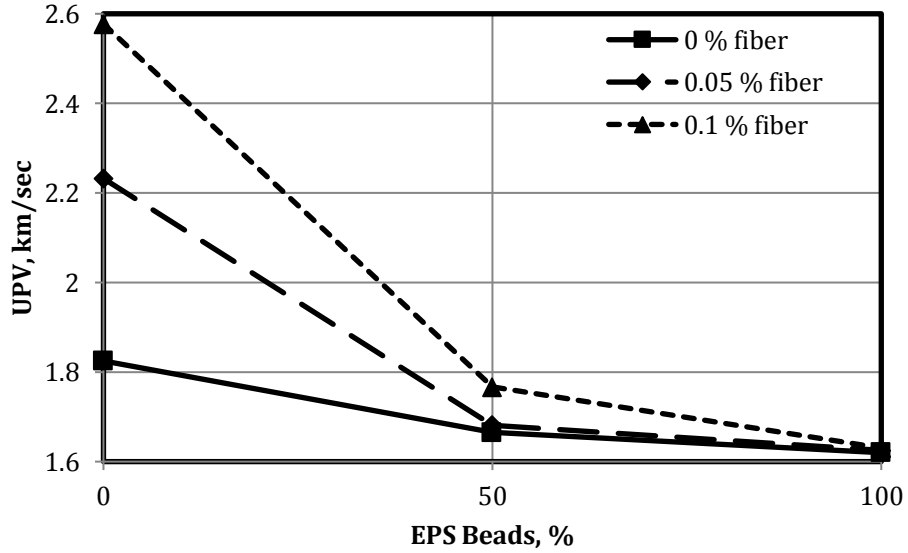

Fig. 4. UPV test results of foam concrete.

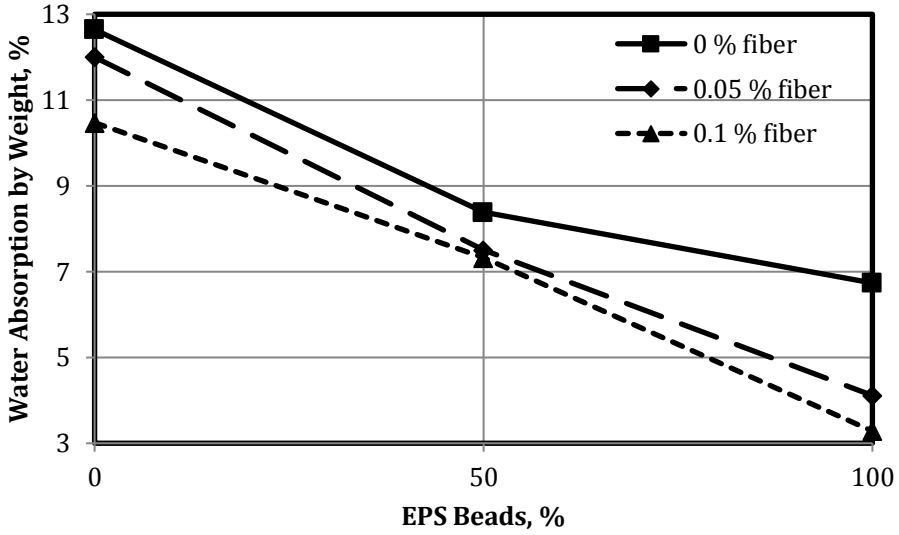

Fig. 5. Change of water absorption rate in foam concrete.

The tensile strength changes of the specimens in splitting depending on the PP fiber and EPS beads ratio are given in Fig. 6. When Fig. 6 was examined, Since EPS beads do not contribute to the strength and act like voids, the splitting tensile strength of the specimens containing EPS beads decreased by up to 70%. The use of PP fiber contributes to the splitting tensile strength, especially in specimens that do not contain EPS beads, and increased the strength by 78%. However; in the specimens containing EPS beads, the positive effect of PP fiber addition on the splitting tensile strength of the specimens decreased to 20%. The PP fibers prevented cracks formed in the specimen under the effect of linear load, spreading brittle suddenly and splitting. In cracks formed under linear load, the PP fibers first began to load with the bridging effect. As a result of the increase in load, its function has ended with the breaking or stripping of the PP fibers. This has resulted in an increase in strength.

Bending test results on foam concrete specimens are present in Fig. 7. When Fig. 7 was examined, the flexural strength of PP fiber addition increased by 70%, similar to splitting tensile strengths. As the EPS beads ratio increased, the flexural strengths decreased by 77%. Since the mid-point loading method was used as the bending test, the PP fibers in this section prevented the splitting into two due to the cracks formed under the bending effect, since the bending effect was created at a single point, similar to the split tensile test.

The changes in compressive strength depending on the EPS beads and PP fiber contained in the foam concrete specimens are given in Fig. 8. When Figure 8 was examined, the compressive strength increased by 55% with the addition of PP fiber. Since the compressive strength affects the entire volume in an area, the PP fibers provided a more controlled growth of micro cracks formed under the pressure effect as the load increased. Therefore, the fibers were effective in increasing the compressive strength regardless of the EPS beads content. Since EPS beads have an easily deformable structure with negligible strength, they acted like a void under pressure and caused their compressive strength to decrease by 60%.

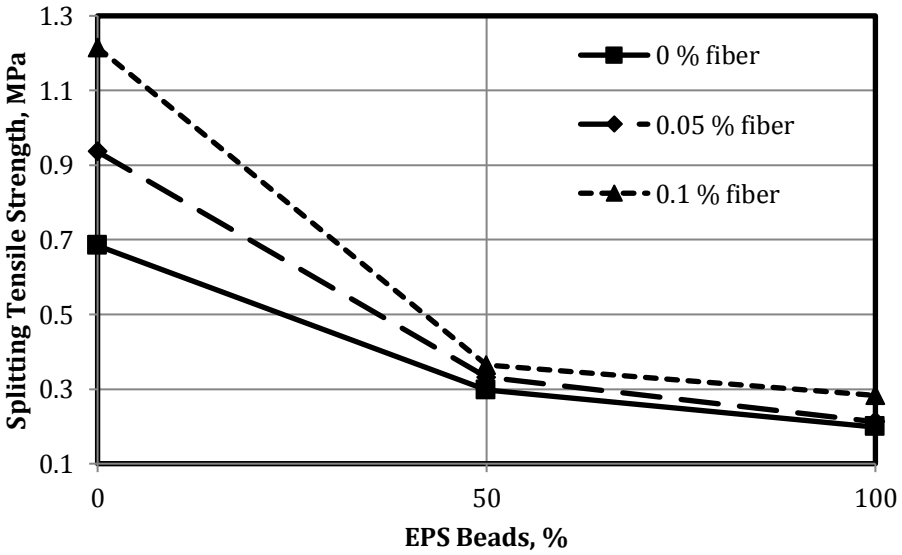

Fig. 6. Splitting tensile strength of foam concrete.

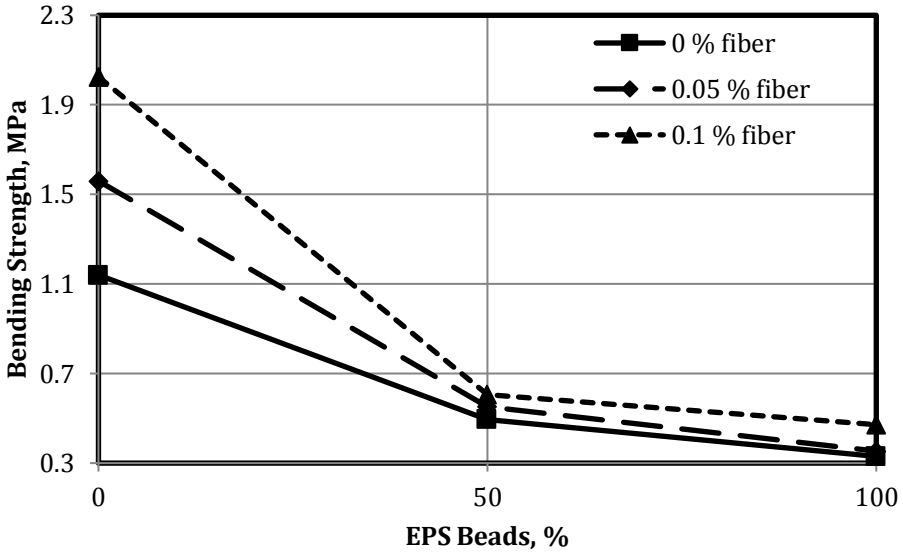

Fig. 7. Bending test results of foam concrete.

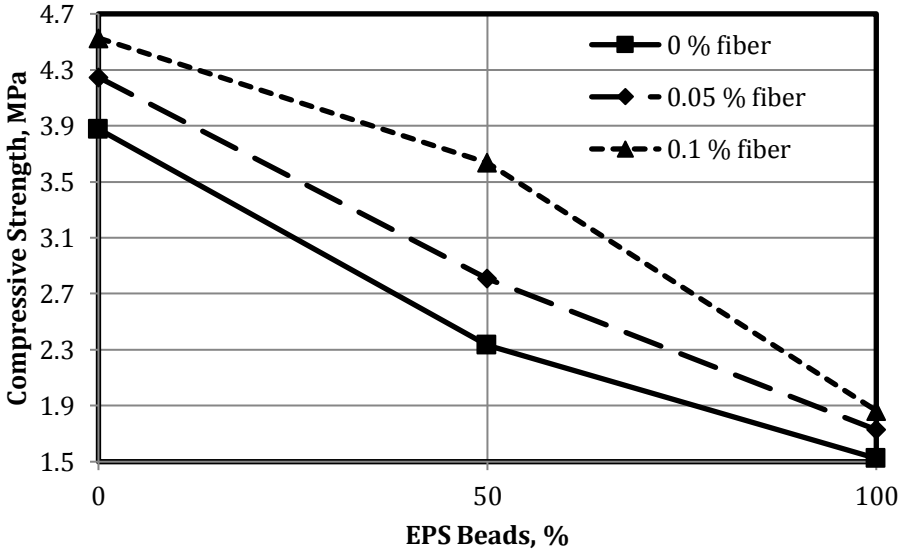

Fig. 8. The change of compressive strength with the ratio of PP fiber and EPS beads in foam concrete.

4. Conclusions

The conclusions of the study are summarized as follows:

- As a result of the substitution of EPS beads instead of aggregate in foam concrete, it observed that the unit weight values decreased below 1000 kg/m^3, ultrasonic pulse velocity decreased by 11% to 1.6 km/sec, water absorption rate by weight decreased by 47%, and decreased below 7%, splitting tensile strength decreased by 70% to below 200 KPa, the bending strength decreased by 70% to below 400 KPa, and the compressive strength decreased by 60% to below 2 MPa.
- In the case of adding PP fiber to foam concrete, unit weights increase by 18% and reach 1350 kg/m^3, ultrasonic pulse velocity increase by 40% and reach 2.6 km/sec, water absorption ratios by weight decrease by 17% and decrease to 10%, splitting tensile strengths It was determined that the flexural strengths increased by 78% and exceeded 1.2 MPa, the flexural strengths increased by 78% and exceeded 2 MPa, and the compressive strengths increased by 17% and exceeded 4.5 MPa.
- In case of adding PP fiber to EPS beads aggregated foam concrete, unit weights increase by 5% and exceed 1000 kg/m^3, ultrasonic pulse velocity exceed 1.63 km/sec with 1% increase, water absorption rates by weight decrease by 50% and reach 3%. , splitting tensile strengths increased by 43% and exceeded 280 KPa, bending strengths increased by 43% and exceeded 470 KPa, compressive strengths increased by 22% and approached 1.9 MPa.

As a result of the study, the use of 0.1% PP fiber in foam concrete is recommended because it improves the mechanical properties despite increasing the unit weight. By using EPS beads instead of aggregate in foam concrete, unit weights can be reduced below 1000

kg/m^3. Considering the mechanical properties of EPS beads aggregate foam concrete, it is seen that it can be used as an insulation plate. For this purpose, it is recommended to measure thermal conductivity values in future studies. In order to further reduce the unit weight values, it is recommended to carry out studies to increase the ratio of the foam solution in the mixture. In case of using EPS beads, it is recommended to investigate the behavior of high temperature and fire effects for new studies.

Acknowledgements

None declared.

Funding

The authors received no financial support for the research, authorship, and/or publication of this manuscript.

Conflict of Interest

The authors declared no potential conflicts of interest with respect to the research, authorship, and/or publication of this manuscript.

References

Alnahhal AM, Alengaram UJ, Yusoff S, Singh R, Radwan MK, Deboucha W (2021). Synthesis of sustainable lightweight foamed concrete using palm oil fuel ash as a cement replacement material. *Journal of Building Engineering*, 35, 1-12.

Al-Shwaiter A, Awang H, Khalaf MA (2022). The influence of superplasticiser on mechanical, transport and microstructure properties of foam concrete. *Journal of King Saud University-Engineering Sciences,* (article in press).

Amran YM, Alyousef R, Alabduljabbar H, Khudhair MHR, Hejazi F, Alaskar A, Siddika A (2020). Performance properties of structural fibred-foamed concrete. *Results in Engineering*, 5, 1-11.

Bindiganavile V, Hoseini MM (2008). Developments in the Formulation and Reinforcement of Concrete: Foamed concrete. Woodhead Publishing, England.

Bing C, Zhen W, Ning L (2012). Experimental research on properties of high-strength foamed concrete. *Journal of Materials in Civil Engineering*, 24(1), 113-118.

Brady KC, Watts GRA, Jones MR (2001). Specification for foamed concrete. Crowthorne, TRL Limited, UK.

Dissanayake DMKW, Jayasinghe C, Jayasinghe MTR (2017). A comparative embodied energy analysis of a house with recycled expanded polystyrene (EPS) based foam concrete wall panels. *Energy and Buildings*, 135, 85-94.

Jiang J, Lu Z, Niu Y, Li J, Zhang Y (2016). Study on the preparation and properties of high-porosity foamed concretes based on ordinary Portland cement. *Materials & Design*, 92, 949-959.

Jones MR, Mccarthy A (2005). Preliminary views on the potential of foamed concrete as a structural material. *Magazine of Concrete Research*, 57(1), 21–31.

Kearsley EP, Wainwright PJ (2001). The effect of high fly ash content on the compressive strength of foamed concrete. *Cement and Concrete Research*, 31(1), 105-112.

Kumar NV, Arunkumar C, Senthil SS (2018). Experimental study on mechanical and thermal behavior of foamed concrete. *Materials Today: Proceedings*, 5(2), 8753-8760.

Lim SK, Tan CS, Li B, Ling TC, Hossain MU, Poon CS (2017). Utilizing high volumes quarry wastes in the production of lightweight foamed concrete. *Construction and Building Materials*, 151, 441-448.

Ma C, Chen B (2017). Experimental study on the preparation and properties of a novel foamed concrete based on magnesium phosphate cement. *Construction and Building Materials*, 137, 160-168.

Mehrani SA, Bhatti IA, Bhatti NB, Jhatial AA, Lohar MA (2019). Utilization of rubber powder of waste tires in foam concrete. *Journal of Applied Engineering Sciences*, 9(1), 87-90.

Nambiar EK, Ramamurthy K (2007). Sorption characteristics of foam concrete. *Cement and Concrete Research*, 37(9), 1341-1347.

Nambiar EK, Ramamurthy K (2008). Fresh state characteristics of foam concrete. *Journal of Materials in Civil Engineering*, 20(2), 111-117.

Priyanka E., Sathyan D, Mini KM (2021). Functional and strength characteristics of EPS beads incorporated foam concrete wall panels. *Materials Today: Proceedings*, 46(10), 5167-5170.

Ramamurthy K, Nambiar EKK, Ranjani GIS (2009). A classification of studies on properties of foam concrete. *Cement and Concrete Composites*, 31(6), 388–396.

Richard AO, Ramli M (2013). Experimental production of sustainable lightweight foamed concrete. *British Journal of Applied Science & Technology*, 3(4), 994-1005.

Sayadi AA, Tapia JV, Neitzert TR, Clifton GC (2016). Effects of expanded polystyrene (EPS) particles on fire resistance, thermal conductivity and compressive strength of foamed concrete. *Construction and Building Materials*, 112, 716-724.

Xie Y, Li J, Lu Z, Jiang J, Niu Y (2018). Effects of bentonite slurry on air-void structure and properties of foamed concrete. *Construction and Building Materials*, 179, 207-219.

Challenge Journal of Concrete Research Letters

Review

Effect and optimization of incorporation of nano-SiO_2 into cement-based materials – a review

Mohammed Gamal Al-Hagri [a,*], Mahmud Sami Döndüren [a]

[a] *Department of Civil Engineering, Konya Technical University, 42130 Konya, Turkey*

ABSTRACT

Incorporation of nanomaterials into cement-based materials has great potentials to improve their performance to great levels and to produce construction materials with superior and unique properties. Various nanoparticles have been utilized in cementitious composites to improve their properties. This paper provides a detailed review about the effect of the most widely incorporated nanomaterial into cement-based materials, namely nano-silica, on different on properties of cement-based materials. The investigated properties are mechanical properties (compressive strength, split tensile strength and flexural strength), durability parameters (permeability, freeze and thaw resistance, high temperature resistance, fire resistance and sulfate attack resistance) and microstructural properties of mortar and concrete. The cost effectiveness of use of nano-silica in cement-based materials is also discussed. The optimum replacement percentage of cement with this nanomaterial to improve the performance of mortar and concrete is also investigated. The investigation showed that nano-silica has the ability to enhance the mechanical properties, durability and microstructural properties of concrete and mortar to a remarkable level. It also showed that the optimum content of nano-silica in concrete and mortar is 1.0-4.0% by weight of binder materials.

ARTICLE INFO

Article history:
Received 3 October 2021
Revised 29 November 2021
Accepted 27 December 2021

Keywords:
Cement-based materials
Durability
Mechanical properties
Microstructural properties
Nano-silica
Optimum content

1. Introduction

Research on use of nano-additives in cement-based materials began with nano-silica (Nano-SiO_2, NS) and then was extended to other nanoparticles (Juenger and Siddique 2015). Nano-silica is an amorphous material that consists of nano-sized particles of silicon dioxide (SiO_2) that have a high surface area to volume ratio, which can lead to a great pozzolanic reactivity (Biricik and Sarier 2014; Zhuang and Chen 2019). NS is one of the materials advancing the field of nanocomposites. It is the most widely incorporated nanomaterial into cementitious composites to enhance their performance due to its pore-filling effect and high pozzolanic reactivity (Aggarwal et al. 2015; Amin and Abu el-Hassan 2015; Ardalan et al. 2017; Behfarnia and Salemi 2013; El-Gamal et al. 2018; Givi et al. 2011; Pengkun Hou et al. 2013; Kawashima et al. 2013; Lazaro et al. 2012). In addition, nano-SiO_2 is becoming a progressively important component of special concretes and other advanced cementitious composites.

This work presents the advantages and disadvantages of use of NS in cementitious composites, and gives a detailed review of the effect of NS on the mechanical properties (compressive strength, split tensile strength and flexural strength), durability and microstructural properties of cement mortar and concrete. It also presents a discussion about the cost effectiveness of us of these nanoparticles. This work also gives a guideline for the optimum content of this nanomaterial in mortar and concrete to improve their performance.

2. Types and Production Methods of Nano-silica

Depending on its produced form, nano-silica has two types: powdery nano-silica and colloidal nano-silica (Biricik and Sarier 2014; Chithra et al. 2016). The SEM

* *Corresponding author*. E-mail address: mg.alhagri@gmail.com (M. G. Al-Hagri)
ISSN: 2548-0928 / DOI: https://doi.org/10.20528/cjcrl.2022.01.004

images of nano-silica in its two forms are presented in Fig. 1. The powdery NS shown in Fig. 1(a) is of an average size of 15 nm (Biricik and Sarier 2014), whereas, the average size of the colloidal NS shown in Fig. 1(b) is 7nm (Chithra et al. 2016). As it can be seen from the SEM images of NS, the particles can be available in a spherical shape. TEM images in diluted form of the two forms of dispersed nano-silica are shown in Fig. 2. As shown in the figure, NS particles are present in an agglomerated form with a number of linked particles. The figure also shows that the particle size and dispersion state of nano-silica vary over a wide range (Bolhassani and Samani 2015).

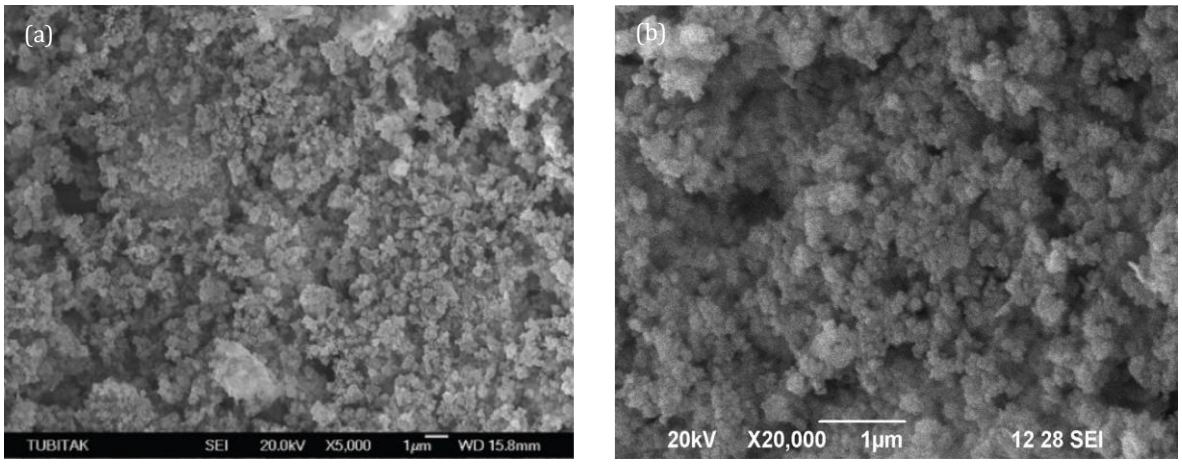

Fig. 1. SEM images of nano-silica: a) Powdery NS (Biricik and Sarier 2014); b) Colloidal NS (Chithra et al. 2016).

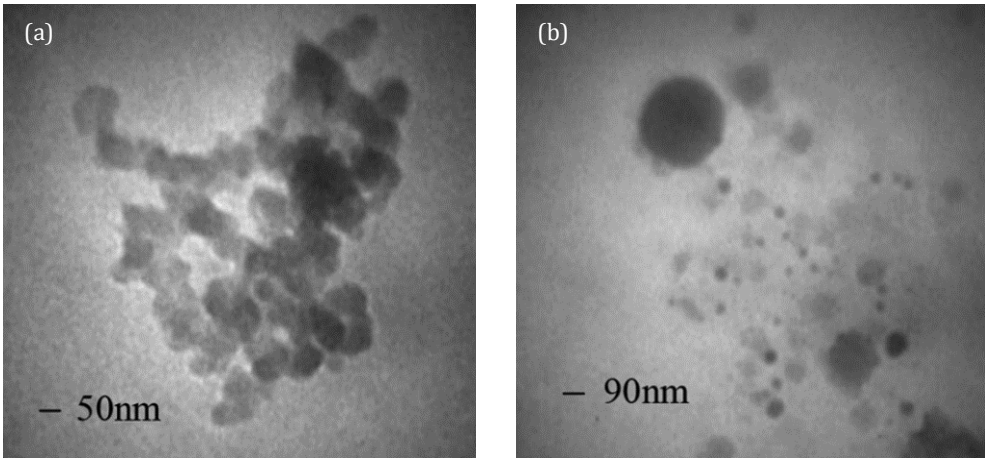

Fig. 2. TEM images of dispersed nano-silica in diluted form: a) Powdery NS; b) Colloidal NS (Bolhassani and Samani 2015).

The investigation of incorporating nano-silica into cementitious materials has become more common because of the successful results of using silica fume to improve the performance of cement-based materials and because of the ability of producing highly pure NS particles compared to silica fume (Bolhassani and Samani 2015). While silica fume, which is a by-product of the ferrosilicon industry, can be produced with a specific surface area (SSA) of 20 m^2/g and 90% purity (Bolhassani and Samani 2015; Li et al. 2017), nano-silica can be produced with a higher specific surface area ranging from 60 to over 600 m^2/g and with a purity up to 99.9% (Beigi et al. 2013; Bolhassani and Samani 2015; Givi et al. 2011, 2010; Jalal et al. 2015, 2012; Janković et al. 2016; Khanzadi et al. 2010; Li et al. 2004; Mohamed and Ragab 2014; Shebl et al. 2009). Due to this high surface area to volume ratio and since the pozzolanic reaction is related to the amount of surface area available for reaction (Givi et al. 2011; Shebl et al. 2009), nano-silica has high pozzolanic activity compared to micro-silica (Behfarnia and Salemi 2013; Ghafari et al. 2014; Givi et al. 2010; Huang et al. 2020; Ji 2005; Seifan et al. 2020). For these reasons, it has been found that nano-SiO_2 is much more effective in improving strength and durability and reducing permeability of cementitious composites than micro-silica, especially at early ages (Ardalan et al. 2017; Behfarnia and Salemi 2013; Bolhassani and Samani 2015; Givi et al. 2011; Jalal et al. 2012; Seifan et al. 2020; Zhang and Islam 2012). It should be mentioned that incorporation of a composition of both nano-SiO_2 and silica fume has been found to be more effective in improving different properties of cementitious composites than the individual use of either one of the two materials (Amin and Abu el-Hassan 2015; Ardalan et al. 2017; Arif et al. 2020; Bi et al. 2012; Jalal et al. 2015; Li et al. 2017; Maheswaran et al. 2013; Nili et al. 2010).

There are two commonly used commercial methods for nano-SiO_2 production; the neutralization of sodium silicate (water-glass or Na_2SiO_4) solutions with acid, such as sulfuric acid (the wet route or sol-gel process) and flame hydrolysis (the thermal route) (Kooshafar and Madani 2020; Lazaro et al. 2013, 2012; Quercia et al. 2013; Quercia and Brouwers 2010). However, because of the energy needed in the processes and the price of the raw materials, nano-SiO_2 produced by these two methods is expensive (Lazaro et al. 2013, 2012). Furthermore, due to the huge amount of CO_2 emitted during these processes, these methods are environmentally unfriendly (Lazaro et al. 2013). Researchers have been trying to overcome such problems through the development of new industrial, low cost, production processes. One example of such processes is the production of nano-SiO_2 by dissolving olivine in acid at low temperatures (50-95°C) (Lazaro et al. 2013, 2012). Using this method, nano-SiO_2 with primary particles of 10-25nm, a specific surface area of 100-400 m^2/g and an impurity content below 5% can be produced (Lazaro et al. 2013, 2012). However, the produced NS was noticed to be agglomerated in 3D chains leading to the reduction of the packing factor of the aggregate mix, and to have a lower pozzolanic activity compared to the standard micro-silica at the same replacement level (Lazaro et al. 2012; Quercia and Brouwers 2010). This process is a convenient alternative method to the existing one because olivine dissolution can be done in a low temperature, making this process cheaper (even cheaper than contemporary micro-silica (Quercia and Brouwers 2010)) and more environmentally friendly (Lazaro et al. 2013). Moreover, used olivine in nano-silica production can be a waste material (Lazaro et al. 2013). Low-cost methods also include the production of nano-SiO_2 from rice husk (Crucho et al. 2018; Mor et al. 2017), barley grain waste (Akhayere et al. 2019), Equisetum arvenses (Carneiro et al. 2015), Sorghum vulgare seed heads (Balamurugan and Saravanan 2012), fly ash (Manchanda et al. 2017) and waste glass powder (Asadi and Norouzbeigi 2018). The production of nano-silica using low-cost methods will reduce its price and lead to more production of nano-silica, leading to more use of it in the construction industry and other industries.

3. Advantages and Disadvantages of Incorporation of Nano-SiO_2 into Cement-based Materials

The effect of using nano-silica in improving mechanical, physical and microstructural properties of cement-based materials has been widely reported (Aggarwal et al. 2015; Arif et al. 2020; Behzadian and Shahrajabian 2019; Biricik and Sarier 2014; Givi et al. 2011; Haruehansapong et al. 2014; Lazaro et al. 2012; H. Li et al. 2004; Rashad 2014; Sikora et al. 2015; Zhang and Islam 2012). These reports have shown that nano-silica leads to significant enhancement in compressive, flexural strength, split tensile strength and elasticity modulus of mortar and concrete. As a result of the high reactivity of these nanoparticles, nano-SiO_2 accelerates the hydration process of dicalcium silicate (C_2S) and tricalcium silicate (C_3S) and increases the amount of calcium silicate hydrate produced in the matrix through intense reaction with crystals of $Ca(OH)_2$, which have adverse effects on strength and durability, leading to exceptional enhancement in different properties of cement-based materials (Aggarwal et al. 2015; Bahadori and Hosseini 2012; Behfarnia and Salemi 2013; Beigi et al. 2013; Biricik and Sarier 2014; Kewalramani and Syed 2018; Ngo et al. 2020; Niewiadomski et al. 2018; Senff et al. 2013; Singh et al. 2013; Zhuang and Chen 2019). Nano-silica addition also fills the voids and improves the microstructure of the final products leading to reduction in porosity and increase in density and in resistance to ion penetration and water permeability, and hence improve the durability (Amin and Abu el-Hassan 2015; Arif et al. 2020; Barbhuiya and Qureshi 2015; Behfarnia and Salemi 2013; Biricik and Sarier 2014; Givi et al. 2011; Kewalramani and Syed 2018; Lazaro et al. 2012; Liu et al. 2020; Quercia et al. 2014; Ying et al. 2017). It also reduces bleeding water, enhances the bond between aggregates and cement paste and increases the cohesiveness of mixtures in the fresh state (Aggarwal et al. 2015; Behfarnia and Salemi 2013; Biricik and Sarier 2014; Carmo et al. 2021; Ji 2005; Lazaro et al. 2012; Nima et al. 2011; Zhang and Islam 2012). Nano-silica has been proved to be beneficial in controlling the leaching of calcium, which is one of the main reasons for various types of concrete degradation (Bahadori and Hosseini 2012; Givi et al. 2011; Nima et al. 2011; Quercia et al. 2013; Singh et al. 2013). Furthermore, NS decreases the setting time of cement-based composites (Aggarwal et al. 2015; Behfarnia and Salemi 2013; Biricik and Sarier 2014; Choolaei et al. 2012; Givi et al. 2011; Rashad 2014; Senff et al. 2009; Zhang and Islam 2012; Zhuang and Chen 2019). The reduction in setting time of cement could increase the throughput of precast plants and also reduce formwork removal time and total time of construction leading to direct economic benefits (Jayapalan et al. 2013). In addition, replacement of cement with nano-SiO_2 should have a great effect on the environment through the considerable reduction of CO_2 emissions caused by cement production (Lazaro et al. 2013; Quercia and Brouwers 2010). Thus, by incorporating NS, cementitious composites with remarkable high performance can be produced (Lazaro et al. 2012).

Despite all the great effects of addition of silica nanoparticles to cement-based materials, use of nano-silica has also some drawbacks. Currently high price of various NS products available in the markets is one of the reasons that limit its commercial applications (Biricik and Sarier 2014). However, some latest studies have focused on solving such problem through developing new less energy consuming methods of production of NS, such as production of NS from olivine (Biricik and Sarier 2014; Lazaro et al. 2013, 2012; Quercia and Brouwers 2010). Furthermore, increasing NS amount more than a specific limit has reverse effects on different properties of cementitious materials due to agglomeration of NS particles and unsuitable dispersion of the nanoparticles (Amin and Abu el-Hassan 2015; Biricik and Sarier 2014; Quercia and Brouwers 2010). Inappropriate dispersion of NS in the mixture affects the rate and extent of hydration

of cement as well as other mechanical and physical properties (Biricik and Sarier 2014). For these reasons, some researchers have suggested to use small amount of NS (1.0-5.0 wt%) unless an appropriate method of dispersion is used (Biricik and Sarier 2014; Senff et al. 2009). Due to its high specific surface area that can absorb some of the water content, NS also reduces the workability of cementitious materials and increases water demands. Every added kilogram of NS requires 0.4 kilogram of water to preserve the same workability (Aggarwal et al. 2015; Al Ghabban et al. 2018; Amin and Abu el-Hassan 2015; Bahadori and Hosseini 2012; Bolhassani and Samani 2015; Givi et al. 2011; Niewiadomski et al. 2018; Rashad 2014; Senff et al. 2009; Siang Ng et al. 2020; Sikora et al. 2015; Singh et al. 2013; Zhuang and Chen 2019). In addition to the fact that the effect of application of NS into cement-based materials is not fully understood yet, due to the insufficient available data related to this topic.

4. Effect of Nano-SiO_2 on Different Properties of Cement-based Materials

Since the final performance of cement-based materials depends to a great deal on the strength assessments and permeability of such materials (Nazari and Riahi 2011a, 2011b), in this section, focus will be on the effect of nano-SiO_2 on the mechanical properties (compressive strength, split tensile strength and flexural strength) and permeability of mortar and concrete. Moreover, to have an idea about the effect of NS on the durability of cementitious composites, some of the main durability parameters have been discussed. In addition, to better understand the changes that happen in the cementitious materials due to the incorporation of nano-additives, the effect of such materials on the microstructural properties have been illustrated through evaluation of some examples of SEM images.

To better understand the effect of nano-silica on the mechanical properties and permeability of concrete and mortar, some examples from the literature have been discussed in this section. The gathered research results have been organized in terms of type of cement-based materials (first for concrete and then for mortar). For concrete, the effect of nano additives on the properties of plain concrete, self-compacting concrete (SCC) and concrete incorporating other additives such as silica fume (SF), fly ash (FA) and copper slag have been respectively discussed. The same has been done for the effect of nano additives on the properties of mortar.

4.1. Effect on mechanical properties

The main characteristic of cement-based materials are mechanical properties, since they directly express the performance of different structural members to the applied loads. Effect nano-SiO_2 on the mechanical properties depends to a great deal on the properties of the used nano-silica, such as specific surface area, particle size etc. (Givi et al. 2010; Haruehansapong et al. 2014). Results found on the literature on the effect of nano-silica on the mechanical properties of cement-based materials vary to some extents from one to another. However, results in some research works were observed to have some similarities. In general, the results show that the incorporation of SiO_2 nanoparticles into cement-based materials can significantly increase the overall compressive strength, split tensile strength and flexural strength at all ages.

Data collected from different research papers on the effect of NS on the compressive strength, split tensile strength and flexural strength of mortar and concrete materials are shown in Table 1**.** As shown in the table, researchers have applied different variables in their research to study the effect of NS on the mechanical properties of cementitious materials. While some researchers investigated the effect of NS on mechanical properties of plain mortar and concrete, some others investigated its effect on other types of cement mortar and concrete, such as mortar and concrete with their cement partially replaced with some other additive, such as silica fume (SF), fly ash (FA) and copper slag etc. The table also shows the optimum percentages of the replacement of cement with NS reported in different research work and their optimum effect on mechanical properties.

It's worth mentioning that when nano silica is incorporated in cement-based materials, the mix design is the same as for normal cement-based materials with one major different. Since nano-silica is usually used as a partial replacement of cement in the mixture, the content of cement is reduced by the chosen replacement percentage and nano-silica is added to the mixture by a weight equal to the replacement percentage. Another important point that should be taken into consideration in the mix design is that nano-silica dramatically reduces the workability of cement-based materials, as mentioned before. Thus, to have a desirable workability, the use an adequate amount of superplasticizer might be needed (Amin and Abu el-Hassan 2015; Chithra et al. 2016; Du et al. 2014). In addition, it has been found that superplasticizer can lead to a better distribution of the nanoparticles in the mixture (Behfarnia and Salemi 2013). Some authors suggested the premixing of the nanoparticles with some quantity of the required superplasticizer and water using a high-speed mixer for few minutes to help distribute the nanoparticles into the mixture (Amin and Abu el-Hassan 2015; Behfarnia and Salemi 2013). While some authors have premixed nanoparticles with the whole required quantity of water and superplasticizer (Behfarnia and Salemi 2013; Kooshafar and Madani 2020), some others have premixed them with only half of the quantity (Amin and Abu el-Hassan 2015). Some other authors such as (Chithra et al. 2016) have premixed nano-silica with 60% of the required water. The rest water quantity was mixed with superplasticizer. It should be noted that some other researchers such as (Du et al. 2014) have not premixed nano-silica with water, and instead, they directly added it to the mixer after mixing the dry materials and adding water to the mixer. Since this paper tries to determine the optimum content of nano-silica in mortar and concrete, only the type of cement-based material, the content of nano-silica used in each study and the optimum content of nano-silica in the related study are mentioned in Table 1.

Table 1. Optimum content of nano-silica in cementitious materials and enhancement percentage of the mechanical properties.

Reference	Mortar/ concrete	NS properties				Optimum content (wt%)	Enhancement in 28-day strength (%)		
		Size (nm)	SSA (m^2/g)	Form	Investigated contents (wt%)		Compressive strength	Split tensile strength	Flexural strength
Li et al. (2004)	mortar	15	-	-	3, 5, 10	10	26	-	-
Givi et al. (2010)	concrete	15	160	powder	0.5, 1, 1.5, 2	1	18.5	83.3	31.8
		80	560			1.5	12	72.2	22.7
Nili et al. (2010)	concrete	50	80	colloidal	1.5, 3, 4.5	4.5	22	-	-
Givi et al. (2011)	concrete	15	160	powder	0.5, 1, 1.5, 2	1	18.5	83.3	31.8
Nazari and Riahi (2011a)	concrete (self-compacting)	15	165	-	1, 2, 3, 4, 5	4	74.37	118.75	64.29
Oltulu and Şahin (2011)	mortar (1)	12	200	powder	0.5, 1.25, 2.5	1.25	11.77	-	-
Zhang and Li (2011)	concrete	10	640	-	1, 3	1	12.3	-	4.21
Ibrahim et al. (2012)	mortar	-	-	colloidal	2.5, 5, 7.5	7.5	37	-	22
Said et al. (2012)	concrete	35	-	colloidal	3, 6	6	25	-	-
Stefanidou and Papayianni (2012)	mortar	14	200	-	0.5, 1, 2, 5	2	15	-	6
Behfarnia and Salemi (2013)	concrete	20	220	-	3,5,7	5	30.1	-	-
Beigi et al. (2013)	concrete (self-compacting)	15	160	-	2, 4, 6	4	18	35	40
Oltulu and Şahin (2013)	mortar (2)	12	200	powder	0.5, 1.25, 2.5	1.25	19.24	-	-
Biricik and Sarier (2014)	mortar (3)	15	640	powder	5, 10	10	83.4	-	31.8
Ghafari et al. (2014)	concrete (4)	15	160	powder	1, 2, 3, 4	3	7.5	-	-
Haruehansapong et al. (2014)	mortar	12	200	-	3, 6, 9, 12	9	23.9	-	-
		20	90			9	52.9	-	-
		40	50			9	54.4	-	-
Shaikh et al (2014)	mortar	25	160	-	1, 2, 4, 6	2	14.29	-	-
Bolhassani and Samani (2015)	mortar	7-25	80 - 380	powder/ colloidal	0.5, 1.5, 3, 5, 7	7	13.1	-	-
Du et al. (2015)	concrete (5)	12.4	220	colloidal	1, 2	2	5.6	-	-
Li et al. (2015)	concrete (6)	20	-	-	0.5, 1, 1.5, 2	1	3.74	-	16.2
Madandoust et al. (2015)	mortar (self-compacting) (7)	15	200	-	1, 2, 3, 4, 5	4	15	-	-
Mohseni et al. (2015)	mortar (self-compacting) (7)	15	200	powder	1, 3, 5	3	7	-	-
Rong et al. (2015)	ultra-high-performance cementitious composites (8)	20	-	-	1, 3, 5	3	22	-	9
Chithra et al. (2016)	concrete (9)	5-40	-	colloidal	0.5, 1, 1.5, 2, 2.5, 3	2	18.2	25.4	36.5
Wu et al. (2016)	concrete (10)	5-35	160	-	0.5, 1, 1.5, 2	1	10	-	11

Ma and Zhu (2017)	concrete	<20	>600	powder	0.6, 1.2, 1.8	1.2	7.07	6.6	-
Ying et al. (2017)	concrete [11]	15 ± 5	-	colloidal	1, 2, 3	2	17	-	-
Al Ghabban et al. (2018)	concrete	40	-	-	1, 2, 3, 4	3	47.17	68.75	63.64
Niewiadomski et al. (2018)	concrete (self-compacting)	10–20	-	powder	0.5, 2, 4	4	8	-	(NS 0.5%) 4
Behzadian and Shahrajabian (2019)	concrete [12]	20-30	-	-	1, 3, 5	3	43.42	48.1	20.34
Arif et al. (2020)	concrete	17	640	-	2.5, 5, 7.5	5	8.5	9	(NS 2.5%) 12.5
Siang Ng et al. (2020)	mortar [13]	20-30	180–600	powder	1, 3, 5	3	38	-	19
Ngo et al. (2020)	concrete [14]	13	-	powder	0.5, 1, 1.5, 2, 2.5, 3	1.5	6.09	-	14.83
Seifan et al. (2020)	mortar	20	-	powder	5, 10, 15	5	31	22	-
Vivek et al. (2020)	concrete	-	202	-	1, 2, 3, 4	4	9.9	17.48	-

Notes:
(1) SF was used by 5 wt% of cement in all mixtures.
(2) FA was used by 15 wt% of cement in all mixtures.
(3) Mortar with good dispersion of NS was studied.
(4) Concrete incorporating SF of around 27 wt% of the total binder content in all mixtures.
(5) Light weight concrete.
(6) Ultra-high-performance concrete (contains silica flour, SF and FA).
(7) FA was used by 25 wt% of cement in all mixtures.
(8) FA was used by 35 wt% of cement in all mixtures.
(9) Concrete with copper slag as 40 wt% partial fine aggregate replacement in all mixtures.
(10) Ultra-high strength concrete (UHSC).
(11) Recycled aggregate concrete.
(12) Concrete incorporating 10 wt% of waste PET aggregates.
(13) FA was used by 30 wt% of the cement in all mixtures.
(14) High performance concrete (SF was used by 5 wt% of the cement in all mixtures.)

4.1.1. Effect of NS on compressive strength

NS effect on the compressive strength of mortar and concrete at different ages has been thoroughly reported in the literature. The results demonstrate that incorporation of NS into mortar and concrete can remarkably enhance their compressive strength at all curing ages. They also show that with the increase in NS content up to a specific limit in the mixture, its effect on the compressive strength increases. This limit is referred to as the optimum content. When the content of NS exceeds the optimum content, its effect starts to decrease. To understand the effect of NS on compressive strength of concrete and mortar at different ages some examples have been provided in this section. More examples can be found in the related references.

Nili et al. (2010) experimentally studied the effect of NS on the compressive strength of concrete. They reported the NS optimum content to be 4.5 wt%, which led to an enhancement in the 7-day, 28-day and 90-day compressive strength of around 20%, 22% and 7%, respectively. Their results also demonstrated that better effect was observed when both SF and NS were used in the same mix. Using 6 wt% SF and 1.5 wt% NS enhanced the 28-day compressive strength by about 29%. Behfarnia and Salemi (2013) found a maximum improvement in the compressive strength with the replacement of cement with 5.0 wt% NS. They reported that this content caused an increase of 15%, 30% and 45% in the 7, 28 and 120-day compressive strength, respectively. Beigi et al. (2013) stated that 2.0, 4.0 and 6.0 wt% NS content led to an increase of 3.0%, 18% and 17%, respectively in the compressive strength after 28 days of curing. Unremarkable difference in the effect of NS on the compressive strength was found for 4.0 wt% and 6.0 wt% content cases.

Nano-silica effect on the compressive strength of mortar at different ages has been also investigated by many researchers. Li et al. (2004) conducted an experimental study on the effect of nano-SiO_2 on compressive strength of plain mortar. They found that while NS of 5.0 wt% had better effect on the 7-day strength (20% higher than plain specimen) compared to 3.0 wt% NS, which only caused an increment of around 6%, higher content of NS (10 wt%) had the same effect as that of 5.0 wt%. However, in the case of 28-day compressive strength, 10 wt% had higher effect (26% higher than plain concrete) on compressive strength compared to 3.0 wt% and 5.0 wt% NS (13.8% and 17%, respectively). Nano-silica effect on the compressive strength of self-compacting mortar was also studied by some researchers such as Madandoust et al. (2015) and Mohseni et al. (2015). In both research work, the authors investigated the effect of NS on the properties of self-compacting mortar incorporating 25% fly ash by weight of cement. While Madandoust et al. (2015) reported that the optimum replacement of cement with NS was 4.0 wt%, and that it increased the 28-day compressive strength by 15%, Mohseni et al. (2015) reported it to be 3.0 wt%, and that it resulted in an improvement in the strength of about 28%, 7% and 15% after 7, 28 and 90 days of curing, respectively. A possible reason for the difference between the optimum replacement content found in these two research work is that Madandoust et al. (2015) have investigated more replacement percentages compared to Mohseni et al. (2015), who haven't investigated the effect of 4 wt% NS.

As can be noticed from the literature review above, replacement of cement with nano-SiO_2 up to the optimum percentage increases the compressive strength of cement-based materials. However, when more content of NS is used, its effect starts to reduce proportional to its content. The improvement in the strength of cementitious materials might be attributed to the behavior of nano-silica as a nano-filler to improve the microstructure and reduce the porosity of the mixture by recovering its particle packing density, as well as an activator to accelerate the pozzolanic reaction (Ghafari et al. 2014; Haruehansapong et al. 2014; Jalal et al. 2012; Kawashima et al. 2013; Siang Ng et al. 2020; Vivek et al. 2020). As a result of its high reactivity and high content of SiO2, NS can accelerate the hydration process of cement paste causing faster consuming of Ca(OH)2, formed mainly at early ages of the cement hydration process (Ghafari et al. 2014; Givi et al. 2011, 2010; Peng-kun Hou et al. 2013; Pengkun Hou et al. 2013; Niewiadomski et al. 2018). This leads to more production of C-S-H gel (Al Ghabban et al. 2018; Givi et al. 2011, 2010; Haruehansapong et al. 2014; Kawashima et al. 2013; Niewiadomski et al. 2018). On the other hand, reduction of strength that happens after exceeding the optimum content could be related to that the quantity of silica nanoparticles that exist in the mix is more than the quantity needed to react with the liberated Ca(OH)2 particles leading to reduction in strength since it partially replaces the binding materials but doesn't contribute to the strength (Ghafari et al. 2014; Givi et al. 2011, 2010). In addition, large content of NS increases the weak zone in the concrete (Behfarnia and Salemi 2013; Ghafari et al. 2014; Seifan et al. 2020; Siang Ng et al. 2020). Reduction in the strength might also happen due to the agglomeration and unsuitable dispersion of silica nanoparticles (Behfarnia and Salemi 2013; Bolhassani and Samani 2015; Ghafari et al. 2014; Seifan et al. 2020). Another reason for the strength reduction might be the insufficient workability, since water available for lubrication is insufficient allowing free movement of particles (Ghafari et al. 2014).

As can be seen from Table 1, different optimum values for the percentage of replacing cement with nano-SiO2 to enhance the compressive strength and other mechanical properties of mortar and concrete have been reported. Finding such optimum content accurately is of a great difficulty, due to the existence of various factors that play role in determining such value and due to the lack of data related to this topic. However, to have an idea about the approximate optimum content of NS, a comparison between all the collected optimum values, regardless of the different variables, can be of a significant help. As can also be seen from the table, mostly the same optimum value has been found for different mechanical properties. It is also obvious that the most investigated mechanical property is the compressive strength. Hence, to make the comparison easier, the collected data related the effect of NS on the compressive strength is shown graphically in Fig. 3. Comparing data in Table 1 and Fig. 3, it's clear that most authors have reported their optimum content to be between 1.0 wt% to 5.0 wt%. Hence, it can be said that the optimum content of NS to enhance different mechanical properties of mortar and concrete is between 1.0-5.0 wt%.

4.1.2. Effect of NS on split tensile strength

Nano-silica effect on the split tensile strength of mortar and concrete has been studied by some researchers. The results show that, similar to the compressive strength case, with the increase of NS content up to the optimum value, its effect on the split tensile strength increases and then starts to decrease. This behavior can be related to the same reasons stated above for the compressive strength. The results also demonstrate that NS can remarkably increase the tensile strength of cementitious composites, and hence solve the problem of low tensile strength related to such materials.

Givi et al. (2010) evaluated the effect of NS of 15nm and 80nm average particle sizes on split tensile strength of plain concrete. They observed that while smaller particle size of NS (15nm) had better performance at early ages, NS with bigger particles size (80nm) had better performance at later ages. The results showed that NS optimum content was 1.0 wt% in the case of the finer NS (15nm) and 1.5 wt% in the case of the courser one (80nm). They also showed that while the optimum content in the case of 15nm NS led to 100%, 83% and 56.5% enhancement in the 7th, 28th and 90th days split tensile strength, respectively, the optimum content in the case of 80nm NS resulted in 93.33%, 72.22% and 100% enhancement. The effect of NS on split tensile strength of SCC was studied by Beigi et al. (2013), who showed that 2.0, 4.0 and 6.0 wt% NS content caused an increase of 7.5%, 35% and 35% in the 28-day split tensile strength, respectively. They also reported that similar to the case of compressive strength the difference between the effect of 4.0 wt% NS and 6.0 wt% NS was negligible. Similarly, Chithra et al. (2016) stated that the development of split tensile strength was similar to the development of compressive strength at all curing ages. The results of their research showed an increment of 21.4%, 25.4% and 25% in the 7, 28 and 90-day strength of concrete incorporating copper slag as 40% by weight of fine aggregate was observed for 2.0 wt% NS content.

As stated before, the optimum content of NS to enhance different mechanical properties is to be taken the same. However, the enhancement percentage of split tensile strength due to the incorporation of the optimum content of NS was observed to be generally higher than that of the compressive strength in different references (see Table 1).

4.1.3. Effect of NS on flexural strength

The effect of nano-SiO_2 on the flexural strength of mortar and concrete has shown a similar trend to that of the compressive strength and split tensile strength. Givi et al. (2010) reported that smaller particles of NS tend to have better effect on flexural strength at early ages of curing while bigger ones tend to have more pronounce effect at later ages. They reported that 1.0 wt% NS of 15nm particle size improved the flexural strength by around 31%, 32% and 32% after 7, 28 and 90 curing days, respectively, compared to 17%, 16% and 45% in

the case of NS of 80nm particle size. However, the optimum content in the case of 80nm (i.e. 1.5 wt%) resulted in 32.8%, 22.7% and 55.3% enhancement in the 7, 28 and 90-day flexural strength, respectively. In their work, Beigi et al. (2013) studied the effect of nano-SiO_2 on flexural strength of SCC and showed that the optimum content (4.0 wt%) increased the strength by 40%. They also reported that while 2 wt% NS only increased the strength by 7.0%, 6.0 wt% NS had strength close to that of the optimum content (39%). Although NS was reported to enhance the flexural strength of concrete remarkably, some authors reported it to only have a small effect on the flexural strength. For instance, Zhang and Li (2011) stated that the optimum content of NS (1.0 wt%) led to only 4.21% increment in the 28-day flexural strength. Moreover, by increasing NS content in the mixture up to 3 wt%, its effect on the strength was found to be even much less. 3.0 wt% NS was found to reduce the flexural strength of concrete by -1.87% compared to the plain concrete.

Nano-silica effect on the flexural strength of mortar has been also investigated by some researchers. Li et al. (2004) showed that by incorporating NS into mortar, the flexural strength could be remarkably improved. They reported that 5.0 wt% NS, which represented the optimum content in their research, improved the flexural strength of mortar by around 27%. These results are close to what Ibrahim et al. (2012) reported in their research. They stated that 7.5 wt% increased the flexural strength by 22%. On the other hand, some other researchers such as Stefanidou and Papayianni (2012) reported an unimportant effect of NS on the flexural strength. They stated that the optimum content (i.e. 2 wt%) caused an enhancement in the flexural strength of only 6%. The inconsistencies found in some references confirm the need for further research.

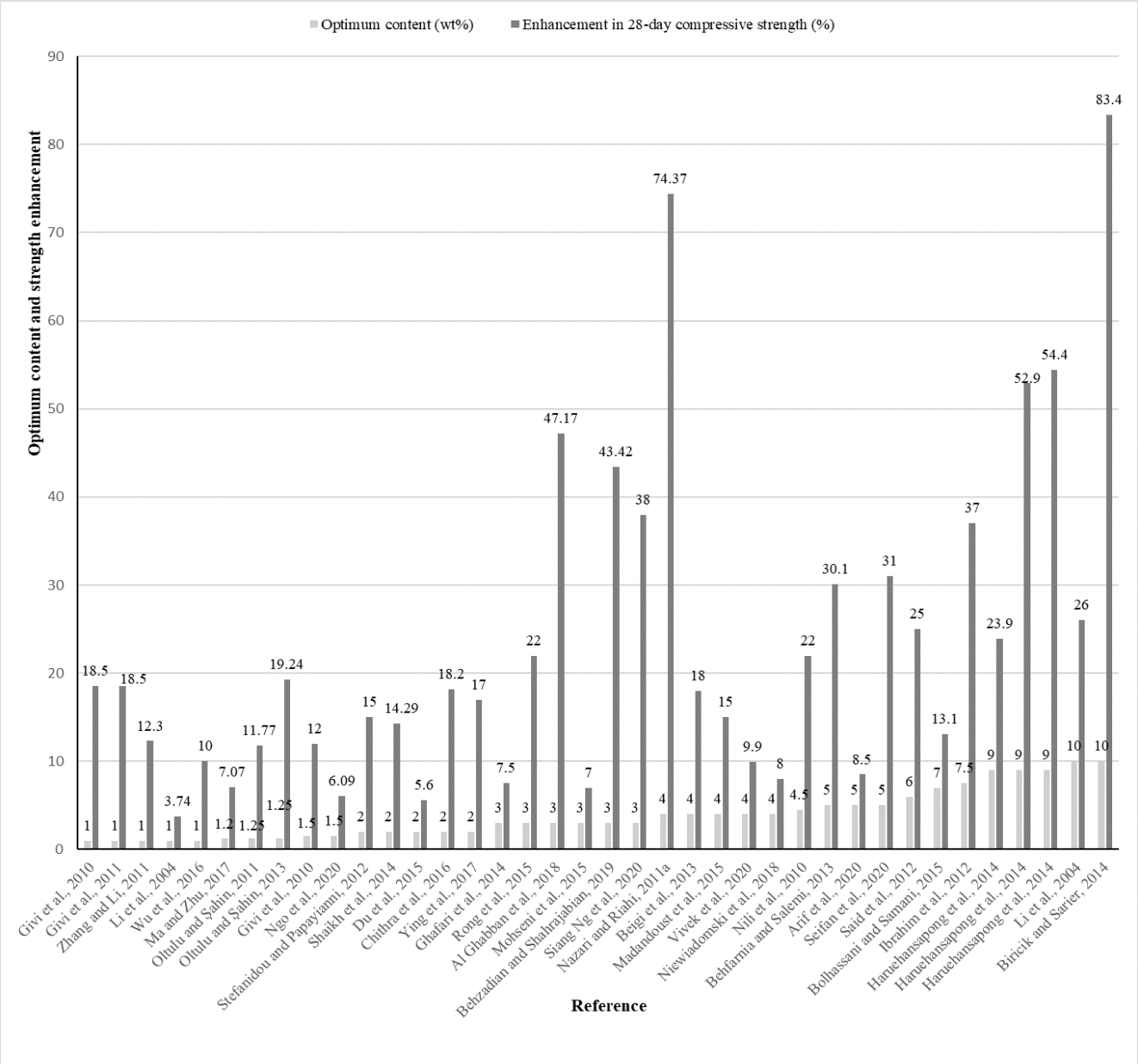

Fig. 3. Different optimum contents of NS to improve the compressive strength of cement-based materials and the related improvement percentage.

4.2. Effect on durability

Nano-silica has been found to improve the durability of cementitious materials due to its high pozzolanic reactivity and its effect on improving the microstructure through increasing compactness and reducing porosity. It also improves the hydration stability and works as a nucleus to bond strongly with C-S-H gel particles (Ashwini and Srinivasa Rao 2021; Du et al. 2014; Farajzadehha et al. 2020; Kooshafar and Madani 2020; Li et al. 2017; Shafiq et al. 2019; Sharaky et al. 2019; Vaz-Ramos et al. 2019). Durability can be evaluated using many parameters, such as permeability (water permeability, chloride permeability etc.), freeze and thaw resistance, wet and dry resistance, fire resistance, high temperature resistance, chemical attacks resistance (sulfate attack, $MgCl_2$ attack, $CaCl_2$ attack etc.), alkali-silica reaction, abrasion resistance, pore structure analysis etc. In this section, the effect of NS on the durability of cement-based materilas is evaluated through discussing permeability, freeze and thaw resistance, high temperature resistance, fire resistance and sulfate attack resistance.

4.2.1. Permeability

Permeability of cement-based products can be defined as the penetration of external substances, such as liquids, gases, harmful ions etc., into a body of such product under a constant pressure gradient (Nazari and Riahi 2011c; Zhang and Li 2011). This property mainly depends on the geometric arrangement and properties of the different components of the materials. Permeability is directly affected by the porosity and solidity of the hydrated product (Jalal 2012; Khoshakhlagh et al. 2012; Nazari and Riahi 2011a). Permeability can be evaluated by many parameters. However, in this section the effect of incorporating silica nanoparticles on the permeability of concrete and mortar are illustrated through studying some of the main parameters; namely percentage of water absorption, chloride permeability, capillary water absorption, water permeability coefficient and gas permeability coefficient.

Silica nanoparticles have been proved to enhance the microstructure of concrete and mortar to a great deal, and accordingly increase its resistance to penetration of different materials (water, chloride, gas etc.) (Aggarwal et al. 2015; Bahadori and Hosseini 2012; Ghafari et al. 2014; Givi et al. 2011; Madandoust et al. 2015; Nili et al. 2010; Quercia et al. 2014; Said et al. 2012; Sikora et al. 2015). It has been noticed that, similar to the effect of NS on the mechanical properties, the permeability of cementitious composites generally decreases with the increase of NS content in the mixture up to the optimum content and then starts to increase.

Table 2 presents some of the published data collected from different references on the effect of nano-SiO_2 on the reduction of different parameters of permeability. The table also shows the optimum percentages for partial cement replacement with NS to reduce the permeability of mortar and concrete and the related reduction percentage of different parameters of permeability. As can be seen from the table, generally, the same optimum content is applicable for different permeability measurements. Comparing Table 1 and Table 2, it can be observed that in some references this optimum content is different from that of the mechanical properties. It should be mentioned that different properties of NS used in the permeability tests are as given in Table 1. It can be realized from Table 2 that the most researched permeability parameters are water absorption and chloride permeability.

Table 2. Optimum content of nano-SiO_2 in cementitious materials for permeability.

Reference	Investigated contents (wt%)	NS optimum content (wt%)	Decrease percentage (%)				
			Water absorption	Chloride permeability	Capillary water absorption	Water permeability coefficient	Gas permeability coefficient
Nili et al. (2010)	1.5, 3, 4.5	3	-	-	40	-	-
Givi et al. (2011)	0.5,1, 1.5,2	2	21.25	-	-	51.4	-
Nazari and Riahi (2011a)	1, 2, 3, 4, 5	4	72.75	-	-	-	-
Oltulu and Şahin (2011)	0.5, 1.25, 2.5	1.25	-	-	15.79	-	-
Zhang and Li (2011)	1, 3	1	-	18.04	-	-	-
Said et al. (2012)	3, 6	3	-	70	-	-	-
Behfarnia and Salemi (2013)	3,5,7	7	23.01	-	-	-	-
Oltulu and Şahin (2013)	0.5, 1.25, 2.5	1.25	-	-	10	-	-
Ghafari et al. (2014)	0.5, 1, 1.5, 2, 2.5, 3	3	33.33	-	-	-	31.9
Madandoust et al. (2015)	1, 2, 3, 4, 5	3	(NS 4%) 6	52	57	-	-
Mohseni et al. (2015)	1, 3, 5	3	3	52	-	-	-
Chithra et al. (2016)	0.5, 1, 1.5, 2, 2.5, 3	2	34.8	38.6	-	-	-
Ying et al. (2017)	1, 2, 3	2	-	26	-	-	-
Al Ghabban et al. (2018)	1, 2, 3, 4	3	22	-	-	-	-

Numerous researchers have investigated nano-silica effect on the reduction of water absorption of cement mortar and concrete. Water absorption is considered to be one the primary tests in evaluating cement-based materials durability. In this test, water penetrates into the matrix voids and saturates them (Bahadori and Hosseini 2012). Percentage of water absorption is an indicator of the porosity volume of the hardened cement-based material (Givi et al. 2011). To have a better understating about the effect of nano-SiO_2 on the reduction of water absorption of mortar and concrete, some examples have been provided. Givi et al. (2011) experimentally evaluated the changes that occur in the water absorption of concrete due to the use of nano-silica. They found that partial cement replacement with nano-SiO_2 led to reduction in the water absorption proportional to the content of NS. When 2.0 wt% NS was used, water absorption was found to decrease by about 1%, 21% and 21% for 7, 28 and 90 curing days, respectively. The effect was observed to increase as the age of the test specimens increased up to 28 days. No difference was observed between the effect of nano-SiO_2 on the 28-day and 90-day waster absorption. Ghafari et al. (2014) demonstrated that incorporating both silica fume and NS together decreased water absorption as the nano-silica replacement percentage increased up to 3.0 wt% and then started to increase. The optimum content was stated to cause a reduction in the water absorption of around 33%. Such behavior has been also reported by Nazari and Riahi (2011a).

Nano-silica effect on the water absorption of mortar has been studied by Madandoust et al. (2015) and Mohseni et al. (2015). They demonstrated that NS positive effect on the water absorption increased in proportion to the increase in its content in the mixture up to the optimum value and then started to decrease. However, they found that NS led to unremarkable reduction in the water absorption of such mortars. While Madandoust et al. (2015) reported a maximum reduction in the water absorption of around 6%, which was observed for 4.0 wt% NS, Mohseni et al. (2015) reported it as 3% and was observed for 3.0 wt% NS. Moreover, Madandoust et al. (2015) stated that higher content of NS caused a revere effect on the water absorption. They stated that 5.0 wt% NS led to more water absorption than that of the reference samples. NS effect on the water absorption of mortar and concrete is graphically shown in Fig. 4(a). The figure. also presents the optimum contents of NS to reduce water absorption collected from different references and the related decrement percentages.

Permeability of cement-based materials has been also evaluated by studying chloride ion penetration. Chloride permeability has been recognized as a main inherent property influencing the durability of reinforced concrete (He and Shi 2008). The results of different research work conducted on the effect of NS on the chloride permeability of concrete and mortar showed that NS had an important potential to increase resistance to chloride ion penetration. Zhang and Li (2011) conducted an experimental investigation on the effect of silica nanoparticles on the chloride permeability of plain concrete. They demonstrated that 1.0 wt% and 3.0 wt% NS could reduce chloride permeability by around 18% and 10%, respectively. Similarly, Said et al. (2012) confirmed that the least chloride permeability in plain concrete was observed in samples incorporating 3.0 wt% NS. This content was found to reduce chloride permeability by 70%. Madandoust et al. (2015) researched the effect of NS on the chloride permeability of self-compacting mortar incorporating a constant amount of FA in all the mixes. They showed that NS incorporation resulted in a significant reduction in the chloride penetration for all the investigated percentages (1.0-5.0 wt%). The best performance was observed for 3.0 wt% NS, which led to a reduction in the permeability of 52%. Similar results were also reported by Mohseni et al. (2015). The optimum contents for the incorporation of NS into cement mortar and concrete to reduce their chloride permeability are shown in Fig. 4(b). The figure also presents the decrement percentage in chloride permeability caused by such contents.

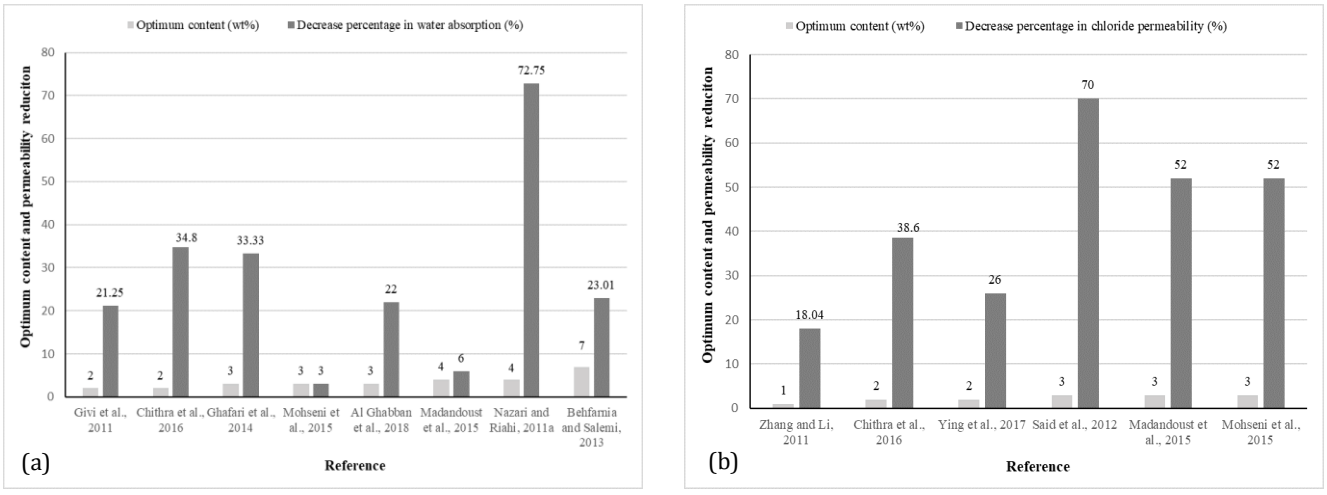

Fig. 4. (a) Different optimum contents of NS to reduce the water absorption; and (b) the chloride permeability of cementitious materials and the related decrease percentage.

Permeability have been also evaluated through finding capillary water absorption. Capillary water absorption is used to estimate the coefficient of water absorption due to the capillary action. In this test samples are partially immersed in water (Madandoust et al. 2015). Results of previous research showed that NS incorporation into cement-based materials could lead to an important reduction in their capillary waster absorption. Nili et al. (2010) demonstrated that the capillary water absorption of concrete got reduced up to about 40% with the increase in the content of NS up to 3.0 wt%. However, higher content of NS (4.5 wt%) was observed not to cause much difference in the capillary water absorption compared to 3.0 wt% NS. Oltulu and Şahin (2011) investigated the effect of nano-SiO_2 on the capillary water absorption of mortar containing SF as 5.0 wt% of cement in all mixtures. The outcomes of their investigation showed that the capillary water absorption got reduced with the increase in the content of NS up to 1.25 wt% and then started to increase. When 1.25 wt% NS was used, the capillary water absorption was found to reduce by around 16% compared to the reference mortar.

Permeability has also been studied by finding water permeability coefficient and gas permeability coefficient of cement-based materials. However, the effect of nano-silica on these two parameters hasn't been sufficiently reported. Water permeability coefficient is a measure of permeability of water in cementitious materials (Nazari and Riahi 2011a). Givi et al. (2011) showed that partial cement replacement with nano-SiO_2 decreased the coefficient of water absorption of plain concrete. This effect was found to increase as the replacement percentage increased. The best results were observed in samples containing the highest investigated replacement percentage (i.e., 2.0 wt%). In this case a reduction in the coefficient of water absorption of around 8%, 51% and 30% at 7, 28 and 90 curing days, respectively, was observed. Gas permeability is primarily related to the percentage and proportion of the open porosity of the hydrated paste and the aggregates in the mixtures (Ghafari et al. 2014). Results reported by Ghafari et al. (2014) indicated that all mixtures incorporating NS (1.0, 2.0, 3.0 and 4.0 wt%) had lower gas permeability coefficient compared to the control samples. It was found that incorporation of 1.0, 2.0, 3.0 and 4.0 wt% NS decreased the coefficient of gas permeability of concrete containing copper slag by 7.5%, 24.2%, 31.9% and 25.7%, respectively.

Since the optimum value to reduce the different permeability parameters was found to be mostly the same, and comparing the results in Fig. 4 and Table 2, it can be said that the optimum content of nano-SiO_2 to reduce the permeability of the concrete and mortar is around 1.0-4.0 wt%. However, to find the overall optimum replacement percentage of cement with NS, we should compare the different obtained optimum values for both the improvement of mechanical properties and the reduction of permeability. Since the optimum content of NS for the improvement of mechanical properties was found to be 1.0-5.0 wt%, and the optimum content for permeability reduction was found to be 1.0-4.0 wt%, it can be said that to get better performance in different properties of concrete and mortar, the content of NS should be 1.0-4.0% by weight of cement. This result is close to what Biricik and Sarier (2014) recommended. They sated that unless a good dispersion of nano-silica particles in the mixture is provided, the content of NS should be between 1.0-5.0 wt%.

4.2.2. Freeze and thaw resistance

Freeze and thaw is a critical problem that causes deterioration of cementitious materials, such as cracking and surface scaling. Freeze and thaw results in a remarkable adverse effects on permeability and mechanical properties of cementitious composites (Li et al. 2020). Nano-silica has been found to improve freeze and thaw resistance of cement-based materials. Ashwini and Srinivasa Rao (2021) investigated the effect of incorporation of 3% nano-silica and 15% alccofine by weight of cement on the freeze and thaw resistance of concrete. Their results revealed that concretes incorporating these additives had lower weight loss, reduction in compressive strength, reduction in density, reduction in ultrasonic pulse velocity and dynamic modulus of elasticity than normal concrete. Zhang et al. (2021) investigated the influence of NS on the freeze and thaw resistance of concrete containing coal fly ash. They found that low percentage of NS (up to 3 wt%) increased the freeze and thaw resistance of concrete remarkably. Higher content of NS showed a reverse effect on the freeze and thaw resistance. The optimum content was found to be 2 wt%. Zhao et al. (2021) conducted an experimental study on the effect of NS on the durability of concrete subjected to freeze and thaw and dry and wet cycles along with $CACl_2$ attack. They found that nano-silica had a great effect on improving the environment resistance of concrete. 1 wt% nano-silica was found to be the optimum content to enhance durability. 1 wt% NS reduced the loss in mass, compressive strength and flexural strength by around 40%, 35%, 22%, respectively, compared to reference concrete, and increased the relative dynamic elastic modulus by around 10%. Shahrajabian and Behfarnia (2018) reported that nano-silica increased the freeze and thaw resistance of alkali-activated slag concrete. They found that smaller content of nano-silica performed marginally better than higher content. Behfarnia and Salemi (2013) studied the effect of nano-silica on compressive strength, mass loss, water permeability and change in length of concrete subjected to a number of freeze and thaw cycles. Their results indicated that nano-silica improved the frost resistance of concrete due to more compacted microstructure in the presence of nano additives.

4.2.3. High temperature resistance

High temperature has a great impact on the properties of cement-based materials. It leads to irreversible changes and a probability of total failure. Elevated temperature results in a sharp reduction in the performance of cement-based materials as the temperature increases (Ibrahim 2017; Sikora et al.

2018). One method to increase the high temperature resistance of cementitious materials is through the use of nanoparticle. Nano-silica has been found to reduce the bad effects of high temperature on strength of cementitious materials. Elkady et al. (2019) studied the effect of 1.5, 3 and 4.5 wt% nano-silica on the compressive strength and bond strength of concrete subjected an indirect elevated temperature of 200 to 600°C. Their results have proved that nano-silica can increase the bond strength of concrete and reduce the lost in strength due to high temperature. Their results showed that while 3 wt% nano-silica was the optimum content for concrete subjected to room temperature, 1.5 wt% NS behaved better when concrete was exposed to a temperature of 600°C. Results also revealed that high percentages of nano-SiO_2 had better mechanical properties than low percentages when the temperatures was between 200°C and 400°C. Reddy Babu et al. (2019) showed that NS increased the resistance of mortar to elevated temperature by up to 94% when 10 wt% NS was used. El-Gamal et al. (2018) reported that NS showed better high temperature resistance than normal concrete. 2 wt% nano-silica was found to be the optimum content to increase the high temperature resistance of cement pastes. Results revealed that as the temperature increased, the effect of silica nanoparticles on high temperature resistance decreased. Horszczaruk et al. (2017) studied the effect of NS (1-5 wt%) on properties of mortar containing different types of aggregates and subjected to high temperature (up to 800°C). The results showed that incorporation of NS up to 3 wt% improved the resistance to high temperature of a range up to 200°C. However, for higher temperatures its effect was less pronounced and not important. Their results also revealed that the effect of NS depended to a great extent on the type of aggregates used. Ibrahim (2017) reported a better residual strength of NS based modified concrete compared to normal concrete. Heikal et al. (2015) stated that the effect of nano-silica on high temperature resistance increased with the use of superplasticizer. Bastami et al. (2014) investigated the effect of high temperature (up to 800°C) on the mechanical strength, spalling, and mass loss of high strength concrete incorporating NS. Their research revealed that use of NS could importantly increase the residual compressive strength and tensile strength, and reduce the spalling and mass loss of concrete.

4.2.4. Fire resistance

Fire is considered to be one of the most severe conditions that a building might be subjected to (Mussa et al. 2021). NS has been reported to have a good effect on the fire resistance of cement-based materials. Mussa et al. (2021) studied the fire resistance of high-volume fly ash RC slab incorporating 2.5 wt% NS. They found that structural members with superior fire resistance could be produced with the incorporating of NS. Nano silica incorporated RC slab was found to have a better thermal conductivity and a higher residual compressive strength than plain RC slab. Tobbala (2021) evaluated the fire influence on compressive strength of concrete incorporating NS. Their results revealed that concrete incorporating NS had good fire resistance compared to normal concrete. 1, 2 and 3 wt% NS was observed to increase the residual compressive strength by around 28, 33 and 48%, respectively. Vaz-Ramos et al. (2019) studied the influence of NS on thermal conductivity of mortar in order to evaluate its effect on fire resistance of cementitious composites. The results showed that NS resulted in a decrease in the thermal conductivity of mortar, which was related to evaporation of free water. High temperature was found to reduce the effect of NS on thermal conductivity of mortar by around 50%. NS was concluded to have the potential to increase fire resistance of cement-based materials. Ibrahim et al. (2012) evaluated the fire resistance of cement mortar containing high-volume fly ash and nano-silica subjected to high temperature. NS led to a higher residual mechanical strength and a less pore size distribution than normal concrete. NS effect on the residual compressive and flexural strengths was found to decrease remarkably as the temperature increased from 400°C to 700°C.

4.2.5. Sulfate attack resistance

Chemical attacks can have a great impact on the overall performance of cement-based materials, since they cause spalling and corrosion. Chemical attacks usually happen to structures exposed to marine environments (Li et al. 2020). Nano silica has been found to increase the resistance of cementitious composites to chemical attacks. One of the most commonly found chemical attack is the sulfate attack. Huang et al. (2020) investigated the impact of NS utilization on the sulfate attack resistance of mortar. They evaluated the sulfate attack impact by means of linear expansion, loss in strength and mass. The results indicated that NS increased the resistance to sulfate attack through the refinement of pores and the reduction of pore connectivity. The effect of NS was reported to be more pronounced in higher content (up to 5 wt%) and in bigger average particle size of NS. Reddy Babu et al. (2019) researched the effect of nano-SiO_2 on the resistance of mortar to magnesium sulfate ($MgSO_4$). They observed that nano-SiO_2 showed better durability performance under chemical attacks than normal concrete. Vargas et al. (2018) conducted an experimental study to evaluate the influence of NS on the durability performance of light weight concrete subjected to magnesium sulfate attack. They reported a higher resistance to the sulfate attack due to the use of NS. However, they found that chemical compositions and porosity of lightweight concrete are the main parameters in defining the durability performance of light weight concrete. Li et al. (2017) found that nano-silica increased the resistance of mortar to sulfate attack. Results revealed that NS reduced the loss in strength due to sulfate attack. This reduction was found to increase as the percentage of NS increased. The results showed that a combination of nano-silica and silica fume increased the resistance of mortar to sulfate attack more than the single use of eighter one of them.

4.3. Effect on microstructural properties

Many reports have been published on the effect of NS on the microstructural properties of cementitious composites. The reports have shown that nano-silica incorporation can greatly improve the microstructure of cementitious materials resulting in a significant reduction in the permeability and an important enhancement in the mechanical and durability properties (Al Ghabban et al. 2018; Arif et al. 2020; Bahadori and Hosseini 2012; Choolaei et al. 2012; Gaitero et al. 2008; He and Shi 2008; Jalal et al. 2012; Ji 2005; Kawashima et al. 2013; Liu et al. 2020; Ma and Zhu 2017; Quercia et al. 2014; Rong et al. 2015). Tests conducted to investigate the microstructural properties have shown that incorporating nano-SiO_2 into cement-based materials results in denser and more compact products (Ardalan et al. 2017; Arif et al. 2020; Behzadian and Shahrajabian 2019; He and Shi 2008; Khalaf et al. 2020; Ma and Zhu 2017). The effect of NS on improving the microstructure of cementitious composites may be ascribed to the following; NS has the ability as a nano-filler to reduce the porosity and fill the voids that exist in the structure of C-S-H gel, leading to a denser matrix (Aggarwal et al. 2015; Bahadori and Hosseini 2012; Cassar et al. 2003; Choolaei et al. 2012; Givi et al. 2011; He and Shi 2008; Jalal et al. 2015, 2012; Ji 2005; Khalaf et al. 2020; Liu et al. 2020; Quercia et al. 2013; Senff et al. 2009; Singh et al. 2013; Zhuang and Chen 2019). Moreover, because of the great pozzolanic reaction and the high content of SiO_2 of nano-silica, it can behave as an activator to accelerate the hydration of cement paste and react with $Ca(OH)_2$ leading to more production of C-S-H products (Aggarwal et al. 2015; Ardalan et al. 2017; Bahadori and Hosseini 2012; Choolaei et al. 2012; Gaitero et al. 2008; He and Shi 2008; Pengkun Hou et al. 2013; Jalal et al. 2015; Ma and Zhu 2017; Reches 2018; Senff et al. 2009; Zhuang and Chen 2019). Pengkun Hou et al. (2013) stated that low stiffness C-S-H products decrease and high-stiffness C-S-H products increase by the incorporation of NS. Crystals of $Ca(OH)_2$, which are hexagonal type of crystals, are located in the ITZ between aggregates and cement paste. These crystals have bad effect on the performance of cement-based materials. Addition of SiO_2 nanoparticle reduces these products and makes the ITZ denser and more compact and improves the overall characteristics of this zone (Ardalan et al. 2017; Bahadori and Hosseini 2012; Du et al. 2015; Jalal et al. 2015; Ji 2005; Said et al. 2012). Additionally, NS can modify the C-S-H internal structure by increasing the silicate chains length (Aggarwal et al. 2015; Cassar et al. 2003; Pengkun Hou et al. 2013). These reasons result in a more stable and more strongly bonded cement paste (Pengkun Hou et al. 2013). It should be mentioned that the positive effect of NS on microstructural properties of cementitious materials increases with the increase in the content of NS up to the optimum value and then starts to decrease, due to the reasons stated before.

Comparing the SEM images of samples with and without nanomaterials can give us a clear idea about the changes that happen in the microstructure of cementitious materials due to the use of nanoparticles. SEM observations of nano-SiO_2 incorporating concrete and mortar have been investigated by a number of researchers (Ardalan et al. 2017; Arif et al. 2020; Biricik and Sarier 2014; Haruehansapong et al. 2014). Fig. 5 presents an example of the SEM images of cement mortar at curing age of 7 days with and without nanoparticles. The used NS was of 40nm particle size and was used as 9.0 wt% replacement of cement, which resulted in the maximum enhancement in the mechanical properties in the related refence (Haruehansapong et al. 2014) (see Table 1). The figure reveals that in the case of the control sample, C-S-H products exist in stand-alone clusters form. These products appear to be lapped and linked by numerous needle hydrates. Whereas, in the sample containing nano-silica, porosity has reduced remarkably, the microstructure has become much denser and more compact. It can be also observed from the figure that by incorporating nano-silica into the mix, the quantity of $Ca(OH)_2$ has reduced and the quantity of C-S-H has increased sharply. The SEM results support the previously concluded findings about the effect of nano-silica on the mechanical properties and permeability and also illustrate the behavior of nano-silica. Similar results were also observed by Biricik and Sarier (2014), who found a heterogeneous dispersion of C-S-H gel and $Ca(OH)_2$ (CH) crystals and needle-like ettringite crystals in the reference mortar after 7 days of curing. Some micro cracks were also observed in the structure. They reported that incorporation of 10 wt% nano-SiO_2 resulted in a very condensed microstructure of mortar. They also stated that the $Ca(OH)_2$ grains in the samples containing NS were less visible than in the control samples. They demonstrated that after 28 days of curing, the microstructure of the specimens got denser and more compact. Large $Ca(OH)_2$ crystals weren't seen through the structure (Fig. 6).

5. Cost Effectiveness of Use of Nano-silica

Nano materials are expensive materials, which have minimized their use in the construction industry, despite of their numerous advantages (Adamu et al. 2021; Crucho et al. 2018; Janković et al. 2016; Mor et al. 2017; Reddy et al. 2020; Safiuddin et al. 2014; Sowjanya and Adiseshu 2022; Varisha et al. 2021). The high price of nano materials is related to the expensive technology and equipment involved (Crucho et al. 2018). Nano-silica has been reported to cost $185 per kg (Zidi et al. 2021). Despite the fact that nano-SiO_2 have been proven to improve the mechanical properties of cement-based materials, these improvements might not justify the huge increase in price of cement-based materials due to the use of nano-silica. However, a life-cycle cost assessment might justify the use of these materials, since nano-silica increases the durability and sustainability of cement-based materials and reduces the maintenance cost (Safiuddin et al. 2014). For this reason, a life-cycle cost analysis of NS incorporating cement-based materials is an important subject to be researched. The cost of nano-silica might be reduced through the production of NS using cost effective methods and through a higher production rate (Mor et al. 2017; Safiuddin et al. 2014). The cost of NS containing cement-based materials can be reduced

by reducing the content of NS in these materials, since higher percentages cause lower or even adverse effects on their properties (Adamu et al. 2021; De la Varga et al. 2019). More research is needed to assess the cost effectiveness of nano-silica use in cementitious materials, and to develop new cheaper and more practical methods of production that may lead to more production and incorporation of such beneficial nanomaterials.

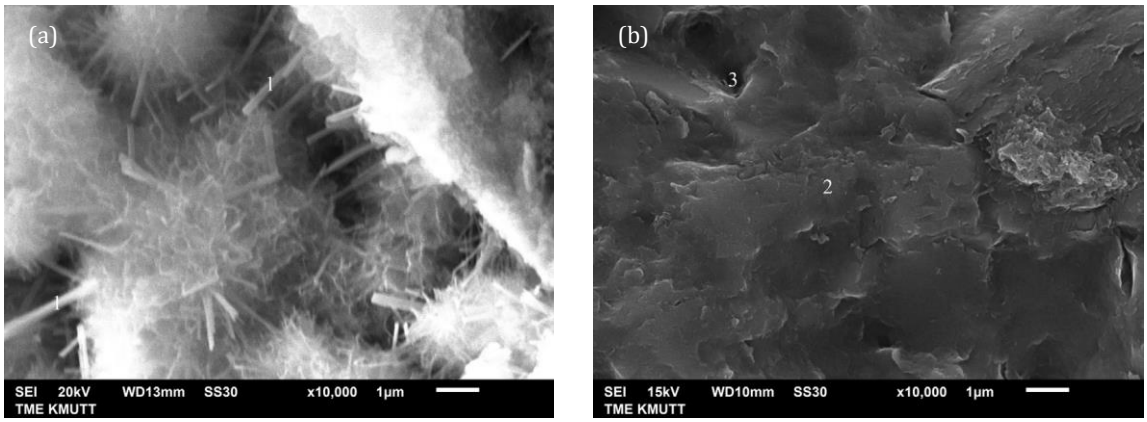

Fig. 5. SEM observations of mortar samples after 7 days of curing:
(a) without NS; (b) with 9.0 wt% NS. 1=CH crystal, 2=C-S-H, 3=pore (Haruehansapong et al. 2014).

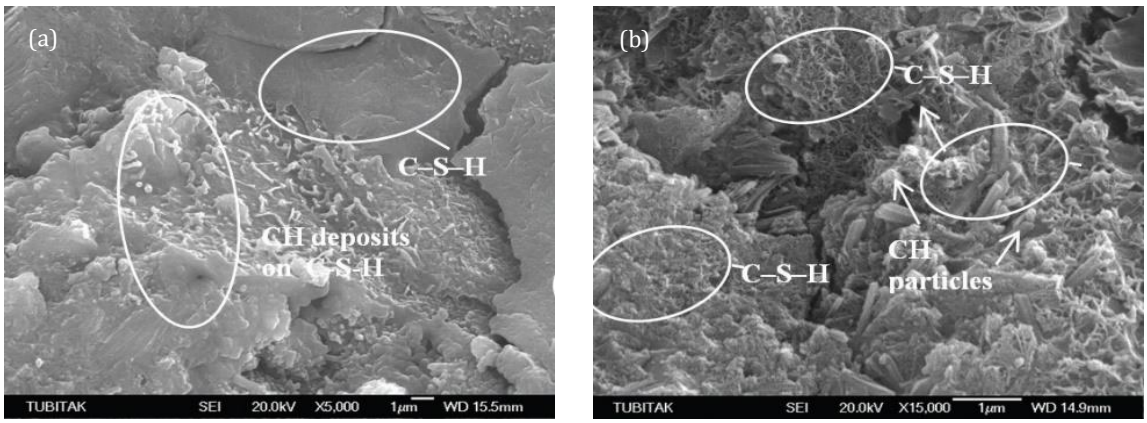

Fig. 6. SEM observations of mortar samples after 28 days of curing:
(a) without NS; (b) with 10 wt% NS (Biricik and Sarier 2014).

6. Conclusions

The present paper discusses the pros and cons of use of NS and reviews the effect of its incorporation on different properties of cement-based materials. Some of the outcomes of the present study can be summarized as:

Nano-SiO_2 incorporation into mortar and concrete with even a small content can remarkably enhance their mechanical properties. This effect is generally more pronounced at early ages than at later ages. The enhancement in strength might be attributed to the behavior of nano-SiO_2 as a nano-filler to improve the microstructure, as well as to the hydration acceleration effect of such nanoparticles. In addition, due to its high pozzolanic reactivity, nano-SiO_2 reacts with $Ca(OH)_2$ and leads to more formation of C-S-H gel.

Nano-silica reduces the permeability of mortar and concrete and increases their resistance to water, chloride and gas penetration. Incorporation of nano-SiO_2 reduces the porosity by recovering the particle packing density, and leads to denser, more compact, less penetrable and more homogeneous microstructure. NS also increases the resistance of cementitious materials to freeze and thaw effect, elevated temperature, fire and sulfate attack.

As a result of its effect in improving the performance of mortar and concrete, nano-silica can improve the durability and sustainability of structures, and reduce their repair and maintenance costs.

The positive effect of nano-SiO_2 on different properties of mortar and concrete increases with the increase in the content of this nanomaterial in the mixture up to the optimum content and then starts to decrease. This reduction in the effect of NS after exceeding the optimum content might be ascribed to the agglomeration and unsuitable dispersion of nanoparticles which lead to formation of weak zones. In addition, the amount of SiO_2 nanoparticles that exist in the paste might be exceeding the needed amount to react with the liberated $Ca(OH)_2$ particles.

Despite the large amount of research carried out on the effect of nano-SiO_2 on different properties of cementitious materials, there still exists a big lack of information related to this topic. In addition, contradictory

results have been reported in different research work. For these reasons, finding a specific optimum content for nano-SiO_2 is of a big difficulty. In spite of that, as a guideline, the optimum replacement percentage of cement with nano-SiO_2 in concrete and mortar to improve their overall performance can be considered as 1.0-4.0 wt%. However, more research is required to confirm these results.

Although use of nano-silica in cementitious materials has great advantages, it also has some disadvantages, such as the high price of nanoparticles that need to be considered in future research. More research is also needed to fully understand the effect of such nano-material on different properties of cement-based materials, and overcome the lack of information related to this topic.

More research on the relationship between the optimum content of nano-additives and the different factors that influence it, such as the properties of the used nano-SiO_2 (specific surface area, dispersion etc.) and the composition of the cement pastes (w/c ratio, content of cement, the addition of other additives etc.), is encouraged. Moreover, there is only little research on the effect of nano-silica on the dynamic properties of cementitious materials, which should be further researched. Future research should also focus on developing equations that describe the relationship between the content of nano-silica and the properties of cement-based materials. The optimum content of other nano-additives to best improve the properties of cement-based materials should also be investigated.

Acknowledgements

None declared.

Funding

The authors received no financial support for the research, authorship, and/or publication of this manuscript.

Conflict of Interest

The authors declared no potential conflicts of interest with respect to the research, authorship, and/or publication of this manuscript.

References

Adamu M, Ibrahim YE, Al-Atroush ME, Alanazi H (2021). Mechanical properties and durability performance of concrete containing calcium carbide residue and nano silica. *Materials*, 14(22), 6960.

Aggarwal P, Singh RP, Aggarwal Y (2015). Use of nano-silica in cement based materials—A review. *Cogent Engineering*, 2(1), 1078018.

Akhayere E, Kavaz D, Vaseashta A (2019). Synthesizing nano silica nanoparticles from barley grain waste: effect of temperature on mechanical properties. *Polish Journal of Environmental Studies*, 28(4), 2513–2521.

Al Ghabban A, Al Zubaidi AB, Jafar M, Fakhri Z (2018). Effect of nano SiO 2 and nano CaCO 3 on the mechanical properties, durability and flowability of Concrete. *IOP Conference Series: Materials Science and Engineering*, 454, 012016.

Amin M, Abu el-Hassan K (2015). Effect of using different types of nano materials on mechanical properties of high strength concrete. *Construction and Building Materials*, 80, 116–124.

Ardalan RB, Jamshidi N, Arabameri H, Joshaghani A, Mehrinejad M, Sharafi P (2017). Enhancing the permeability and abrasion resistance of concrete using colloidal nano-SiO2 oxide and spraying nanosilicon practices. *Construction and Building Materials*, 146, 128–135.

Arif M, Al-Hagri MG, Shariq M, Rahman I, Hassan A, Baqi A (2020). Mechanical properties and microstructure of micro- and nano-additives-based modified concrete composites: A sustainable solution. *Journal of The Institution of Engineers (India): Series A*, 101(1), 89–104.

Asadi Z, Norouzbeigi R (2018). Synthesis of colloidal nanosilica from waste glass powder as a low cost precursor. *Ceramics International*, 44(18), 22692–22697.

Ashwini K, Srinivasa Rao P (2021). Freeze and thaw resistance of concrete using alccofine and nano-silica. *Materials Today: Proceedings*, 47, 4336–4340.

Bahadori H, Hosseini P (2012). Reduction of cement consumption by the aid of silica nano-particles (investigation on concrete properties). *Journal of Civil Engineering and Management*, 18(3), 416–425.

Balamurugan M, Saravanan S (2012). Producing nanosilica from Sorghum vulgare seed heads. *Powder Technology*, 224, 345–350.

Barbhuiya S, Qureshi M (2015). Handbook of Research on Diverse Applications of Nanotechnology in Biomedicine, Chemistry, and Engineering. Soni S, Salhotra A, Suar M. *Applications of Nanotechnology in Cement and Concrete Science.* Engineering Science Reference, USA, 624-639.

Bastami M, Baghbadrani M, Aslani F (2014). Performance of nano-silica modified high strength concrete at elevated temperatures. *Construction and Building Materials*, 68, 402–408.

Behfarnia K, Salemi N (2013). The effects of nano-silica and nano-alumina on frost resistance of normal concrete. *Construction and Building Materials*, 48, 580–584.

Behzadian R, Shahrajabian H (2019). Experimental study of the effect of nano-silica on the mechanical properties of concrete/PET Composites. *KSCE Journal of Civil Engineering*, 23(8), 3660-3668.

Beigi MH, Berenjian J, Omran OL, Nik AS, Nikbin IM (2013). An experimental survey on combined effects of fibers and nanosilica on the mechanical, rheological, and durability properties of self-compacting concrete. *Materials & Design*, 50, 1019–1029.

Bi J, Pane I, Hariandja B, Imran I (2012). The Use of nanosilica for improving of concrete compressive strength and durability. *Applied Mechanics and Materials*, 204–208, 4059–4062.

Biricik H, Sarier N (2014). Comparative study of the characteristics of nano silica-, silica fume-and fly ash-incorporated cement mortars. *Materials Research*, 17(3), 570–582.

Bolhassani M, Samani M (2015). Effect of type, size, and dosage of nanosilica and microsilica on properties of cement paste and mortar. *ACI Materials Journal*, 112(2), 1–7.

Carmo R, Costa H, Soldado E, Júlio E (2021). Influence of nano-SiO2, nano-Al2O3, and nano-ZnO additions on cementitious matrixes with different powder and steel fibers content. *Journal of Advanced Concrete Technology*, 19(1), 40–52.

Carneiro ME, Magalhães W LE, Muñiz GI de, Nisgoski S, Satyanarayana KG (2015). Preparation and characterization of nano silica from equisetum arvenses. *Journal of Bioprocessing & Biotechniques*, 05(02).

Cassar L, Pepe C, Tognon G, Guerrini GL, Amadelli R (2003). White cement for architectural concrete, possessing photocatalytic properties. *Proceedings of the 11th International Congress on the Chemistry of Cement*, Durban, South Africa, 2012–2021.

Chithra S, Kumar SRRS, Chinnaraju K (2016). The effect of colloidal nano-silica on workability, mechanical and durability properties of high performance concrete with copper slag as partial fine aggregate. *Construction and Building Materials*, 113, 794–804.

Choolaei M, Rashidi AM, Ardjmand M, Yadegari A, Soltanian H (2012). The effect of nanosilica on the physical properties of oil well cement. *Materials Science and Engineering: A*, 538, 288–294.

Crucho JML, Neves JMC das, Capitão SD, Picado-Santos LG de (2018). Mechanical performance of asphalt concrete modified with nanoparticles: Nanosilica, zero-valent iron and nanoclay. *Construction and Building Materials*, 181, 309–318.

De la Varga I, Muñoz JF, Spragg RP, Nickel CA, Bohn L, Fay A, Graybeal BA (2019). Nanosilica coatings to improve the tensile bond strength of cementitious grouts. *Transportation Research Record: Journal of the Transportation Research Board*, 2673(10), 586–594.

Du H, Du S, Liu X (2015). Effect of nano-silica on the mechanical and transport properties of lightweight concrete. *Construction and Building Materials*, 82, 114–122.

Du H, Du S, Liu X (2014). Durability performances of concrete with nano-silica. *Construction and Building Materials*, 73, 705–712.

El-Gamal SMA, Abo-El-Enein SA, El-Hosiny FI, Amin MS, Ramadan M (2018). Thermal resistance, microstructure and mechanical properties of type I Portland cement pastes containing low-cost nanoparticles. *Journal of Thermal Analysis and Calorimetry*, 131(2), 949–968.

Elkady HM, Yasien AM, Elfeky MS, Serag ME (2019). Assessment of mechanical strength of nano silica concrete (NSC) subjected to elevated temperatures. *Journal of Structural Fire Engineering*, 10(1), 90–109.

Farajzadehha Soroush, Mahdikhani M, Moayed R, Farajzadehha Soheil (2020). Experimental study of permeability and elastic modulus of plastic concrete containing nano silica. *Structural Concrete*, e202000551, 1–12.

Gaitero JJ, Campillo I, Guerrero A (2008). Reduction of the calcium leaching rate of cement paste by addition of silica nanoparticles. *Cement and concrete research*, 38(8–9), 1112–1118.

Ghafari E, Costa H, Júlio E, Portugal A, Durães L (2014). The effect of nanosilica addition on flowability, strength and transport properties of ultra high performance concrete. *Materials & Design*, 59, 1–9.

Givi AN, Rashid SA, Aziz FNA, Salleh MAM (2011). The effects of lime solution on the properties of SiO2 nanoparticles binary blended concrete. *Composites Part B: Engineering*, 42(3), 562–569.

Givi AN, Rashid SA, Aziz FNA, Salleh MAM (2010). Experimental investigation of the size effects of SiO2 nano-particles on the mechanical properties of binary blended concrete. *Composites Part B: Engineering*, 41(8), 673–677.

Haruehansapong S, Pulngern T, Chucheepsakul S (2014). Effect of the particle size of nanosilica on the compressive strength and the optimum replacement content of cement mortar containing nano-SiO2. *Construction and Building Materials*, 50, 471–477.

He X, Shi X (2008). Chloride permeability and microstructure of Portland cement mortars incorporating nanomaterials. *Transportation Research Record: Journal of the Transportation Research Board*, 2070, 13–21.

Heikal M, Al-Duaij OK, Ibrahim NS (2015). Microstructure of composite cements containing blast-furnace slag and silica nano-particles subjected to elevated thermally treatment temperature. *Construction and Building Materials*, 93, 1067–1077.

Horszczaruk E, Sikora P, Cendrowski K, Mijowska E (2017). The effect of elevated temperature on the properties of cement mortars containing nanosilica and heavyweight aggregates. *Construction and Building Materials*, 137, 420–431.

Hou Pengkun, Kawashima S, Kong D, Corr DJ, Qian J, Shah SP (2013). Modification effects of colloidal nanoSiO2 on cement hydration and its gel property. *Composites Part B: Engineering*, 45(1), 440–448.

Hou Peng-kun, Kawashima S, Wang K, Corr DJ, Qian J, Shah SP (2013). Effects of colloidal nanosilica on rheological and mechanical properties of fly ash–cement mortar. *Cement and Concrete Composites*, 35(1), 12–22.

Huang Q, Zhu X, Zhao L, Zhao M, Liu Y, Zeng X (2020). Effect of nanosilica on sulfate resistance of cement mortar under partial immersion. *Construction and Building Materials*, 231, 117180.

Ibrahim KIM (2017). The effect of high elevated temperatures on nano silica high strength concrete [NSHSC]. *IOSR Journal of Mechanical and Civil Engineering*, 14(04), 61–66.

Ibrahim RK, Hamid R, Taha MR (2012). Fire resistance of high-volume fly ash mortars with nanosilica addition. *Construction and Building Materials*, 36, 779–786.

Jalal M (2012). Durability enhancement of concrete by incorporating titanium dioxide nanopowder into binder. *Journal of American Science*, 8(4), 289–294.

Jalal M, Mansouri E, Sharifipour M, Pouladkhan AR (2012). Mechanical, rheological, durability and microstructural properties of high performance self-compacting concrete containing SiO2 micro and nanoparticles. *Materials & Design*, 34, 389–400.

Jalal M, Pouladkhan A, Harandi OF, Jafari D (2015). Comparative study on effects of Class F fly ash, nano silica and silica fume on properties of high performance self compacting concrete. *Construction and Building Materials*, 94, 90–104.

Janković K, Stanković S, Bojović D, Stojanović M, Antić L (2016). The influence of nano-silica and barite aggregate on properties of ultra high performance concrete. *Construction and Building Materials*, 126, 147–156.

Jayapalan AR, Lee BY, Kurtis KE (2013). Can nanotechnology be 'green'? Comparing efficacy of nano and microparticles in cementitious materials. *Cement and Concrete Composites*, 36, 16–24.

Ji T (2005). Preliminary study on the water permeability and microstructure of concrete incorporating nano-SiO2. *Cement and Concrete Research*, 35(10), 1943–1947.

Juenger MCG, Siddique R (2015). Recent advances in understanding the role of supplementary cementitious materials in concrete. *Cement and concrete research*, 78, 71–80.

Kawashima S, Hou P, Corr DJ, Shah SP (2013). Modification of cement-based materials with nanoparticles. *Cement and Concrete Composites*, 36, 8–15.

Kewalramani MA, Syed ZI (2018). Application of nanomaterials to enhance microstructure and mechanical properties of concrete. *International Journal of Integrated Engineering*, 10(2).

Khalaf MA, Cheah CB, Ramli M, Ahmed NM, Al-Shwaiter A (2020). Effect of nano zinc oxide and silica on mechanical, fluid transport and radiation attenuation properties of steel furnace slag heavyweight concrete. *Construction and Building Materials*, 121785.

Khanzadi M, Tadayon M, Sepehri H, Sepehri M (2010). Influence of nano-silica particles on mechanical properties and permeability of concrete. *The 2nd International Conference on Sustainable Construction Materials and Technologies*, Ancona, Italy, 1–7.

Khoshakhlagh A, Nazari A, Khalaj G (2012). Effects of Fe2O3 nanoparticles on water permeability and strength assessments of high strength self-compacting concrete. *Journal of Materials Science & Technology*, 28(1), 73–82.

Kooshafar M, Madani H (2020). An investigation on the influence of nano silica morphology on the characteristics of cement composites. *Journal of Building Engineering*, 30, 101293.

Lazaro A, Quercia G, Brouwers HJH (2012). Production and application of a new type of nano-silica in concrete, in: Proceedings of the International Conference on Building Materials. Finger-Institut Fur Baustoffkunde, Weimar, Germany. pp. 1–6.

Lazaro A, Quercia G, Brouwers HJH, Geus JW (2013). Synthesis of a green nano-silica material using beneficiated waste dunites and its application in concrete. *World Journal of Nano Science and Engineering*, 3(3), 41–51.

Li H, Xiao HG, Yuan J, Ou J (2004). Microstructure of cement mortar with nano-particles. *Composites Part B: Engineering*, 35(2), 185-189.

Li J, Wu Z, Shi C, Yuan Q, Zhang Z (2020). Durability of ultra-high performance concrete – A review. *Construction and Building Materials*, 255, 119296.

Li LG, Zhu J, Huang ZH, Kwan AKH, Li LJ (2017). Combined effects of micro-silica and nano-silica on durability of mortar. *Construction and Building Materials*, 157, 337–347.

Li W, Huang Z, Cao F, Sun Z, Shah SP (2015). Effects of nano-silica and nano-limestone on flowability and mechanical properties of ultra-high-performance concrete matrix. *Construction and Building Materials*, 95, 366–374.

Liu R, Xiao H, Geng J, Du J, Liu M (2020). Effect of nano-CaCO3 and nano-SiO2 on improving the properties of carbon fibre-reinforced concrete and their pore-structure models. *Construction and Building Materials*, 244, 118297.

Ma Q, Zhu Y (2017). Experimental research on the microstructure and compressive and tensile properties of nano-SiO2 concrete containing basalt fibers. *Underground Space*, 2(3), 175–181.

Madandoust R, Mohseni E, Mousavi SY, Namnevis M (2015). An experimental investigation on the durability of self-compacting mortar containing nano-SiO2, nano-Fe2O3 and nano-CuO. *Construction and Building Materials*, 86, 44–50.

Maheswaran S, Bhuvaneshwari B, Palani GS, Nagesh R, Kalaiselvam S (2013). An overview on the influence of nano silica in concrete and a research initiative. *Research Journal of Recent Sciences*, 2(ISC-2012), 17–24.

Manchanda CK, Khaiwal R, Mor S (2017). Application of sol–gel technique for preparation of nanosilica from coal powered thermal power plant fly ash. *Journal of Sol-Gel Science and Technology*, 83(3), 574–581.

Mohamed SAE-A, Ragab AE-R (2014). Physico-mechanical properties and microstructure of blended cement incorporating nano-silica. *International Journal of Engineering Research & Technology*, 3(7), 339–358.

Mohseni E, Miyandehi BM, Yang J, Yazdi MA (2015). Single and combined effects of nano-SiO2, nano-Al2O3 and nano-TiO2 on the mechanical, rheological and durability properties of self-compacting mortar containing fly ash. *Construction and Building Materials*, 84, 331–340.

Mor S, Manchanda CK, Kansal SK, Ravindra K (2017). Nanosilica extraction from processed agricultural residue using green technology. *Journal of Cleaner Production*, 143, 1284–1290.

Mussa MH, Radzi NAM, Hamid R, Mutalib AA (2021). Fire Resistance of High-Volume Fly Ash RC Slab Inclusion with Nano-Silica. *Materials*, 14(12), 3311.

Nazari A, Riahi S (2011a). The effects of SiO2 nanoparticles on physical and mechanical properties of high strength compacting concrete. *Composites Part B: Engineering*, 42(3), 570–578.

Nazari A, Riahi S (2011b). The effects of TiO2 nanoparticles on properties of binary blended concrete. *Journal of Composite Materials*, 45(11), 1181–1188.

Nazari A, Riahi S (2011c). TiO2 nanoparticles effects on physical, thermal and mechanical properties of self compacting concrete with ground granulated blast furnace slag as binder. *Energy and Buildings*, 43(4), 995–1002.

Ngo V-T, Bui T-T, Lam T-Q-K, Nguyen T-T-N, Nguyen V-H (2020). Experimental evaluation of nano silica effects to high performance concrete strength in early age. *IOP Conference Series: Materials Science and Engineering*, 869, 032011.

Niewiadomski P, Hoła J, Ćwirzeń A (2018). Study on properties of self-compacting concrete modified with nanoparticles. *Archives of Civil and Mechanical Engineering*, 18(3), 877–886.

Nili M, Ehsani A, Shabani K (2010). Influence of nano-SiO2 and micro-silica on concrete performance. *Second international conference on sustainable construction materials and technologies*, Ancona, Italy, 67-73.

Nima F, Ali AAA, Demirboga R (2011). Development of nanotechnology in high performance concrete. *Advanced Materials Research*, 364, 115–118.

Oltulu M, Şahin R (2013). Effect of nano-SiO2, nano-Al2O3 and nano-Fe2O3 powders on compressive strengths and capillary water absorption of cement mortar containing fly ash: A comparative study. *Energy and Buildings*, 58, 292–301.

Oltulu M, Şahin R (2011). Single and combined effects of nano-SiO2, nano-Al2O3 and nano-Fe2O3 powders on compressive strength and capillary permeability of cement mortar containing silica fume. *Materials Science and Engineering: A*, 528(22–23), 7012–7019.

Quercia G, Brouwers HJH (2010). Application of nano-silica (nS) in concrete mixtures. *8th fib PhD Symposium*, Lyngby, Denmark, 431-436.

Quercia G, Lazaro A, Geus JW, Brouwers HJH (2013). Characterization of morphology and texture of several amorphous nano-silica particles used in concrete. *Cement and Concrete Composites*, 44, 77–92.

Quercia G, Spiesz P, Hüsken G, Brouwers HJH (2014). SCC modification by use of amorphous nano-silica. *Cement and Concrete Composites*, 45, 69–81.

Rashad AM (2014). A comprehensive overview about the effect of nano-SiO2 on some properties of traditional cementitious materials and alkali-activated fly ash. *Construction and Building Materials*, 52, 437–464.

Reches Y (2018). Nanoparticles as concrete additives: Review and perspectives. *Construction and Building Materials*, 175, 483–495.

Reddy AN, Reddy PN, Kavyateja BV, Reddy GGK (2020). Influence of nanomaterial on high-volume fly ash concrete: a statistical approach. *Innovative Infrastructure Solutions*, 5(3), 88.

Reddy Babu G, Ramana NV, Naresh Kumar T, Visesh Kumar K (2019). Effect of nanosilica on properties and durability in cement. *Materials Today: Proceedings*, 19, 599–605.

Rong Z, Sun W, Xiao H, Jiang G (2015). Effects of nano-SiO2 particles on the mechanical and microstructural properties of ultra-high performance cementitious composites. *Cement and Concrete Composites*, 56, 25–31.

Safiuddin M, Gonzalez M, Cao J, Tighe SL (2014). State-of-the-art report on use of nano-materials in concrete. *International Journal of Pavement Engineering*, 15(10), 940–949.

Said AM, Zeidan MS, Bassuoni MT, Tian Y (2012). Properties of concrete incorporating nano-silica. *Construction and Building Materials*, 36, 838–844.

Seifan M, Mendoza S, Berenjian A (2020). Mechanical properties and durability performance of fly ash based mortar containing nano- and micro-silica additives. *Construction and Building Materials*, 252, 119121.

Senff L, Labrincha JA, Ferreira VM, Hotza D, Repette WL (2009). Effect of nano-silica on rheology and fresh properties of cement pastes and mortars. *Construction and Building Materials*, 23(7), 2487–2491.

Senff L, Tobaldi DM, Lucas S, Hotza D, Ferreira VM, Labrincha JA (2013). Formulation of mortars with nano-SiO2 and nano-TiO2 for degradation of pollutants in buildings. *Composites Part B: Engineering*, 44(1), 40–47.

Shafiq N, Kumar R, Zahid M, Tufail RF (2019). Effects of modified metakaolin using nano-silica on the mechanical properties and durability of concrete. *Materials*, 12(14), 2291.

Shahrajabian F, Behfarnia K (2018). The effects of nano particles on freeze and thaw resistance of alkali-activated slag concrete. *Construction and Building Materials*, 176, 172–178.

Shaikh FUA, Supit SWM, Sarker PK (2014). A study on the effect of nano silica on compressive strength of high volume fly ash mortars and concretes. *Materials & Design*, 60, 433–442.

Sharaky IA, Megahed FA, Seleem MH, Badawy AM (2019). The influence of silica fume, nano silica and mixing method on the strength and durability of concrete. *SN Applied Sciences*, 1(6), 575.

Shebl SS, Allie L, Morsy MS, Aglan HA (2009). Mechanical behavior of activated nano silicate filled cement binders. *Journal of Materials Science*, 44(6), 1600–1606.

Siang Ng D, Paul SC, Anggraini V, Kong SY, Qureshi TS, Rodriguez CR, Liu Q, Šavija B (2020). Influence of SiO2, TiO2 and Fe2O3 nanoparticles on the properties of fly ash blended cement mortars. *Construction and Building Materials*, 258, 119627.

Sikora P, Abd Elrahman M, Stephan D (2018). The influence of nanomaterials on the thermal resistance of cement-based composites—A review. *Nanomaterials*, 8(7), 465.

Sikora P, Łukowski P, Cendrowski K, Horszczaruk E, Mijowska E (2015). The effect of nanosilica on the mechanical properties of polymer-cement composites (PCC). *Procedia Engineering*, 108, 139–145.

Singh LP, Karade SR, Bhattacharyya SK, Yousuf MM, Ahalawat S (2013). Beneficial role of nanosilica in cement based materials – A review. *Construction and Building Materials*, 47, 1069–1077.

Sowjanya S, Adiseshu S (2022). Statistical analysis of the physical properties of ternary blended concrete. *Innovative Infrastructure Solutions*, 7(1), 10.

Stefanidou M, Papayianni I (2012). Influence of nano-SiO2 on the Portland cement pastes. *Composites Part B: Engineering*, 43(6), 2706–2710.

Tobbala DE (2021). Comparative study on the durability of nano-silica and nano-ferrite concrete. *East African Scholars Journal of Engineering and Computer Sciences*, 4(9), 124–131.

Vargas P, Marín NA, Tobón JI (2018). Performance and microstructural analysis of lightweight concrete blended with nanosilica under sulfate attack. *Advances in Civil Engineering*, 2018, 1–11.

Varisha, Zaheer MM, Hasan SD (2021). Mechanical and durability performance of carbon nanotubes (CNTs) and nanosilica (NS) admixed cement mortar. *Materials Today: Proceedings*, 42, 1422–1431.

Vaz-Ramos J, Santiago A, Portugal A, Durães L (2019). Synthesis of silica nanoparticles to enhance the fire resistance of cement mortars. *Fire Research*, 3(1).

Vivek D, Elango KS, Saravanakumar R, Mohamed Rafek B, Ragavendra P, Kaviarasan S, Raguram E (2020). Effect of nano-silica in high performance concrete. *Materials Today: Proceedings*, 37(2), 1226-1229.

Wu Z, Shi C, Khayat KH, Wan S (2016). Effects of different nanomaterials on hardening and performance of ultra-high strength concrete (UHSC). *Cement and Concrete Composites*, 70, 24–34.

Ying J, Zhou B, Xiao J (2017). Pore structure and chloride diffusivity of recycled aggregate concrete with nano-SiO2 and nano-TiO2. *Construction and Building Materials*, 150, 49–55.

Zhang M-H, Islam J (2012). Use of nano-silica to reduce setting time and increase early strength of concretes with high volumes of fly ash or slag. *Construction and Building Materials*, 29, 573–580.

Zhang M, Li H (2011). Pore structure and chloride permeability of concrete containing nano-particles for pavement. *Construction and Building Materials*, 25(2), 608–616.

Zhang P, Sha D, Li Q, Zhao S, Ling Y (2021). Effect of nano silica particles on impact resistance and durability of concrete containing coal fly ash. *Nanomaterials*, 11(5), 1296.

Zhao Y, Cui N, Zhao S, Zhu Y, Hou P, Feng L, Xie N (2021). Aggressive Environment resistance of concrete products modified with nano alumina and nano silica. *Frontiers in Materials*, 8 (695624), 1-12.

Zhuang C, Chen Y (2019). The effect of nano-SiO2 on concrete properties: a review. *Nanotechnology Reviews*, 8(1), 562–572.

Zidi Z, Ltifi M, Zafar I (2021). Comparative study: nanosilica, nanoalumina, and nanozinc oxide addition on the properties of localized geopolymer. *Journal of the Australian Ceramic Society*, 57(3), 783–792.